PNWD-3180

Simulation of Water Balance and Forest Treatment Effects at the H.J. Andrews Experimental Forest

Scott R. Waichler, Mark S. Wigmosta, and Beverley C. Wemple

Pacific Northwest National Laboratory
MSIN K9-36, P.O. Box 999
Richland, Washington, 99352
scott.waichler@pnl.gov

November 2002

Prepared for
National Council for Air and Stream Improvement (NCASI)
Battelle Agreement 40686

LEGAL NOTICE

Abstract

The watershed model DHSVM was applied to the small watersheds WS1,2,3 in H.J. Andrews Experimental Forest (HJA), Oregon and tested for skill in simulating observed forest treatment effects on streamflow. These watersheds in the rain-snow transition zone underwent road and clearcut treatments during 1959-66 and subsequent natural regeneration. DHSVM was applied with 10 m and 1 hr resolution to 1958-98, most of the period of record. Methods for generating hourly meteorological values from daily data were developed and tested for the period WY80-98 when hourly data are available, then applied to WY58-79, when hourly data are not available. Water balance for old-growth WS2 indicated that evapotranspiration and streamflow were unlikely to be the only loss terms, and groundwater recharge was included to account for about 12% of precipitation; this term was assumed zero in previous studies. After limited calibration, overall efficiency in simulating hourly streamflow exceeded 0.7, and mean annual error was less than 10%. Model skill decreased at the margins, with overprediction of low flows and underprediction of high flows. However, statistical analyses of simulated and observed peakflows yielded similar characterizations of treatment effects. Primary simulation weaknesses were snowpack accumulation, snowmelt under rain-on-snow conditions, and production of stormflow. This challenging test of DHSVM moved the model closer to a practical tool for forest management.

Keywords

watershed modeling, forest treatment, hydrology, meteorology, peakflows, DHSVM, HJ Andrews, HJA

Acknowledgments

Financial support was provided by the National Council for Air and Stream Improvement (NCASI), Battelle-Pacific Northwest Division, and Pacific Northwest National Laboratory. We thank Don Henshaw/OSU, for his assistance in obtaining climate and streamflow data; and Robert Thomas, for his assistance with implementing the statistical methods used on peakflows. Data sets were provided by the Forest Science Data Bank, a partnership between the Department of Forest Science, Oregon State University, and the U.S. Forest Service Pacific Northwest Research Station, Corvallis, Oregon. Funding for these data was provided by the Long-Term Ecological Research (LTER) program and other National Science Foundation programs (NSF), Oregon State University, and U.S. Forest Service Pacific Northwest Research Station. NSF grants: DEB-7611978, BSR-9011663.

List of Symbols and Acronyms

B_1	coefficient in Chapman-Richards equation
H_o	overstory canopy height
LAI_o	overstory leaf area index
LAI_u	understory leaf area index
LAI_{max}	old-growth, maximum leaf area index
$\hat{y}$	fitted response variable, natural log of streamflow, original units m^3/s
t	explanatory variable, time since treatment ended (yr)
x	explanatory variable, natural log of streamflow, original units m^3/s
d_1'	baseline-adjusted modified index of agreement
ΔS	change in storage (water balance)
E_2	efficiency (Nash and Sutcliffe, 1970)
E_1	first-degree efficiency
E_1''	baseline-adjusted first-degree
E_1'	baseline-adjusted first-degree efficiency
ET	evapotranspiration (water balance)
G	groundwater recharge or deep flux (water balance)
i_c	infiltration capacity (m/s)
K_g	vertical hydraulic conductivity for groundwater recharge (m/s)
K_l	lateral hydraulic conductivity (m/s)
K_v	vertical hydraulic conductivity (m/s)
P	precipitation (water balance)
P_d	daily precipitation (mm)
Q	streamflow (water balance)
H_{max}	daily maximum relative humidity (%)
H_{min}	daily minimum relative humidity (%)
R^2	square of Pearson’s product-moment correlation coefficient
T_{dew}	dewpoint air temperature (C)

T_{max}	daily maximum air temperature (C)
T_{min}	daily minimum air temperature (C)
CS2MET	WS2 climatic station
DEM	digital elevation model (an elevation grid)
DHSVM	Distributed Hydrology-Soil-Vegetatation Model
GIS	geographic information system
HJA	H.J. Andrews Experimental Forest
J&G	Jones and Grant (1996)
LAI	leaf area index
LTER	Long Term Ecological Research Network
met	meteorological
PRIMET	primary meteorological station at HJA
R	R is a language and environment for statistics and graphics; an open-source version of Splus.
RHESSys	Regional HydroEcological Simulation System
T&M	Thomas and Megahan (1998); Thomas (2002)
WS	small watershed at HJA
WY	water year, beginning October 1 of the previous calendar year

Contents

Figures

Tables

1 Introduction

The impacts of forest practices on catchment hydrology are an important issue to resource managers and the public. Numerous paired-basin field studies have evaluated the effects of road construction and vegetation removal on basin hydrologic response at the H.J. Andrews Experimental Forest, Oregon (HJA), including annual water yield (Rothacher, 1970), peak streamflows (Harr and McCorison, 1979; Jones and Grant, 1996; Thomas and Megahan, 1998; Jones, 2000; Beschta et al., 2000), and summer low flows (Rothacher, 1965). Most of these studies did find forest treatment effects on streamflow, with varying degrees of significance. The goal of this study is to evaluate how well the physically-based Distributed Hydrology Soil Vegetation Model (DHSVM) can reproduce observed forest treatment effects, using the small watersheds WS1,2,3 at the HJA as the test case.

Recent analysis of long-term hydrologic records from HJA has raised questions about the magnitude and persistence of forest treatment effects on streamflow. Jones and Grant (1996) (J&G) compiled and analyzed peak stream discharges for 34 years of record on WS1,2,3. Using analysis of variance to detect differences between treated and control basins, they found statistically significant differences in peakflow magnitudes following clearcut harvesting in WS1 that were detectable 22 years after harvesting. In WS3, where road construction was followed four years later by harvesting 25% of basin area, statistically significant increases in peakflow magnitudes were detected only after forest harvesting occurred but were still detectable 25 years after harvest. Thomas and Megahan (1998) (T&M) reanalyzed these data using linear regression and presented new statistical models for the effects of treatment with time. Both studies documented similar magnitudes in peakflow increases following forest treatments, particularly for the smallest flow events. T&M did not find statistically significant treatment effects on WS3 more than 10 years after harvesting. They showed that treatment effects diminished with time, and concluded that flow increases were detectable only for flows less than the 2-year recurrence interval. Similarly, Beschta et al. (2000) evaluated the same data and concluded that peakflow increases diminished with the size of the recurrence interval. These studies have spurred ongoing debate about the mechanisms responsible for changes in peakflows in these basins, the effects of forest clearing and roads on large floods, and the persistence of forest treatment effects through time.

Empirical studies provide insight into the effects of forest treatments in the experimental basins and describe the behavior of the local hydrologic system, but provide limited ability to extrapolate to other settings. Part of the promise of process-based modeling is to provide a means of evaluating the impacts of forest practices in areas lacking extensive empirical work. Recent applications of DHSVM have evaluate the impacts of forest harvesting and road construction on watersheds in western Washington (Storck et al., 1998; LaMarche and Lettenmeier, 2001; Bowling and Lettenmaier, 1997) and western British Columbia (Wigmosta and Perkins, 1997). The HJA is one of the longest-running field sites in the Long Term Ecological Research Network (LTER) and has produced a great deal of research on the hydrology of steep, forested catchments and the impacts of road-building and timber harvest. However, most of the hydrologic research has been empirical and statistical in nature. Relatively little testing and improvement of process-based models has been done at HJA, and no previous efforts have attempted to simulate basin hydrology at a fine temporal resolution over the entire period of record. Only two published studies and two theses have modeled the catchment hydrology with physically-based models, and these did so on limited timespans and watersheds (Tague and Band, 2001b,a; Duan, 1996; Bredensteiner, 1998). We applied DHSVM to WS1,2,3 at the HJA to assess our ability to

reproduce observed forest treatment effects on streamflow, including changes in peakflows that have been observed statistically. We simulated 41 years, most of the record, in all three watersheds at 10 m and 1 hr resolution.

In the rest of this report we first present an overview of DHSVM structure, and describe the spatial model inputs to DHSVM and the generation of hourly meteorology from daily data for use in driving DHSVM. A special challenge for this study was to reproduce the hydrology of the regrowing forest. We limited calibration to the control watershed, WS2, and the pretreatment period of WS1, accounting for watershed variability in terrain, soil type, and forest treatment with model input, and assessed our ability to reproduce observed flows. We reviewed previously published water balances and field measurements of evapotranspiration rates in this environment, inferred an additional loss term not present in previous studies, and incorporated this loss as a groundwater recharge term in the model. We compared streamflow under no treatment and treatment states using combinations of observed and simulated flows for WS1 and WS2. We also compared non-historical treatment and no-treatment scenarios using WS1 as the test case. Finally, we applied the statistical methods of Thomas and Megahan (1998) as later revised by Thomas (personal communication, 2002), to assess our ability to reproduce the statistical tendencies of the observed data in our simulation results. Figures and tables are grouped at the end of each section for easier navigation. A list of definitions for symbols and acronyms is given on page v. The Appendices include definitions for goodness-of-fit statistics, and the main DHSVM input files.

2 Methods

HJA is located in the Western Cascades province of Oregon (Figure 2.1) and its maritime climate is dominated by frontal systems from the Pacific Ocean during November-May, and by high-pressure systems producing warm, dry conditions the rest of the year. Average annual precipitation at WS2 is 2300 mm, with a mean temperature of 9 C. The small watersheds WS1,2,3 range from 0.6 to 1.0 km^2 in area, and have elevations ranging from 450 to 1000 m (Table 2.1), placing them in the rain-snow transition zone. All three watersheds were covered with old-growth Douglas fir-Western hemlock forest before forest treatments began in the late 1950s and early 1960s. WS2 has served as a control for the paired watershed experiment; its vegetation has remained old-growth.

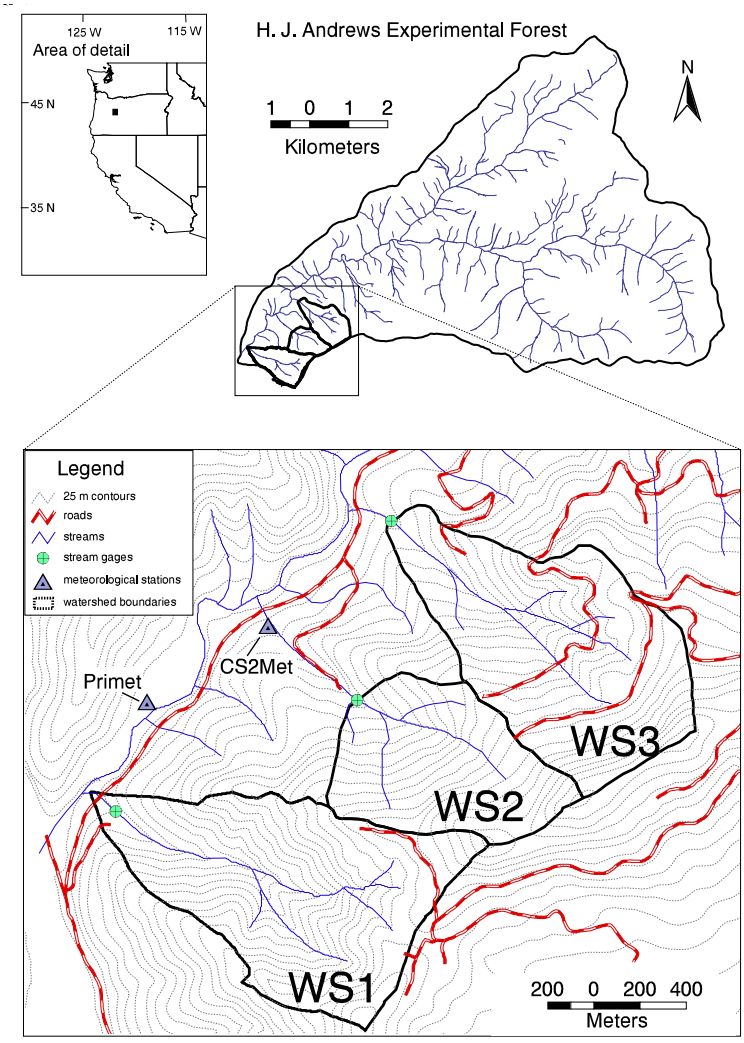

Figure 2.1: H.J. Andrews Experimental Forest, small watersheds WS1,2,3, and climate stations.

Table 2.1: HJA small watersheds WS1,2,3.

Basin	Size km^2	Elevation (m)	Road density (km/km^2)	Treatment (change from old-growth forest)
WS1	0.96	460-990	0	Clearcut 1962-66; burned 10/66
WS2	0.60	530-1070	0	Untreated
WS3	1.01	490-1070	3.0	Roaded 1959; 25% patch cut 1963

2.1 Description of DHSVM

The Distributed Hydrology Soil Vegetation Model (DHSVM) is a process-based, distributed parameter hydrologic model designed for simulating runoff processes in forested, mountainous environments (Wigmosta et al., 1994, 2002). A particular strength of DHSVM is its grid-based representation of the watershed, allowing specification of vegetation and soil types at the resolution of the digital elevation model (DEM), stored as a GIS layer. Elevation data of the DEM are used to simulate topographic controls on absorbed shortwave radiation, precipitation, air temperature and downslope water movement.

Major processes simulated by DHSVM are canopy interception, evaporation, transpiration, snow accumulation and melt in the canopy and on the ground, vertical unsaturated water flow, and lateral saturated groundwater flow. The major inputs are grids of surface elevation, soil type, soil thickness, vegetation type; tables of soil and vegetation biophysical parameter values keyed to type; and timeseries of the meteorological variables air temperature, precipitation, wind speed, relative humidity, solar radiation, and longwave radiation from one or more stations. Canopy evapotranspiration is simulated for each cell with the Penman-Monteith equation and local aerodynamic and canopy resistances. An explicit energy-balance approach is used for snow accumulation and ablation, both in the canopy and on the ground. Unsaturated soil water movement is downward only and driven by a unit gradient with hydraulic conductivity as a function of soil moisture content, using the Brooks-Corey equation. Lateral saturated soil water movement is simulated with Darcy's Law, where hydraulic gradient is based on either land surface or water table elevations (land surface option was used here).

Surface overland flow is generated where the water table rises above the land surface, or where infiltration capacity is limiting. Macropore flow is an important mechanism for streamflow generation in steep, temperate forests, and is accounted for in DHSVM by diverting some of the water from normal soil infiltration to the surface storage term, similar to the approach of Szilagyi and Parlange (1999). Water in the surface store is routed downgradient with either a constant velocity ($\Delta x/\Delta t$), or a slower kinematic approach based on the method of Szilagyi and Parlange (1999). The constant velocity method is the upper limit in terms of possible flow rate (all of the surface water in a cell is moved to the next cell). Both methods move the surface water faster than subsurface Darcian flow, but the water moves just one cell per timestep and can infiltrate in downgradient cells. To represent macropore flow in this study, we used variable infiltration of the Holtan equation (Holtan, 1961) to divert some of the water to the non-matric (surface) store, then routed it using the constant velocity method. Streamflow is generated by channel interception of surface and subsurface runoff.

Vegetation may be represented with up to two layers. An overstory, if present, may cover all or some fraction of the cell. An understory, if present, is assumed to cover the entire cell. Vegetation types ranging from bare soil to low-lying vegetation to closed-canopy forests with understory may be specified. Climate variables are specified at a height above the top of the vegetation. Wind

speed and solar radiation are attenuated down through the vegetation layers based on fractional area covered, vegetation height, and leaf area index (LAI). Stomatal resistance is computed separately for each root zone-vegetation layer combination, using soil moisture (Feddes et al., 1978), air temperature, vapor pressure deficit, and solar radiation (Dickinson et al., 1991).

Most details of applying DHSVM to the HJA were addressed in the pre- and post-processing tasks. A few changes related to meteorologic and vegetation input were made in the model code itself, as discussed below.

2.2 Meteorology

Simulation of hydrological processes at timescales less than a day requires the hydrologic model to operate at subdaily timesteps and to utilize diurnal variation in meteorological forcing. For example, DHSVM is designed to work best at a timestep of 3 hours or less. Required meteorological (hereafter, “met”) input for DHSVM consists of air temperature, precipitation, relative humidity, wind speed, solar radiation, and longwave radiation at the same timestep as the output. For most mountain watersheds only a few daily met variables are readily available at nearby met stations; typically minimum and maximum air temperature, daily total precipitation, and perhaps humidity. At HJA, hourly data were not available for the met variables of interest prior to WY80, so disaggregation and estimation of required but unmeasured met parameters were done. Previous studies have focused on generating daily met data at specific sites (Running et al., 1987) or over large areas (Thornton et al., 1997; Thornton and Running, 1999). As part of the preparation to satisfy the main NCASI objectives for simulating streamflow, we calibrated and verified models for predicting hourly values from a few daily variables. We also explored the significance of the met modeling for the hydrology simulation.

The met measurement program at HJA (Henshaw et al., 1998; Bierlmaier and McKee, 1989) includes hourly observations since the 1970s and provides a rich opportunity for the development and verification of local met models. We focused on the two met stations closest to WS1,2,3, PRIMET and CS2MET (Figure 2.1), and evaluated how well we could predict hourly values. We then evaluated the significance of the hourly met synthesis for hydrology, by simulating the hydrology of WS2 during WY80-98, using both observed and generated met values, and compared output hourly streamflow and several annualized fluxes.

Climate data were obtained from the primary met station PRIMET and another station located adjacent to WS2, CS2MET (Figure 2.1) (Henshaw et al., 1998). PRIMET is located at 430 m elevation in a valley-bottom clearing. The valley bottom is approximately 200 m wide and is subject to early morning and late afternoon topographic shading. CS2MET is located at 485 m elevation in a smaller clearing within the forest and is subject to shading from both canopy and topography. Hourly met values for WY80-98 were estimated from daily PRIMET data using common disaggregation and estimation techniques (Table 2.2), and compared to the hourly observations. Hourly met values at PRIMET were also estimated from daily CS2MET data, because CS2MET has a longer record and is needed for hydrologic modeling prior to 1979.

Thirteen sets of met input representing different levels of quality and met modeling assumptions were used to drive DHSVM (Table 2.3), and the significance of the met modeling assumptions for hydrology simulation were evaluated. The met inputs included the PRIMET observed hourly (P1) and fully-developed simulated sets (P2), plus eleven additional inputs (P3,P4,C1-C9) intended to highlight relative sensitivities to particular met variables and met simulation assumptions.

2.2.1 Hourly Meteorological Modeling

Daily minimum air temperature (T_{min}), maximum air temperature (T_{max}), precipitation (P_d), minimum relative humidity (H_{min}), maximum relative humidity (H_{max}), and mean wind speed (W) were used to predict hourly values of air temperature (T), precipitation (P), relative humidity (H), wind speed (W), and solar radiation (R_s) at PRIMET. Hourly data from WY80-89 were used to calibrate the disaggregation methods, and data from WY90-98 were used for verification. No data for longwave radiation were available, so we used without verification the method of Bras (1990) and Bowling and Lettenmaier (1997), which is based on hourly air temperature, relative humidity, and daily atmospheric transmittance. A longer, daily met record was available at CS2MET, and was used to generate the hourly met input for the years WY58-79. Model skill at reproducing the hourly data was quantified with a bias measure, and three increasingly stringent tests of efficiency (see Appendix A for definitions of goodness-of-fit statistics). Bias was defined as $\overline{S}/\overline{O}$, where $\overline{S}$ is mean of simulated values and $\overline{O}$ is mean of observed values. For the least stringent efficiency statistic, E_2, a value less than about 0.6 is typically considered a poor fit, while a value greater than about 0.8 is considered a very good fit. Many hydrologists modeling streamflow are satisfied with a value of around 0.7.

Some hourly timesteps in the PRIMET record for WY80-98 were missing from the raw data files, or had variables that were flagged as missing or questionable. Substitutions with baseline means were made to render a complete hourly record for each of the five variables. For air temperature, the baseline [month,hour] mean was substituted. The square brackets are used here to denote categorical variables. In the case of a [month,hour] baseline, there were $(12 \cdot 24 =)$ 288 means computed from the available data. Wind speed and solar radiation had similar substitutions (Table 2.4). Relative humidity was more complicated because no hourly measurements were available before 7/7/88. Before that date, hourly values were computed from CS2MET H_{max} and T_{min} or PRIMET air temperature at midnight if T_{min} was missing. For precipitation, $1/24$ of the daily total at PRIMET was used for flagged timesteps; if the PRIMET daily total was unavailable, then the CS2MET daily total was used. Precipitation values at all timesteps were obtainable with this combination of methods. The numbers of missing or questionable values were less than 3% for air temperature, wind speed, solar radiation, and relative humidity after 7/7/88; and less than 8% for precipitation (Table 2.4). Similar information for CS2MET daily met variables is given in Tables 2.5, 2.6. Missing or questionable CS2MET daily data were replaced with [month] means computed from WY58-98. No precipitation values were missing, but about 2% and 12% of temperature and relative humidity values, respectively, were affected (Table 2.5).

Two types of baseline means and bias corrections were used in the modeling of hourly met values, where baseline refers to a domain defined by categorical factors denoted with square brackets. The first type used month and hour ([month,hour]); the second used those factors plus daily precipitation status (wet or dry) ([month,hour,precip]). Baseline means and bias corrections were computed from data in the calibration period. Baseline means were used as another predictor for air temperature, atmospheric transmittance, humidity, and wind speed (methods 1c, 3c, 4e, 5b, respectively). Baseline bias corrections were used to account for differences between CS2MET and PRIMET stations when generating met input for the hydrologic model. The difference between hourly estimated CS2MET and observed PRIMET baseline means were computed and added to CS2MET hourly values to get the final, unbiased estimate for the PRIMET location. The most efficient method for each variable was used to generate the “best” simulated hourly met values of input sets P2 and C1. Inputs P4 and C2-C9 differ from P2 and C1, respectively, only with respect to one variable, as described in Table 2.3 and in the paragraphs below. Met input P3 was generated using just T_{min}, T_{max}, and P_d with no other site knowledge, and represents a input set that would be generated with limited data under typical circumstances in many watershed applications.

Simulation of all met variables except wind speed was good when the "best" set of techniques was used (i.e., the techniques for input sets P2 and C1). Bias was close to 1.0 except for wind speed during the verification period (Table 2.7). Air temperature, atmospheric transmittance, and relative humidity actually had higher efficiency values during the verification period than during the calibration period.

Air Temperature. Hourly values of T were generated by computing a modified sine curve from daily T_{min} and T_{max}, following the method of Running et al. (1987); Parton and Logan (1981). First, monthly means were substituted for missing, questionable, and ($T_{min} > T_{max}$) days (1.6% of timeseries). Daylight air temperature was modeled using three quadrants of a sine wave ($-\pi/2$ to π) with the minimum value at sunrise, maximum value at solar noon ($\pi/2$), and mean value at sunset (π). Sunrise and sunset times were computed with a solar geometry model (Gates, 1980; Bowling and Lettenmaier, 1997), assuming level ground free from topographic shading. Nighttime air temperature was modeled as a linear interpolation between sunset T of the previous day and sunrise T of the following day. The modified sine curve approach can be viewed as the minimum viable method for generating T (method 1a in Table 2.2). Shifting the resulting sine curve two hours earlier yielded the best match to the observations (method 1b).

To generate hourly air temperature using CS2MET data, [month,hour,precip] bias corrections were computed from data in the calibration period and added to the modified sine curve based on CS2MET T_{min} and T_{max} to yield the final air temperatures (Figure 2.2). For wet days, the bias correction was 1-2 C during the wet season. Cloud cover associated with wet days reduced night time cooling, producing a smaller range in diurnal temperature. For dry days, a strong diurnal pattern was evident, with the maximum bias correction (up to 6 C) occurring around midday, and the minimum occurring around dawn. For comparison, the difference between these stations according to the mean lapse rate of -4.2 C/km (Rosentrater, 1997) would be only 0.2 C. The effect of siting independent of elevation difference indicates the potential difficulty in spatial interpolation or extrapolation, even in small areas.

The modified sine curve method with a two-hour shift (method 1b) resulted in the best fit to the observations (Table 2.7, Figures 2.3, 2.4). The least successful predictor of air temperature was the baseline means model (method 1c). Air temperature modeling had the most skill of the five met variables, with bias close to 1.0 and efficiency values among the highest obtained. The efficiency statistics have a possible range of $-\infty$ to 1.0. A value of 0 indicates the model is no better or worse than the observed mean as a predictor. Efficiency generally declines from calibration to verification, and from using a less specific mean to a more specific mean for comparison (e.g., from grand mean to [month,hour,precip] baseline mean).

Precipitation. Hourly P values were generated as $1/24$ of daily precipitation P_d. When using CS2MET data, a bias correction factor (=0.956) was computed as the ratio of total PRIMET to CS2MET precipitation during WY80-98, and applied to all hourly simulated values.

Precipitation goodness-of-fit was much lower than for air temperature, as expected with the assumption of uniform precipitation over 24 hours (Table 2.7). Observed precipitation values greater than 6 mm/hr were underpredicted, and values greater than 10 mm/hr were underpredicted by 50% or more (Figures 2.5, 2.6).

Solar Radiation. Atmosphere-incident solar radiation R_a was calculated from latitude and time of year using the solar geometry model (Gates, 1980). The Bristow and Campbell (1984) model (BC) was used to predict daily atmospheric transmittance (T_r), and together with the atmosphere-incident solar model, hourly solar radiation R_s. BC estimates daily atmospheric transmittance from time of year and difference between daily minimum and maximum

temperature,

$$T_r = Ap(1 - e^{-B_m \Delta T^C}) \tag{2.1}$$

where

$A =$ coefficient, equivalent to the maximum atmospheric transmittance
$p =$ coefficient, 1.0 on dry days, < 1.0 on wet days
$B_m =$ coefficient that varies by month
$\Delta T =$ T_{max} - T_{min}
$C =$ coefficient

Atmospheric transmittance derived from dividing observed solar radiation at PRIMET by radiation incident to the atmosphere exhibits a weak relationship to daily ΔT (Figure 2.7). Maximum transmittance A was estimated from the ratio of observed solar radiation on clear days to modeled radiation at the top of the atmosphere (R_a) during the calibration period. Mean hourly R_a and observed clear sky radiation on dry days were plotted for each month (Figure 2.8). Existence of topographic shading was inferred from the data because morning values were much lower than afternoon during the winter months, but not during the summer months. Therefore, a conservative subset of the early afternoon hours, 1300-1500, were used to compute transmittance for the whole day. To obtain a sample of days that were reasonably certain to be clear, the eight (2.5%) of days with the highest mean 1300-1500 radiation were chosen. The observed radiation on these days were then divided by the corresponding R_a. The maximum value was A=0.73, similar to 0.70 cited in Bristow and Campbell (1984) for Pullman, Washington. Next, p and C were fitted by trial-and-error to the nearest 0.01, and B_m for each month was fitted with a non-linear regression function, using all days in the calibration period. On dry days, p was fixed to 1.0, and a single value was found for all wet days. The parameter set with the maximum efficiency E_1' value was selected: A =0.73, C =0.70, p =0.65 (wet days), B_m =[0.2089 (Jan), 0.2857, 0.2689, 0.2137, 0.1925, 0.2209, 0.2527, 0.2495, 0.2232, 0.1728, 0.1424, 0.1422 (Dec)]. Model skill was evaluated with respect to daily atmospheric transmittance rather than hourly solar radiation because of topographic shading at PRIMET. Finally, hourly solar radiation incident to level ground (R_s) was computed as R_s=$T_r R_a$.

The BC model calibrated for local conditions (method 3b) was the best method for predicting daily atmospheric transmittance T_r (Figures 2.9, 2.10) but efficiency was much lower than for air temperature or precipitation (Table 2.7). It was slightly more efficient than using [month,hour,precip] means to predict T_r. The BC model with parameter values from Bristow and Campbell (1984) (method 3a) had the lowest efficiency.

Humidity. Hourly PRIMET relative humidity prior to 7/8/88 was not available, so the calibration and verification periods were shortened to WY89-93 and WY94-98, respectively. The minimal method (4a) for estimating hourly H assumes that daily minimum air temperature is the same as dewpoint, $T_{min} = T_{dew}$, then uses

$$H = \frac{V_s(T_{dew})}{V_s(T)}, \tag{2.2}$$

where $V_s(T_{dew})$ equals saturation vapor pressure at T_{dew}, and $V_s(T)$ equals saturation vapor pressure at T. A slightly better approach (Running et al., 1987) uses a simple linear regression and is feasible if an independent measurement of T_{dew} is available (method 4b):

$$T_{dew} = a_0 + a_1 T_{min}. \tag{2.3}$$

For WY80-89, $a_0 = 1.95$ and $a_1 = 0.938$; both terms were significant (p-value< 0.0001; $R^2 = 0.88$).

Since daily H_{min} and H_{max} were available, hourly values could also be estimated as (methods 4c,d)

$$H = H_{max} + \frac{(T - T_{min})}{(T_{max} - T_{min})}(H_{min} - H_{max}). \tag{2.4}$$

For relative humidity, the only method with efficiency consistently greater than zero was the [month,hour,precip] means model (method 4e) (Table 2.8, Figures 2.11, 2.12). The next best predictor was Equation 2.4 with a two-hour shift (method 4d). Humidity actually had higher efficiency values during the verification period than during the calibration period.

Wind speed. Hourly met modeling was least successful for wind speed. The [month,hour,precip] means model (method 5b) was a better predictor than the mean daily wind speed (method 5a) during both periods (Table 2.8). However, there was significant positive bias in the WY90-98 verification run of method 5b for most months, especially around mid-day (Figures 2.13, 2.14). The +29% bias in predicted wind speed for WY90-98 may have been caused in part by a reduction in the measurement height, which occurred close to the end of the calibration period. On 1/1/1989 the measurement height was reduced from 12 m to 10 m.

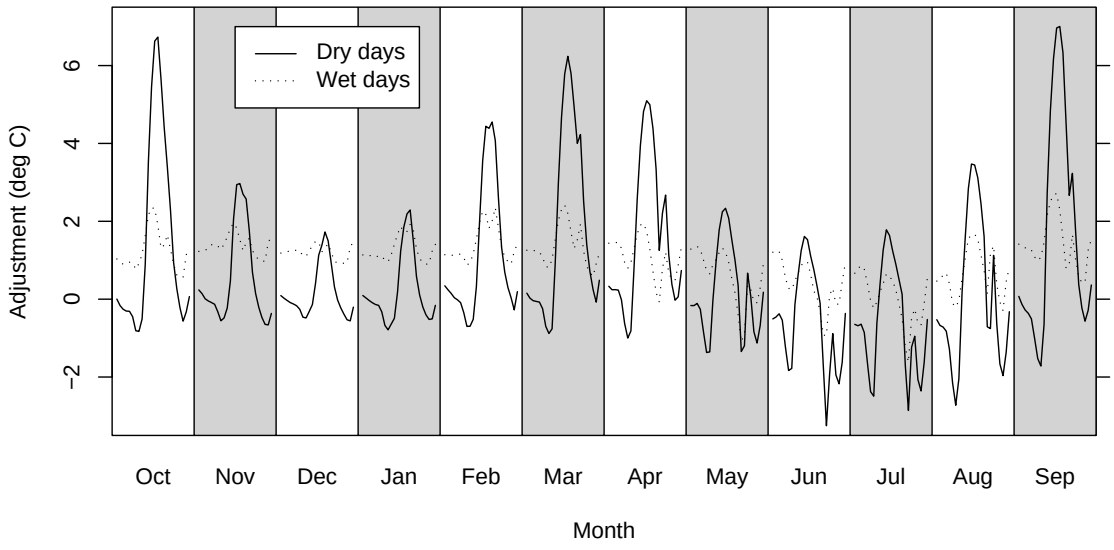

Figure 2.2: Bias corrections for CS2MET air temperature. The correction corresponding to a particular [month,hour,precip] combination was applied after generating hourly values using the modified sine curve method and a two-hour shift. The corrected timeseries represented the unbiased estimate of PRIMET air temperature from CS2MET daily data.

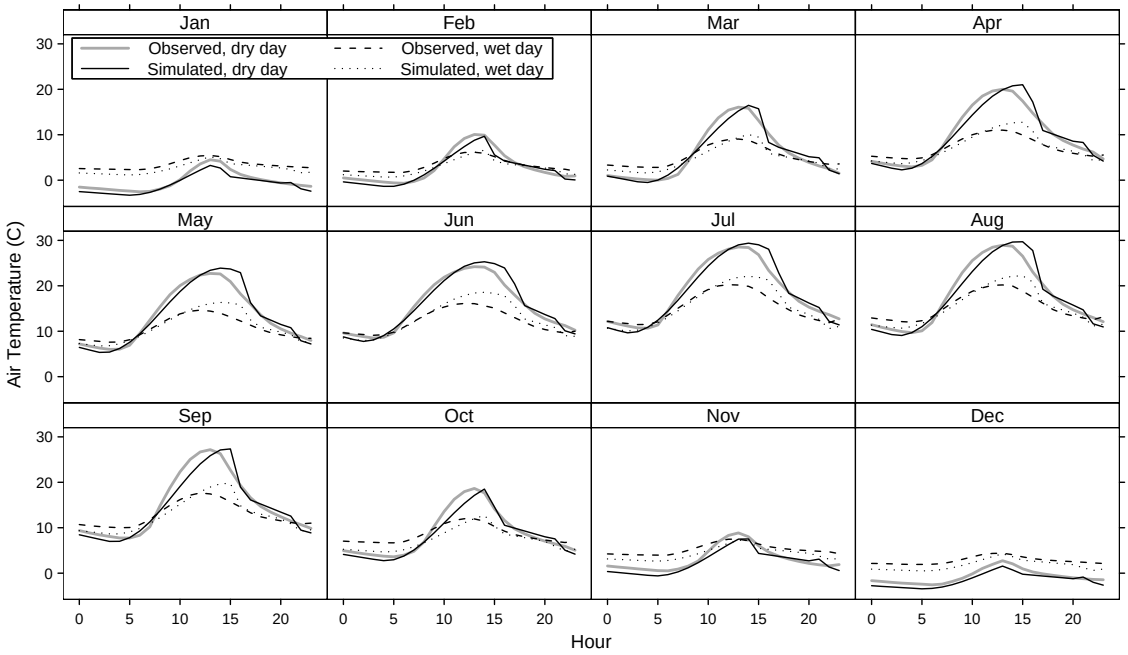

Figure 2.3: Mean hourly temperature by month, verification period (WY90-98). Simulated values from PRIMET daily data, sine curve, and 2-hour shift (method 1b, Table 2.2).

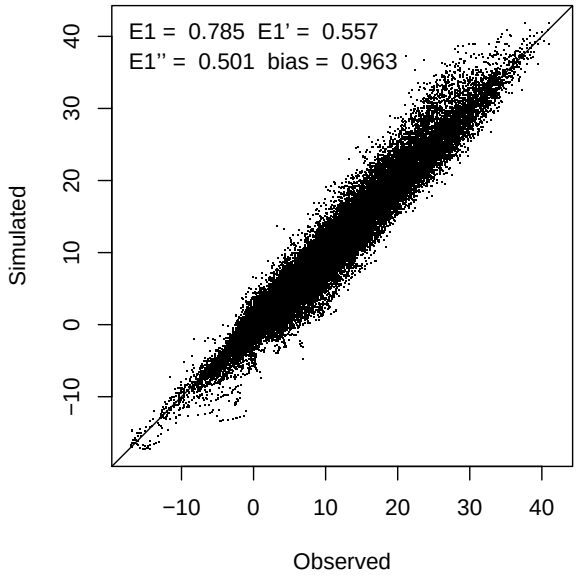

Figure 2.4: Hourly temperature 1:1 plot, verification period (WY90-98). Simulated values from PRIMET daily data, sine curve, and 2-hour shift (method 1b, Table 2.2).

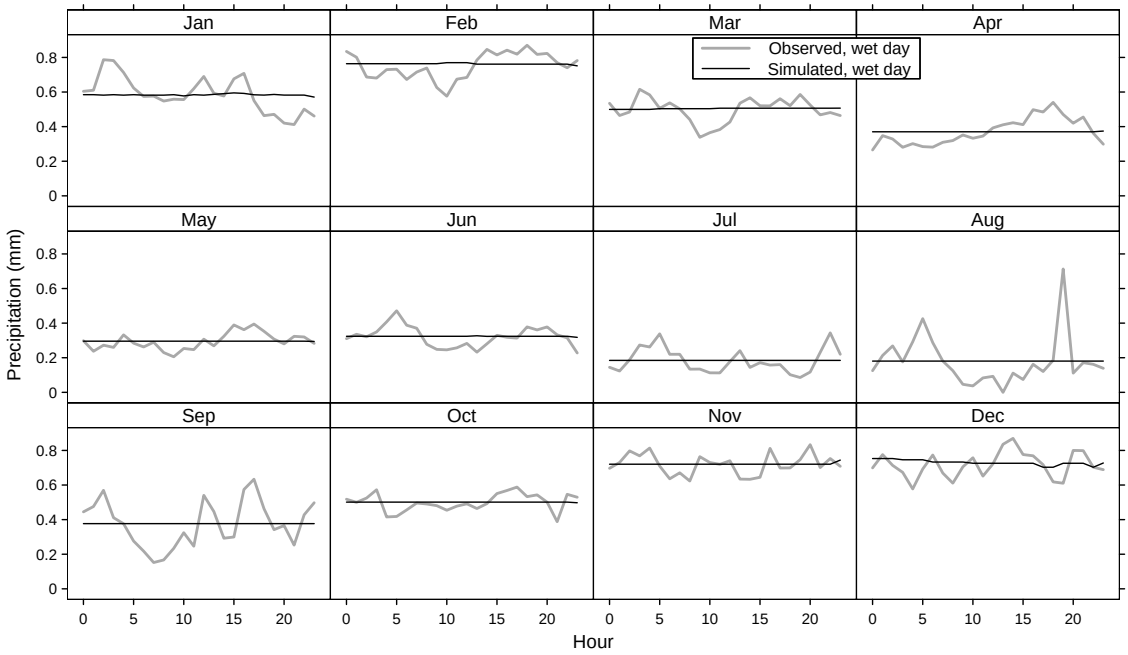

Figure 2.5: Mean hourly precipitation on wet days, by month, verification period (WY90-98). Simulated values $= P_d/24$ (method 2, Table 2.2).

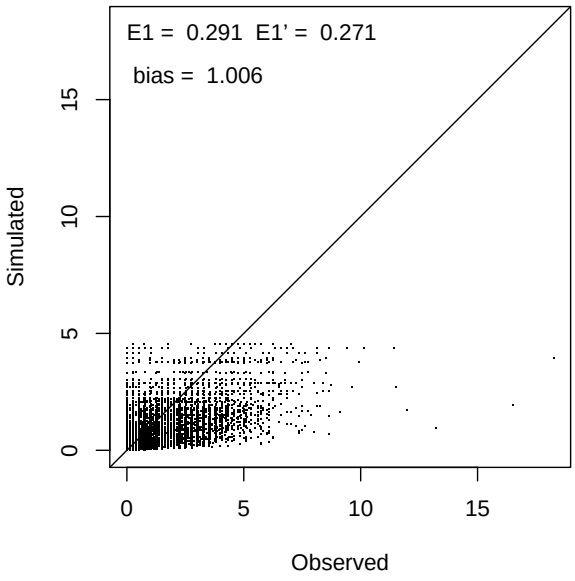

Figure 2.6: Hourly precipitation on wet days, 1:1 plot, verification period (WY90-98). Simulated values $= P_d/24$ (method 2, Table 2.2).

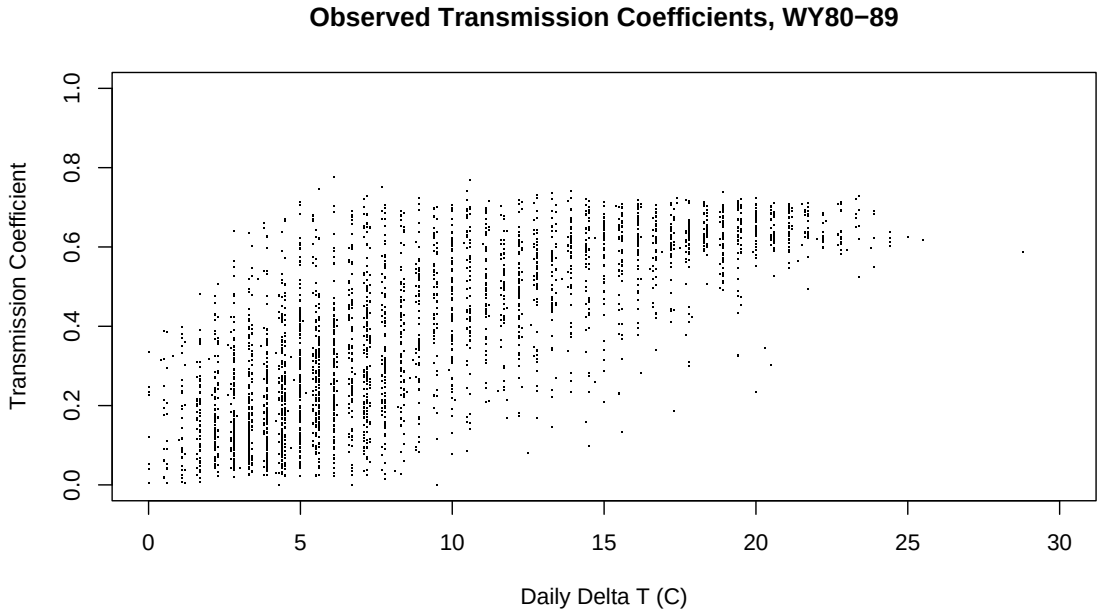

Figure 2.7: Observed daily atmospheric transmittance coefficients vs. ΔT, calibration period (WY80-98).

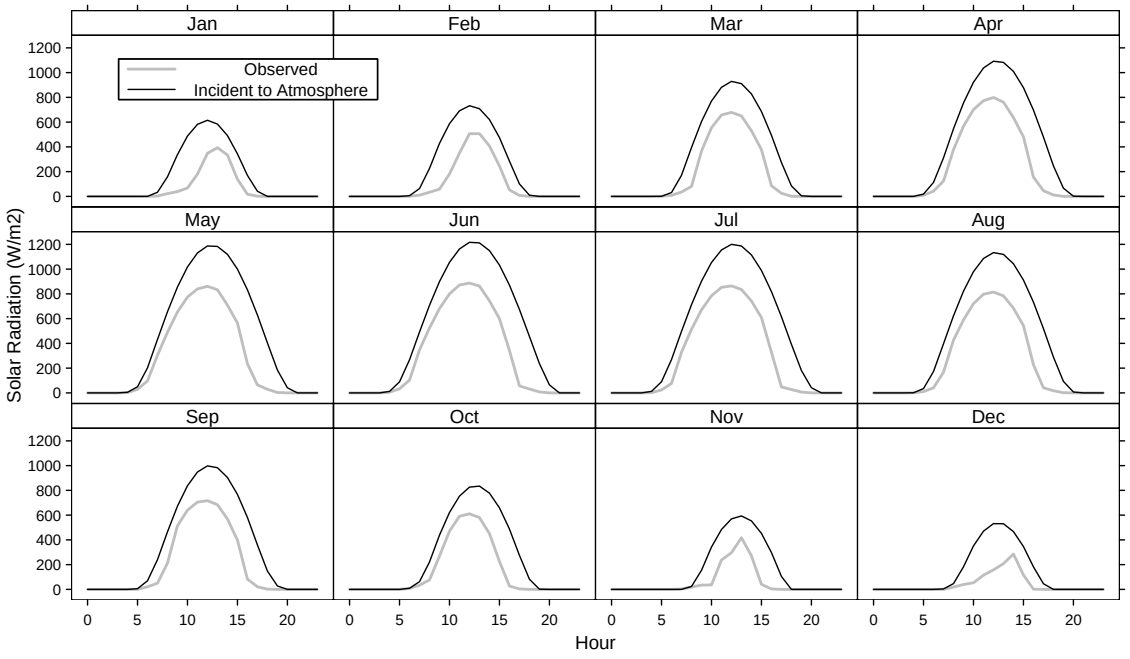

Figure 2.8: Mean hourly radiation by month, observed PRIMET WY80-89, and radiation incident to atmosphere (R_a), based on days where mean observed radiation during hours 1300-1500 was within 50% of R_a.

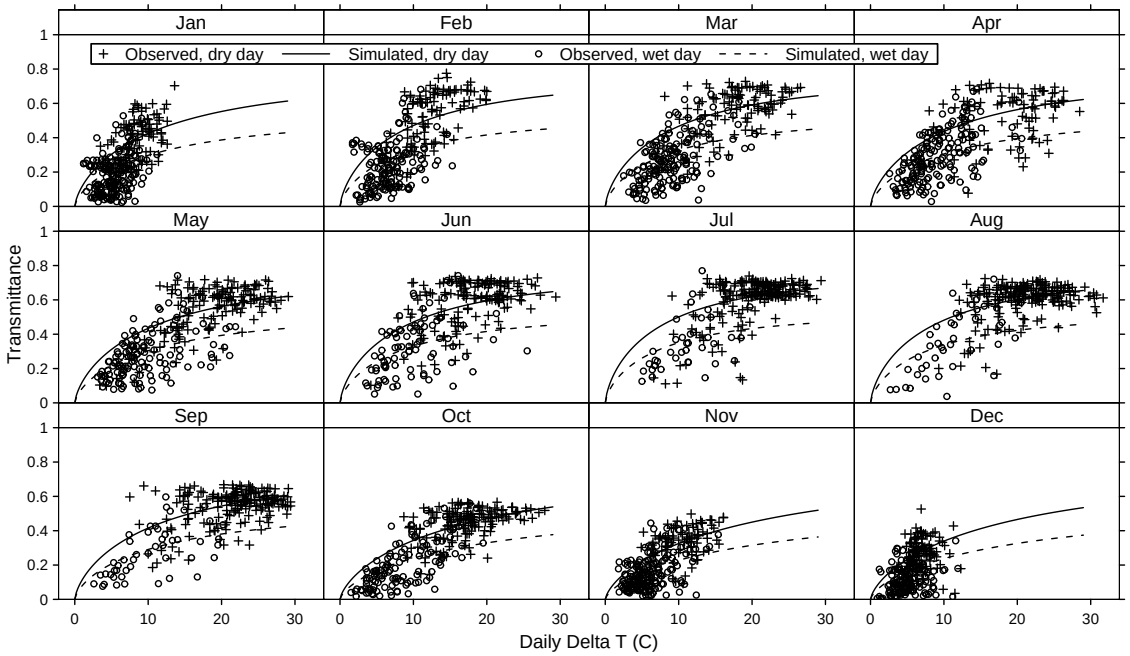

Figure 2.9: Daily atmospheric transmittance by month, verification period (WY90-98). Simulated values using Bristow-Campbell coefficients tuned for HJA (method 3b, Table 2.2).

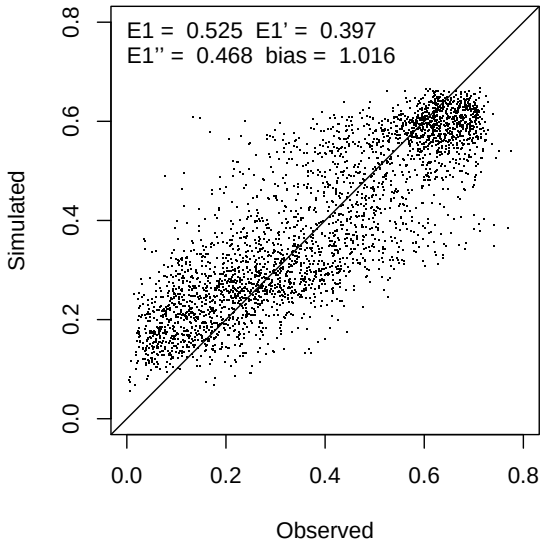

Figure 2.10: Daily atmospheric transmittance 1:1 plot, verification period (WY90-98). Simulated values using Bristow-Campbell coefficients tuned for HJA (method 3b, Table 2.2).

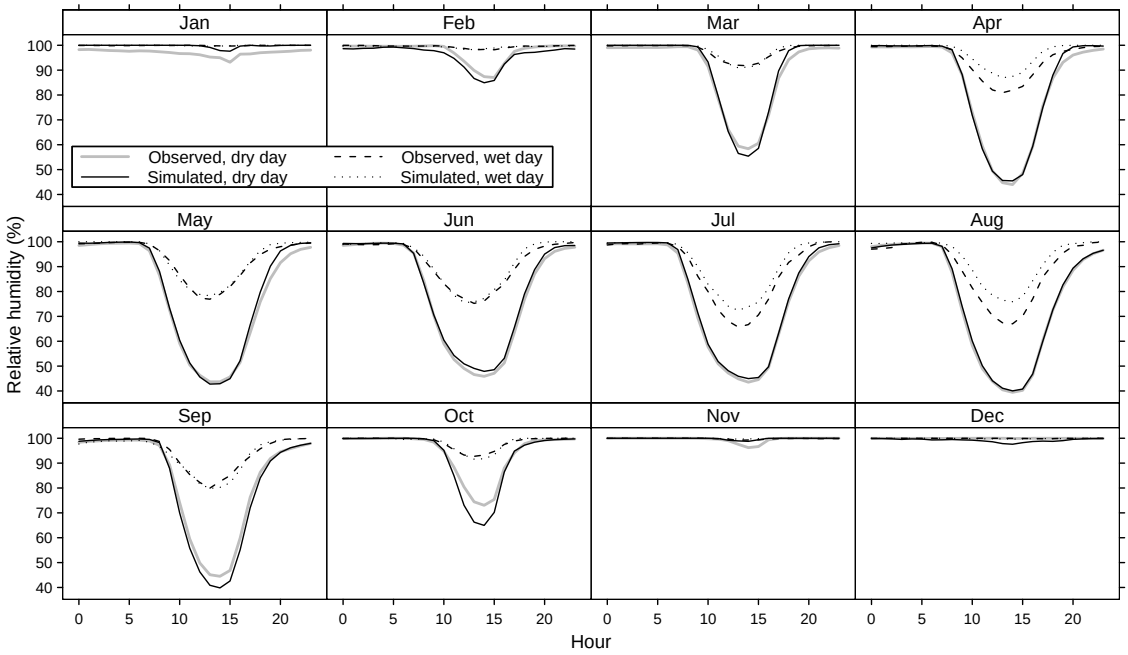

Figure 2.11: Mean hourly relative humidity by month, verification period (WY94-98). Simulated values using [month,hour,precip] means from calibration period (method 4e, Table 2.2).

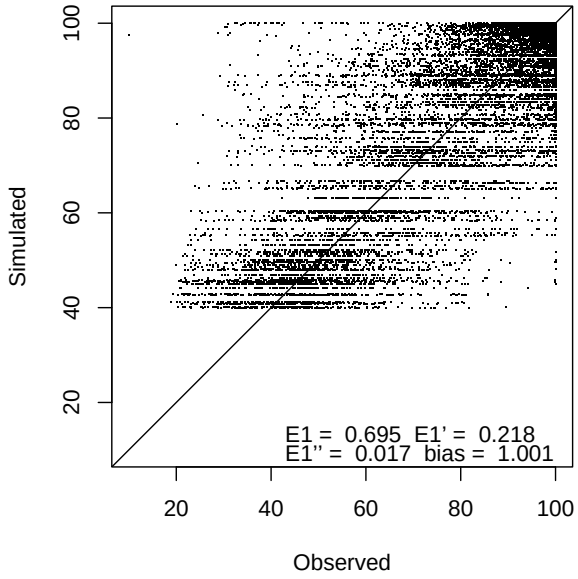

Figure 2.12: Hourly relative humidity 1:1 plot, verification period (WY94-98). Simulated values using [month,hour,precip] means from calibration period (method 4e, Table 2.2).

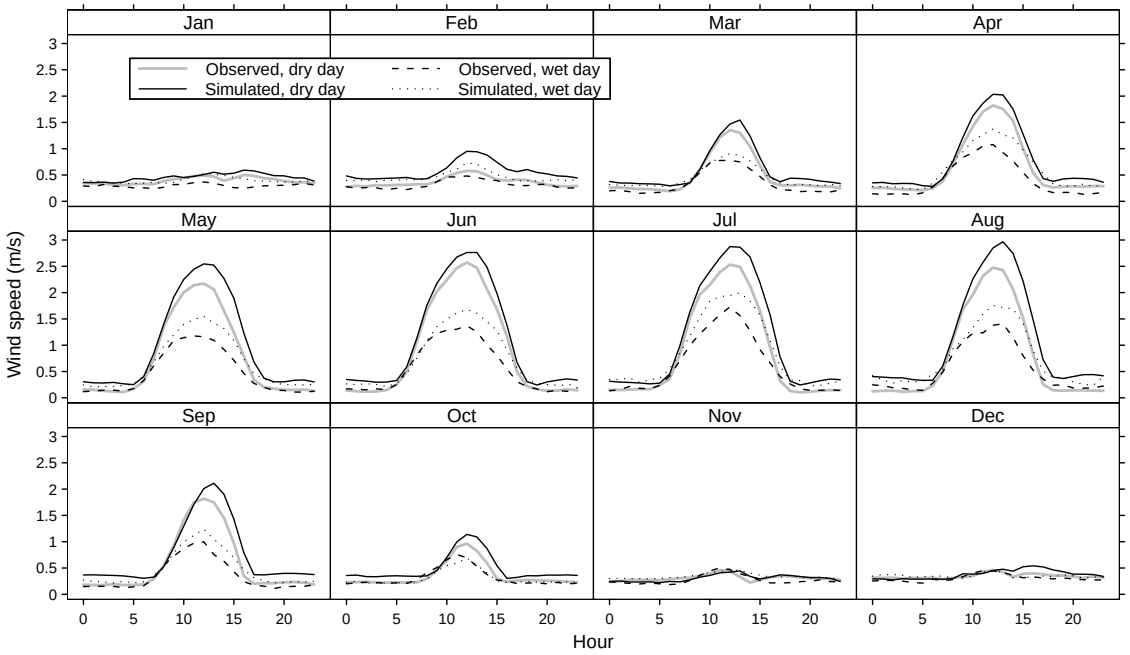

Figure 2.13: Mean hourly wind speed by month, verification period (WY90-98). Simulated values are [month,hour,precip] means from calibration (method 5b, Table 2.2).

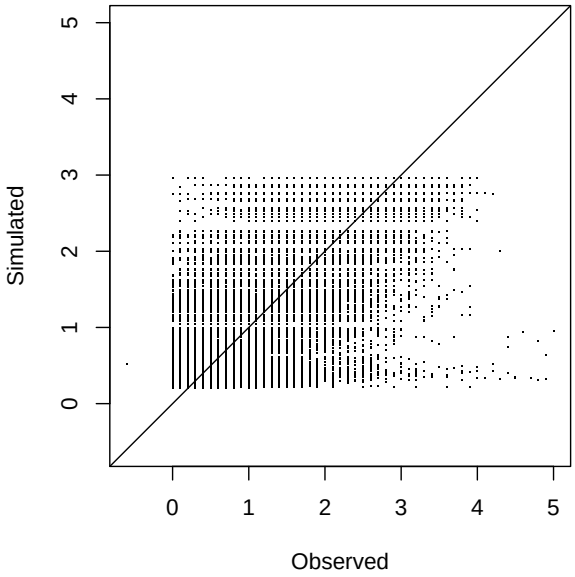

Figure 2.14: Hourly wind speed 1:1 plot, verification period (WY90-98). Simulated values are [month,hour,precip] means from calibration (method 5b, Table 2.2).

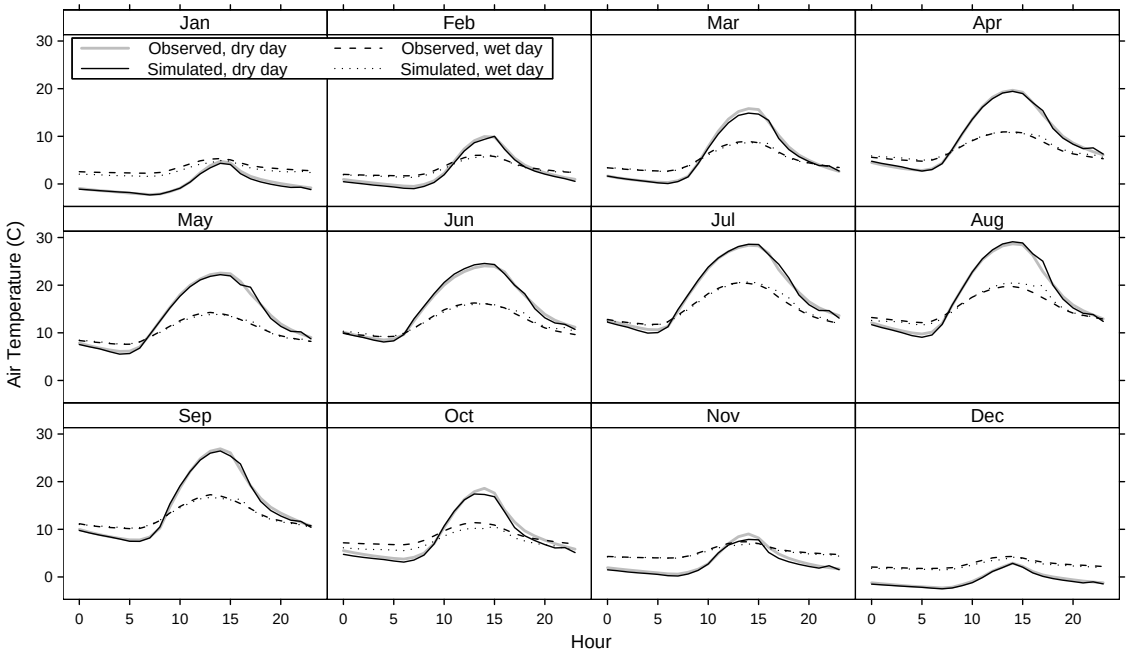

Figure 2.15: Mean hourly temperature by month, CS2MET to PRIMET, verification period (WY90-98). Simulated values from CS2MET daily data, using method 1b and bias correction (Table 2.2).

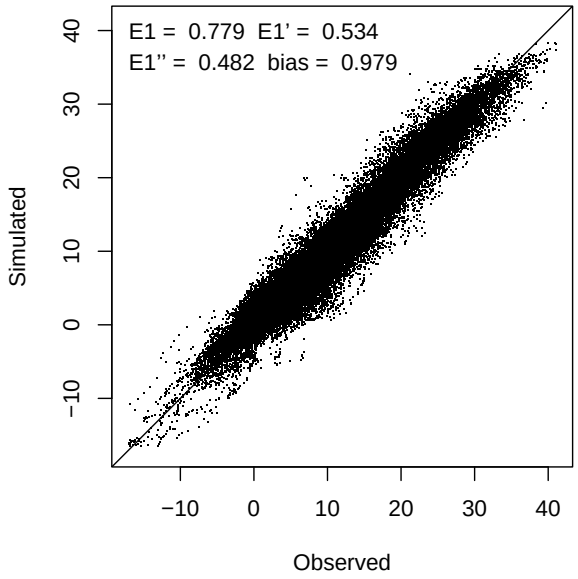

Figure 2.16: Hourly temperature 1:1 plot, verification period (WY90-98). Simulated values from CS2MET daily data, using method 1b and bias correction (Table 2.2).

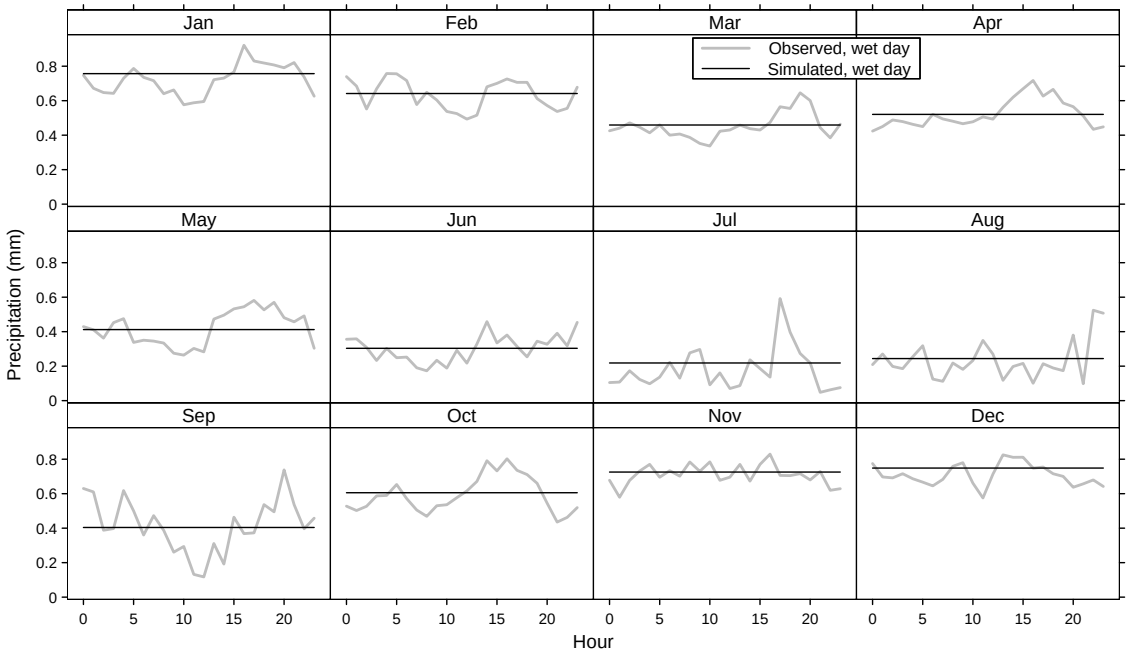

Figure 2.17: Mean hourly precipitation on wet days, by month, verification period (WY90-98). Simulated values from CS2MET daily data, method 2 and bias correction (Table 2.2).

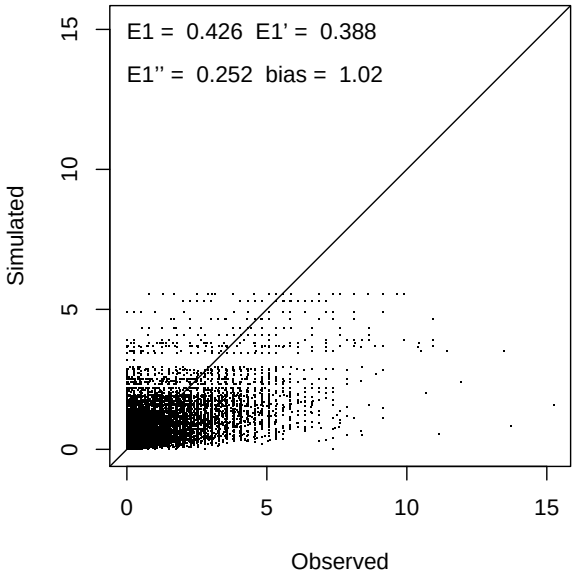

Figure 2.18: Hourly precipitation on wet days, 1:1 plot, verification period (WY90-98). Simulated values from CS2MET daily data, method 2 and bias correction. (Table 2.2)

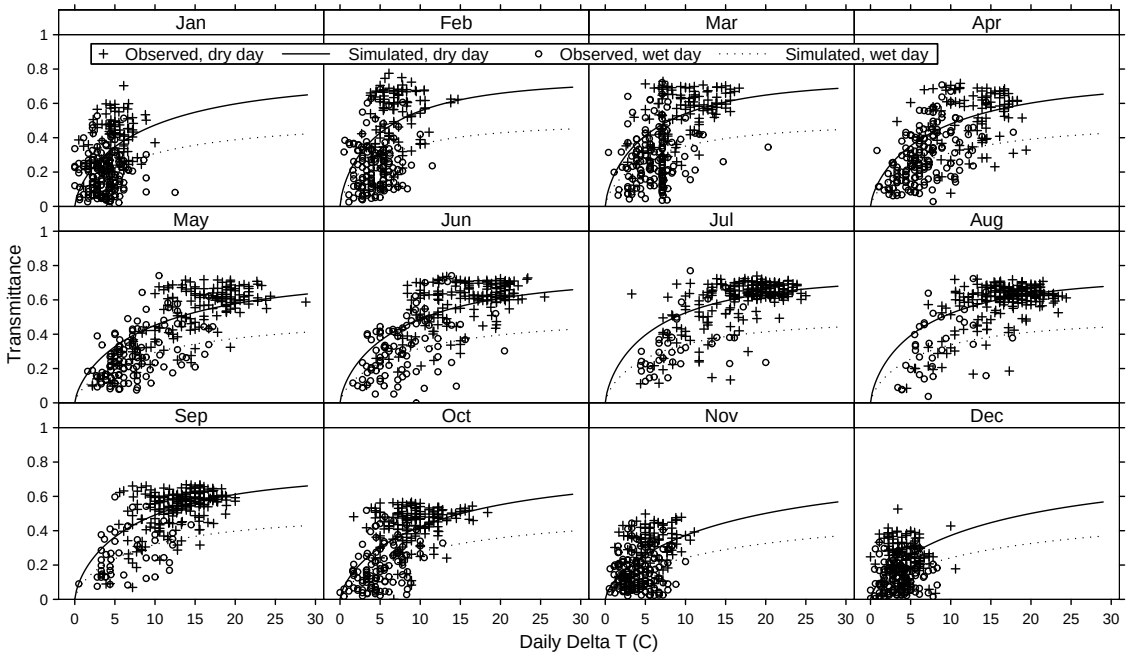

Figure 2.19: Daily atmospheric transmittance by month, verification period (WY90-98). Simulated values computed with CS2MET daily data and method 3b (Table 2.2).

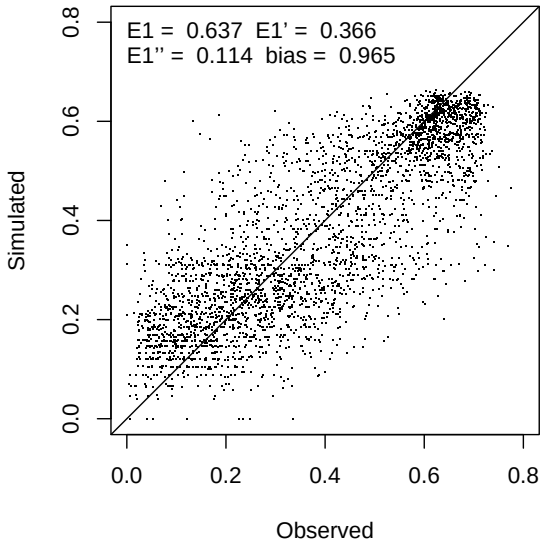

Figure 2.20: Daily atmospheric transmittance 1:1 plot, verification period (WY90-98). Simulated values computed with CS2MET daily data and method 3b, Table 2.2).

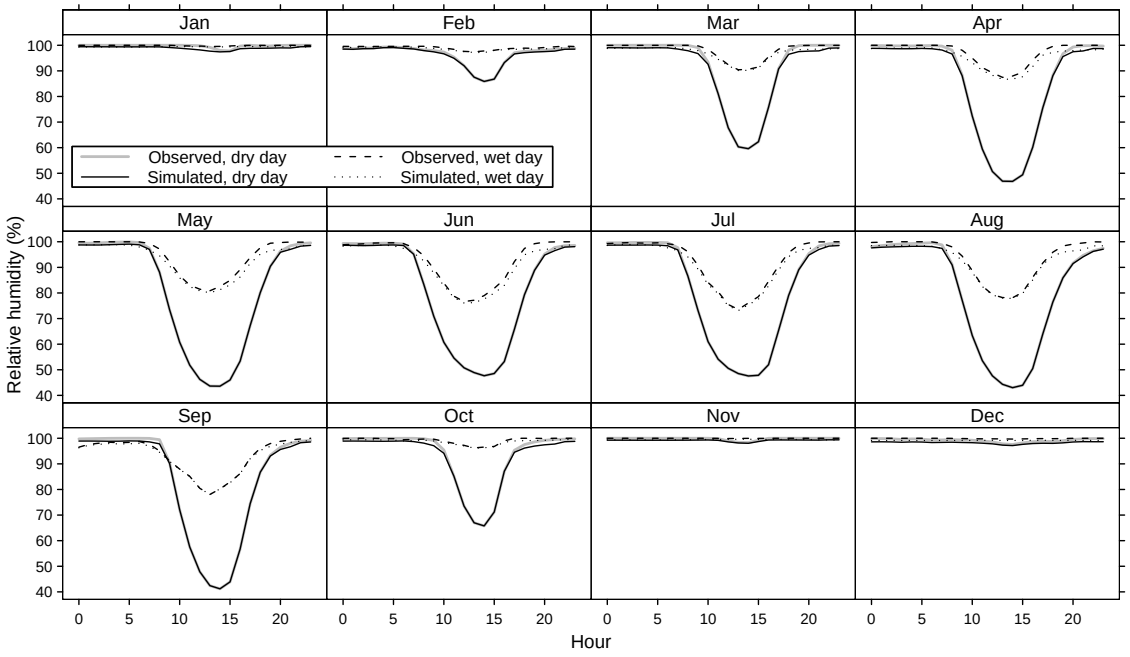

Figure 2.21: Mean hourly relative humidity by month, verification period (WY94-98). Simulated values using CS2MET daily data and method 4d (Table 2.2).

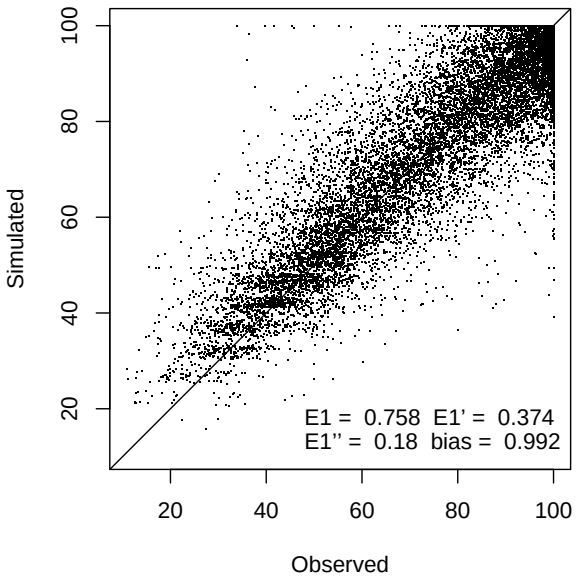

Figure 2.22: Hourly relative humidity 1:1 plot, verification period (WY94-98). Simulated values using CS2MET daily data and method 4d (Table 2.2).

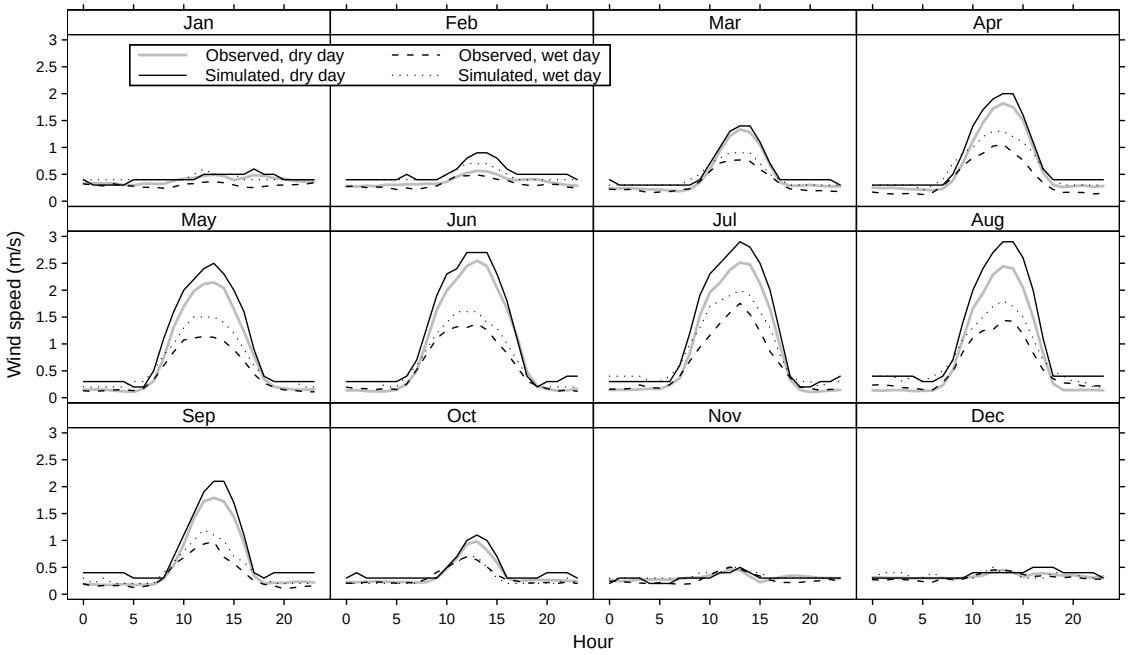

Figure 2.23: Mean hourly wind speed by month, verification period (WY90-98). Simulated values using method 5b and CS2MET daily precipitation status.

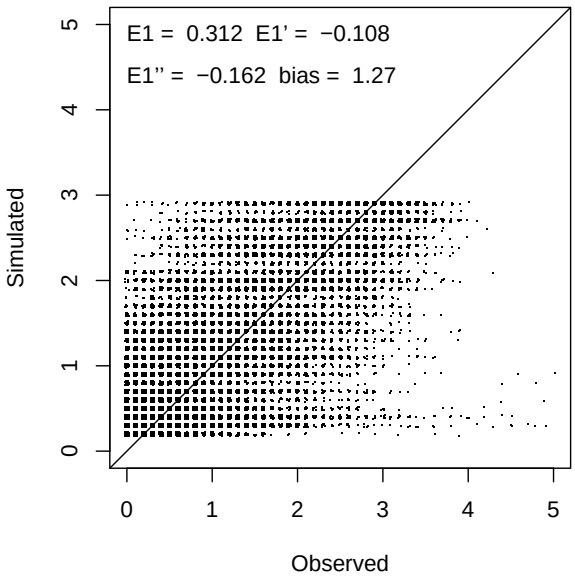

Figure 2.24: Hourly wind speed 1:1 plot, verification period (WY90-98). Simulated values using method 5b and CS2MET daily precipitation status. Points are jittered to reduce overlap.

Table 2.2: Daily to hourly disaggregation and estimation methods for meteorological variables. If calibration equals yes, prior inspection or calculation using some hourly data is involved.

#	Parameter	Description	Calibration
1a	Air temperature	Modified sine curve	no
1b	Air temperature	Modified sine curve and 2-hour shift	yes
1c	Air temperature	[month,hour,precip] means	yes
2	Precipitation	1/24th daily total	no
3a	Atmospheric transmittance	BC model with Pacific Northwest parameters from Bristow and Campbell (1984)	no
3b	Atmospheric transmittance	Bristow-Campbell model with HJA parameters	yes
3c	Atmospheric transmittance	[month,precip] means	yes
4a	Relative humidity	$T_{dew} = T_{min}$	no
4b	Relative humidity	$T_{dew} = aT_{min} + b$	yes
4c	Relative humidity	H_{min}, H_{max}, Equation 2.4	no
4d	Relative humidity	H_{min}, H_{max}, Equation 2.4, and 2-hour shift	yes
4e	Relative humidity	[month,hour,precip] means	yes
5a	Wind speed	daily mean	no
5b	Wind speed	[month,hour,precip] means	yes

Table 2.3: Meteorology inputs to DHSVM.

Input[a]	**Description**
P1. Observed	PRIMET hourly data
P2. Full simulated	From PRIMET daily data, using all available variables and methods to get best match for each hourly input variable (methods 1b, 2, 3b, 4e, 5b)
P3. Minimum simulated	From PRIMET daily data and PRIMET wind, using only T_{min}, T_{max}, P_d, and wind=0.65 m/s (methods 1a, 2, 3a, 4a)
P4. Uniform precipitation	PRIMET hourly data except precip = PRIMET daily total / 24 (method 2)
C1. Full simulated	From CS2MET daily data, using all available variables and methods to get best possible match to PRIMET data for each hourly input variable (methods 1b, 2, 3b, 4e, 5b)
C2. Basic air temperature	Sine curve used, but not shift or bias corrections (method 1a)
C3. Dewpoint humidity	Based on dewpoint = T_{min} (method 4a)
C4. Enhanced dewpoint humidity	Based on enhanced dewpoint model, $T_{dew} = aT_{min} + b$ (method 4b)
C5. Sine humidity	Sine curve used, but not shift or bias corrections (method 4c)
C6. Wind = 0.65	Constant wind speed = 0.65 m/s (grand mean)
C7. General solar	Bristow and Campbell (1984) model with their parameters based on Pullman, Seattle, and Great Falls ($A = 0.70$, $C = 2.4$, and $B = 0.036e^{-0.154\overline{\Delta T}}$, where $\overline{\Delta T}$ = mean monthly temperature difference) (method 3a)
C8. Baseline solar	[month,hour,precip] means from calibration period (method 3c)
C9. Basic precip	No bias correction

[a] C2-C9 are identical to C1 except for the variable noted

Table 2.4: Missing and questionable data in PRIMET hourly record, WY80-98.

Variable	Quantity (%)	Replacement method
Air temperature	0.5	[month,hour] mean from WY80-98
Wind speed	2.9	”
Solar radiation[a]	1.1	[month,hour] mean from 1/1/80 - 9/30/98
Relative humidity before 7/7/88	100	Computed from CS2MET H_{max}, and T_{min} or PRIMET $T_{midnight}$
Relative humidity after 7/6/88	0.6	[month,hour] mean from 7/7/88 - 9/30/98
Precipitation	3.6	$\frac{1}{24}\times$ daily PRIMET precip
Precipitation	4.3	$\frac{1}{24}\times$ daily CS2MET precip

[a] converted from langleys/hr to W/m^2

Table 2.5: Missing and questionable data in CS2MET daily record, WY80-98.

Variable	Quantity (%)	Replacement method
Minimum air temperature	1.9	[month] mean from WY58-98
Maximum air temperature	1.8	”
Minimum relative humidity	11.8	”
Maximum relative humidity	11.5	”
Precipitation	0	

Table 2.6: Missing and questionable data in CS2MET daily record, WY58-79.

Variable	Quantity (%)	Replacement method
Minimum air temperature	0.5	[month] mean from WY58-98
Maximum air temperature	0.4	”
Minimum relative humidity	5.0	”
Maximum relative humidity	4.8	”
Precipitation	0	

Table 2.7: Meteorological model skill for T, P, and T_r. Hourly variables except atmospheric transmittance, which is daily. See appendix for efficiency equations.

Model	Period	Bias[a]	E_1[b]	E_1'[c]	E_1''[d]
Air Temperature					
1a	WY80-89	0.951	0.616	0.206	0.094
1b	WY80-89	0.951	0.788	0.561	0.5
1c	WY80-89	1	0.576	0.123	0
1a	WY90-98	0.963	0.595	0.166	0.06
1b	WY90-98	0.963	0.785	0.557	0.501
1c	WY90-98	0.963	0.564	0.089	-0.025
Precipitation					
2	WY80-89	1.013	0.941	0.265	—
2	WY90-98	1.025	0.94	0.257	—
Atmospheric transmittance					
3a	WY80-89	1.4450	-0.096	-0.429	-0.879
3b	WY80-89	0.983	0.506	0.356	0.152
3c	WY80-89	1	0.423	0.247	0
3a	WY90-98	1.419	0.004	-0.266	-0.116
3b	WY90-98	1.016	0.525	0.397	0.468
3c	WY90-98	1.002	0.451	0.302	0.385

[a] ratio of simulated to observed mean

[b] efficiency relative to grand mean of observations

[c] efficiency relative to [month,hour] baseline mean, except [month] for atmospheric transmittance

[d] efficiency relative to [month,hour,precip] baseline mean, except [month,precip] for atmospheric transmittance

Table 2.8: Meteorological model skill for H and W. Hourly variables except atmospheric transmittance, which is daily. See appendix for efficiency equations.

Model	Period	Bias[a]	E_1[b]	E_1'[c]	E_1''[d]
Relative humidity					
4a	WY80-89	0.831	-0.183	-2.054	-2.981
4b	WY80-89	0.935	0.417	-0.506	-0.963
4c	WY80-89	0.941	0.435	-0.46	-0.903
4d	WY80-89	0.941	0.544	-0.176	-0.534
4e	WY80-89	1	0.703	0.233	0
4a	WY90-98	0.832	-0.284	-2.296	-3.141
4b	WY90-98	0.938	0.392	-0.559	-0.959
4c	WY90-98	0.946	0.356	-0.652	-1.076
4d	WY90-98	0.946	0.534	-0.195	-0.502
4e	WY90-98	1.001	0.695	0.218	0.017
Wind speed					
5a	WY80-89	0.98	0.179	-0.296	-0.353
5b	WY80-89	1	0.393	0.042	0
5a	WY90-98	1.002	0.139	-0.379	-0.451
5b	WY90-98	1.288	0.295	-0.13	-0.189

[a] ratio of simulated to observed mean

[b] efficiency relative to grand mean of observations

[c] efficiency relative to [month,hour] baseline mean, except [month] for atmospheric transmittance

[d] efficiency relative to [month,hour,precip] baseline mean, except [month,precip] for atmospheric transmittance

2.2.2 Impact of Meteorologic Modeling on Hydrologic Modeling

Methods. To evaluate the hydrologic significance of the met assumptions, we applied DHSVM with thirteen sets of met input (Table 2.3). Model skill in simulating hourly streamflow, and predicted major fluxes of the water balance were compared across met inputs. Simulation using the met input with observed hourly data (P1) was compared to simulations using derived hourly values, either the full set of techniques for best fit (P2), or the minimal set of techniques (P3). Met input P3 was generated using just T_{min}, T_{max}, P_d, and the grand mean wind speed, and represents a typical hourly met input that would be generated with limited data under typical circumstances in many watershed applications. Met input P4 was identical P1 except for precipitation, which was the observed daily total distributed uniformly over 24 hours. We also compared met inputs based on CS2MET daily data because we needed the longer record at CS2MET for met input before WY80. The set of best techniques and baseline bias corrections were used to develop met input C1. Inputs C2-C9 are variants of C1, where one of the variables was predicted with a simpler technique, as described in Table 2.3.

Hourly met values were representative of the PRIMET location at 430 m elevation. Spatial distribution of the PRIMET point values to all grid cells in WS2 was required to run DHSVM. Air temperature and solar radiation were the only variables involving significant modification from the point values. Air temperature was lapsed with a positive rate corresponding to a lower inversion zone below 700 m elevation, and an upper negative rate, using monthly breakpoint

elevations and lapse rates (Table 2.9, Rosentrater (1997)). Means and standard deviations for the lower and upper lapse rates were (2.7, 1.3 C/km) and (-5.2, 1.1 C/km), respectively. Solar radiation was distributed by taking into account local slope and aspect (but not topographic shading) for the direct beam component. Precipitation in the real WS2 probably has a positive lapse rate with elevation, but it was not lapsed in the model because of water balance difficulties discussed in Section 2.4. Relative humidity and incoming longwave radiation were distributed without modification, a reasonable assumption for this small watershed. The PRIMET wind speed was distributed without modification except to enforce a minimum of 0.01 m/s to avoid divide-by-zero when computing aerodynamic resistance. For simplicity, a single lapse rate was used for calculation of air pressure in DHSVM.

Results. The derived met input for PRIMET using the set of best techniques (P2) resulted in slightly lower efficiency and more error in mean annual streamflow compared to using the observed data for met input (P1) (Figure 2.25). The most important difference between the two simulations was the air temperature input, which was slightly colder on average with the derived input P2 and caused more precipitation to fall as snow. The different outcomes of P2 and P3, where P3 had the met input derived with the minimal set of techniques, are best understood after considering the single-variable differences in C2-C9 compared to C1, and P4 compared to P1.

Met inputs C2-C9 were identical to C1 except for one variable. In C2, a lack of shift and bias corrections for air temperature caused temperature to be colder on average than C1, greatly increasing the amount of snowfall, and lowering evapotranspiration slightly in C2. In C3, the $T_{dew}=T_{min}$ assumption for generating hourly humidity resulted in significantly higher ET and lower streamflow. In the real system, the dewpoint is often reached before the minimum air temperature, and therefore the atmosphere is often saturated and ET is reduced over a portion of the day. In C4, the enhanced dewpoint model (method 4b) resulted in a smaller but still noticeable ET increase. In C5, a similar result was obtained when a sine curve without shift and bias corrections was used for humidity (method 4c). In C6, using the grand mean to set a constant wind speed of 0.65 m/s resulted in a slight decrease in ET and increase in streamflow. In C7, the large positive bias in atmospheric transmittance stemming from use of the literature parameter values in the BC model (method 3a) caused R_s and ET to increase. In C8, using the baseline means model for T_r had little effect on the hydrology. In C9, the lack of the -4.4% bias correction for precipitation resulted in a positive streamflow error of 10% and reduced efficiency, confirming the sensitivity of streamflow to this primary term in the water balance.

Hydrology results from the minimal met input P3 were much different from results with the observed met input P1. The annual streamflow error was -20% with P3, caused by much higher evapotranspiration (ET). The main reason for the much higher ET in the P3 run was the $T_{dew}=T_{min}$ assumption for generating humidity. The large positive bias in atmospheric transmittance associated with method 3a also contributed to the large ET in P3, as did the higher temperatures with method 1a. Between P2 and C1, the two met inputs derived the set of best-fit techniques, C1 had higher efficiency because the use of bias corrections in C1 caused air temperature to more closely match the data than in P2. Making precipitation uniform over the day caused efficiency of predicted streamflow in P4 to decrease slightly compared to P1. Evapotranspiration was slightly increased in P4 due to greater interception of precipitation, but much less so than in P3, with the result that mean annual streamflow error was much lower in P4 than P3.

Change in hydrology model skill was evaluated for several subperiods within WY80-98 (Table 2.10). As expected, skill was higher during the calibration period than the verification period. DHSVM was calibrated using periods with a range of dry to wet years, and bias is opposite in sign for dry and wet periods for most met inputs. Bias was superior during the relatively dry period of WY90-92. Efficiency was higher during the relatively wet period of WY95-97. Worst affected during the dry period was E_1', which is more sensitive to model fit at low flows than E.

As a final exploration of the hydrologic consequence of the various met assumptions, the observed and simulated streamflows were processed with the USGS statistical model for flood frequency, using a log-Pearson Type III distribution for annual maximum flows (USGS, 1982). Point estimates and 95 percent confidence intervals (CI) for flows corresponding to recurrence intervals 1.1, 2, 5, 10, and 20 years were computed. A regional skew coefficient of 0.12 was used to compute a weighted skew coefficient. There were no outliers, and the rest of the computations followed the USGS methods. The CIs for all simulated streamflows (P1-C9) were compared to the CI for the observed streamflow, and in all cases there was overlap, indicating no significant difference between the flood streamflows predicted by the statistical model (Figure 2.26). However, the point estimate from the observations was markedly higher than the simulations at recurrence intervals above 2 years. These two results indicate that the met inputs were equally satisfactory for applying the USGS method, but overall the simulations lost value compared to the data as the recurrence interval and flood magnitude increased.

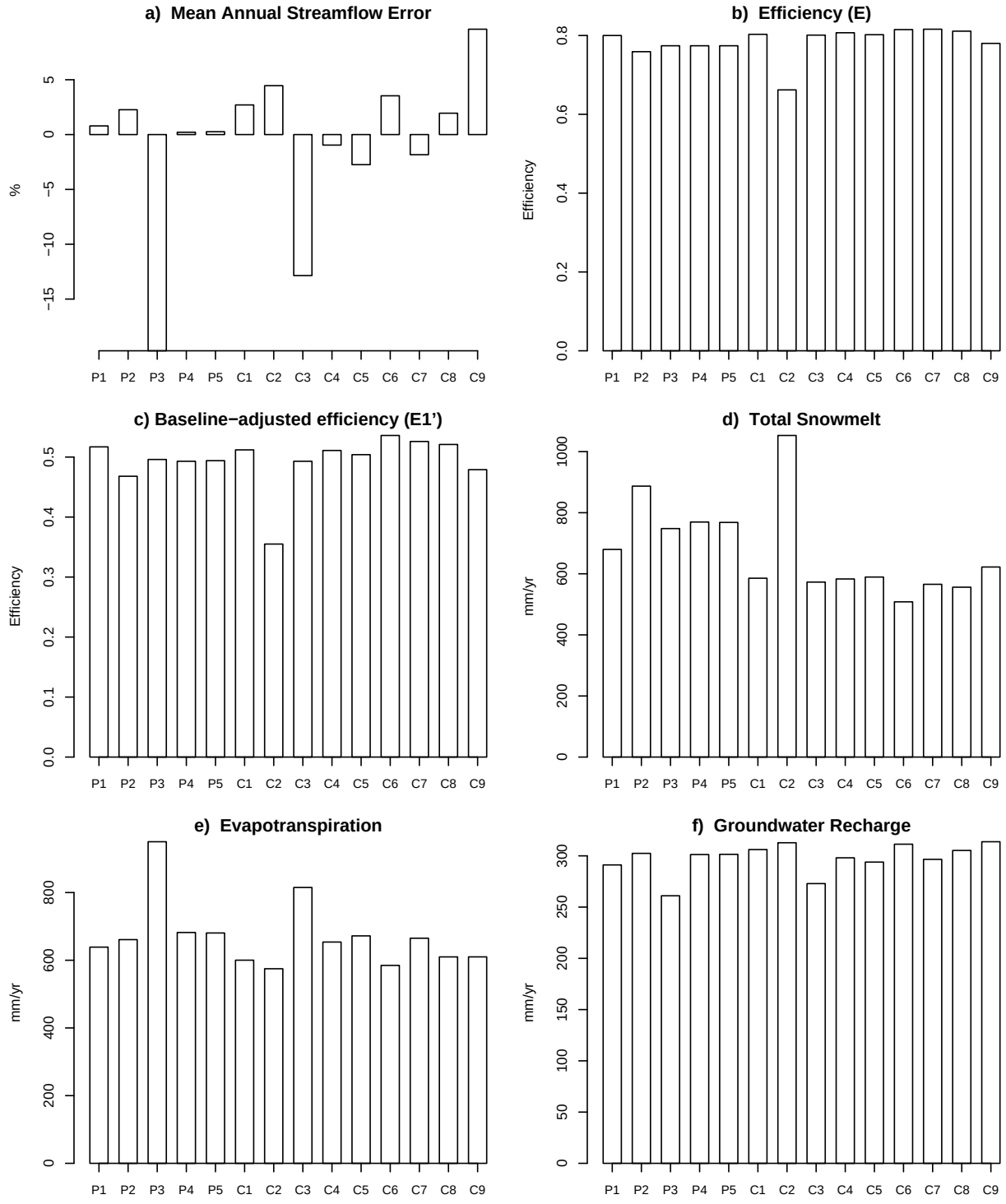

Figure 2.25: Comparison of WS2 hydrologic results across alternative meteorology inputs. Period is WY80-98. Total snowmelt varied among model runs with identical temperature and precipitation inputs because sublimation varied.

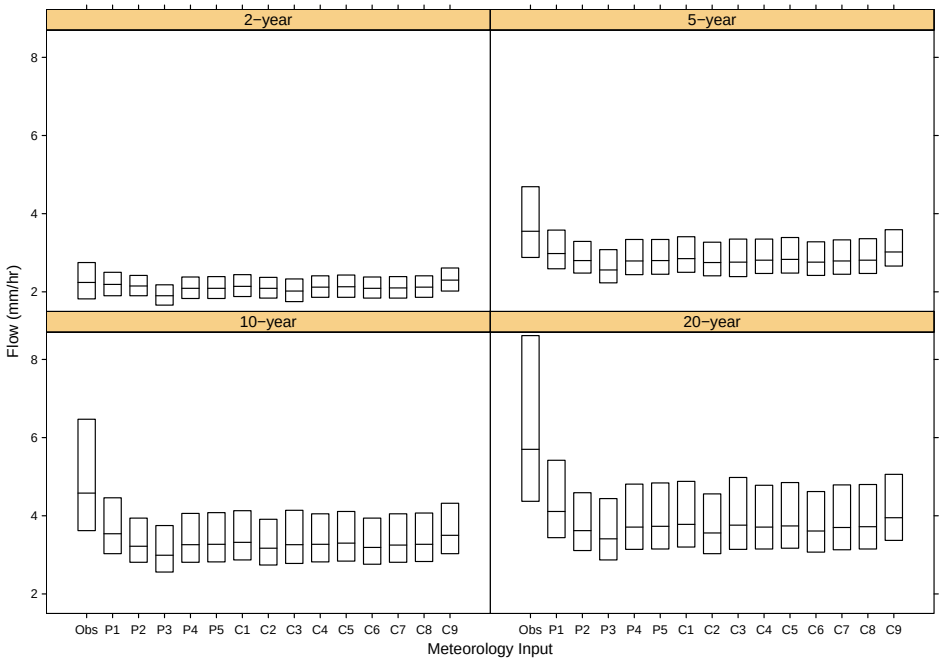

Figure 2.26: Flood magnitudes, from applying the log-Pearson Type III model (USGS, 1982) to WS2 hourly streamflows simulated with alternative meteorology inputs. Middle line is point estimate for flood flow; top and bottom lines denote 95% confidence interval. "Obs" is observed streamflow dataset.

Table 2.9: Monthly lapse rates for air temperature and precipitation.

Month	Lower air temp lapse rate (deg C/km)[a]	Breakpoint elevation (m)[a]	Upper air temp lapse rate (deg C/km)[a]	Single air temp lapse rate (deg C/km)[b]	Precipitation (mm/100m)[c]
Oct	3.7	700	-3.8	-2.65	4.2
Nov	2.0	700	-5.2	-4.20	11.2
Dec	2.3	700	-3.2	-2.65	9.9
Jan	3.9	700	-4.0	-2.54	8.9
Feb	3.2	700	-5.4	-3.61	8.5
Mar	1.3	700	-5.4	-4.97	7.7
Apr	1.5	650	-6.5	-6.10	4.4
May	2.4	650	-7.0	-6.34	3.2
Jun	1.5	650	-5.9	-5.30	2.6
Jul	2.8	700	-5.8	-4.82	0.8
Aug	2.1	700	-5.2	-4.02	0.7
Sep	5.9	700	-5.1	-3.18	2.6

[a]From Rosentrater (1997), Table 4.
[b]From Rosentrater (1997), Table 3.
[c]Computed from PRISM maps, Forest Science Data Bank, Oregon State University.

Table 2.10: Change (%) in WS2 streamflow modeling skill from entire period (WY80-98) to sub-periods.

Stat.[a]	Period[b]	P1	P2	P3	P4	C1	C2	C3	C4	C5	C6	C7	C8	C9
bias	Calibration	-3	3	5	-4	0	0	0	0	0	0	1	0	0
bias	Verification	3	-4	-6	4	0	0	0	0	0	0	-1	0	0
bias	Dry	13	1	-5	10	1	2	-1	2	-3	1	-1	1	1
bias	Wet	0	-6	-4	1	-1	-2	2	-1	1	-1	-1	-1	-2
E	Calibration	2	1	6	3	3	7	3	3	3	3	3	3	3
E	Verification	-1	-1	-5	-3	-3	-7	-3	-3	-3	-2	-3	-2	-3
E	Dry	-9	-1	-1	-2	-9	-11	-7	-8	-5	-10	-8	-10	-13
E	Wet	3	0	-7	-1	0	-2	-1	0	0	-1	0	0	3
E_1'	Calibration	-2	-7	3	-1	2	6	1	1	3	0	1	0	1
E_1'	Verification	1	7	-4	0	-2	-8	-2	-2	-3	0	-1	-1	-3
E_1'	Dry	-16	-5	-9	-9	-17	-12	-15	-14	-13	-18	-16	-18	-20
E_1'	Wet	9	11	-5	6	6	-9	6	7	4	5	7	6	8

[a]Bias is the ratio of mean simulated to mean observed streamflow. E=efficiency; E_1'=first-degree efficiency based on [month,hour] means.

[b]Periods refer to meteorology input. Cal (Calibration)=WY80-89, Ver (Verification)=WY90-98, Dry=WY90-92, Wet=WY95-97.

2.2.3 Discussion of Meteorological Modeling

The motivation for the met modeling was to extend the hourly record back in time to WY58 and thus encompass most of the HJA paired watershed study period. The availability of an hourly dataset starting in WY80 made it possible to do this with methods tuned to local conditions. It also provided an opportunity to evaluate common assumptions for generating subdaily met values from limited daily data, and to evaluate the consequences of those assumptions on hydrologic modeling.

The usefulness of the modified sine curve method for predicting air temperature was confirmed by this study. The beneficial effect of the two-hour phase shift for the air temperature and relative humidity timeseries was somewhat surprising, however. The shift probably accounts for a sunset time that is earlier than predicted by the solar model because of the valley-bottom setting of PRIMET. However, local sunrise time is later, so warming of the local air mass should be delayed in the morning. Perhaps atmospheric turbulence plays a role in the timing of diurnal temperature change. The bias corrections used to complete the synthesis of PRIMET air temperature from CS2MET daily T_{min} and T_{max} were substantial and significantly affected precipitation phase in DHSVM. Without the mostly positive corrections, much more snowfall was predicted.

The superior fit of the baseline means model for atmospheric transmittance as compared to the BC model with literature parameter values was also unexpected. This indicates that using the data directly rather than running the uncalibrated BC model may be more productive in locations where some solar radiation data exists. For relative humidity, the baseline means model had the best fit of five tested models, including two models that used daily H_{min} and H_{max}.

DHSVM was calibrated with met input P1, so it was anticipated that the corresponding model

skill would be among the highest. The least model skill resulted with input C2, which had air temperature generated with the basic method and no shift or bias corrections. This highlights the sensitivity of snowfall, and wintertime streamflow, to precipitation phase in this rain-snow transition zone.

Streamflow modeling was moderately sensitive to whether precipitation was distributed throughout the day as observed (P1) or uniformly over the day (P4). We expected that hourly observations of precipitation would have had more impact on model skill in this steep and small watershed. This lack of sensitivity was more important as the recurrence interval of the event increased.

2.3 Topography, Soils, Vegetation, and Channel Networks

A regional 10-meter digital elevation model (DEM) and stream gage locations were obtained from the HJA databank and used to define the simulated terrain and extent of WS1,2,3. Standard ArcInfo algorithms (ESRI, 1999) were used to process the DEM to fill erroneous sinks, calculate flow direction and flow accumulation, and delineate the watersheds (Figure 2.27).

2.3.1 Soils

A soil type map in vector format was obtained from the HJA databank and converted to a 10-meter grid cell format using the ArcInfo polygrid function (Figure 2.28). Soils were characterized as having three rooting zone layers, plus a lower layer to bedrock. Soil depth, bulk density, and percent sand and clay for the seven soil types in the small watersheds were measured by Dyrness (1969) and compiled by Bredensteiner (1998). Soil depths were initially increased by 20 percent to account for the presence of regolith, resulting in depths from 0.7 to 2.0 m. Then soil depths less than 1.0 m were increased to 1.0 m to simplify the designation of root zone depths. Porosity (ϕ), matric potential at saturation (ψ_s), and exponent b were estimated from percent sand and clay using coefficients from Cosby et al. (1984). Volumetric field capacity and wilting point were estimated using the above ψ_s, b and the equation of Clapp and Hornberger (1978). Pore size distribution and bubbling pressure were estimated from the above soil texture information using Table 5.3.3 in Maidment (1993).

In-situ percolation rates measured by Rothacher et al. (1967) at multiple depths were averaged (weighted by depth) into a single rate for each soil. Then the ratio of each soil type to the minimum rate was computed, resulting in the following values: Flunky=1.0, Rockland=1.36, Slipout=1.63, Limberlost=4.22, Budworm=14.02, Frissell=15.25, and McKenzie River=15.79. Then an initial value for lateral hydraulic conductivity K_l was determined from the average percolation rate for Flunky=$5.18 \times 10^{-5} m\,s^{-1}$. K_l was subsequently adjusted during calibration by scaling the values of all soil types up or down uniformly, thereby preserving the relative differences among soil types. Vertical hydraulic conductivity for the lower soil layers was set as $K_v = 0.1(K_l)$. The ratio of K_v to K_l for the surface soil layer was calibrated, as explained in Section 2.4. Even though infiltration capacity i_c in the HJA setting is nonlimiting in the real system, we limited the surface layer K_v and thereby i_c to partition some of the water into the non-matric surface store, where it was routed with the non-linear reservoir approach of Szilagyi and Parlange (1999) to emulate the effect of macropore flow on streamflow generation. Fitted values from Szilagyi and Parlange (1999) were used for infiltration and macropore (quick) flow coefficients that were uniform across soil types.

2.3.2 Vegetation

The spatial distribution of old-growth and clearcut areas was obtained from the HJA databank. Two vegetation types were specified: 1) old-growth, with steady-state properties; 2) clearcut/regrown forest, with transient leaf area and height. WS2 is entirely old-growth, WS1 is entirely regrown forest, and WS3 has patches of regrown forest inside an old-growth matrix (Figure 2.29). Both types were characterized as a two- layer system with an overstory and understory. The old-growth type was defined as having an overstory leaf area index (LAI) of 8.5, and a height of 60 m. The old-growth understory was defined with LAI=0.5 and height=1 m. For the regrown forest, overstory and understory LAI and overstory height were set equal to the old-growth values during the pre-treatment period, then declined uniformly during the treatment period, then recovered non-linearly after treatment ended (Figure 2.30). LAI was assumed to decrease linearly during treatment to almost zero; overstory height was reduced to 0.1 m and understory height was assumed constant. Regrowing overstory LAI was simulated with an exponential growth function (Richards, 1959; Duan, 1996)

$$LAI_O = LAI_{Omax}(1 - e^{-B_1 t}), \tag{2.5}$$

where $LAI_{Omax} = 8.5$, t is time (fractional years), and $B_1 = 0.065$. Regrowing understory leaf area (LAI_U) was simulated with a modified version of Equation 2.5 to take into account the shading effect of the overstory:

$$LAI_U = LAI_{Umax}(1 - e^{-B_1 t}) - 0.15 LAI_o, \tag{2.6}$$

where $LAI_{Umax} = 2.0$, and $B_1 = 1.0$. Regrowing overstory height was simulated with

$$H_O = H_{Omax}(1 - e^{-B_1 t}), \tag{2.7}$$

where $H_{Omax} = 60$ m and $B_1 = 0.05$. Physiological properties were set the same for both vegetation types (see Appendix B for a complete listing of soil and vegetation properties).

In addition to trying to simulate historical conditions, we also simulated alternative treated/untreated scenarios for WS1, where the treatment was 100% clear-cut imposed at dates different from historical reality. For these simulations, the harvest was assumed to end immediately before the start of the run, so that regrowth began on 10/1/57 and 10/1/79 for the periods WY58-79 and WY80-98, respectively. The scenario of no treatment was defined as constant old-growth conditions.

2.3.3 Stream and Road Networks

Standard ArcInfo algorithms (ESRI, 1999) were used to calculate flow direction and flow accumulation for each grid cell, according to the method originally described by Jenson and Domingue (1998). The stream channel network was defined using a minimum contributing area of 35 cells (0.35 ha), then manually revised to more closely match USGS 7.5-minute hydrography of the HJA. Locations of roads in WS3 were obtained from the H.J. Andrews databank, and culvert locations were mapped by Wemple (1998). A series of ArcInfo scripts (Wigmosta and Perkins, 1997) were run on stream and road networks to create input files for DHSVM. These scripts partition road and stream networks into a series of reaches defined by stream and road junctions. The scripts sample DEM grid cell elevations along each reach to calculate local slope, flow direction and segment ordering. Locations of road and stream networks used as model input are shown in Figure 2.27.

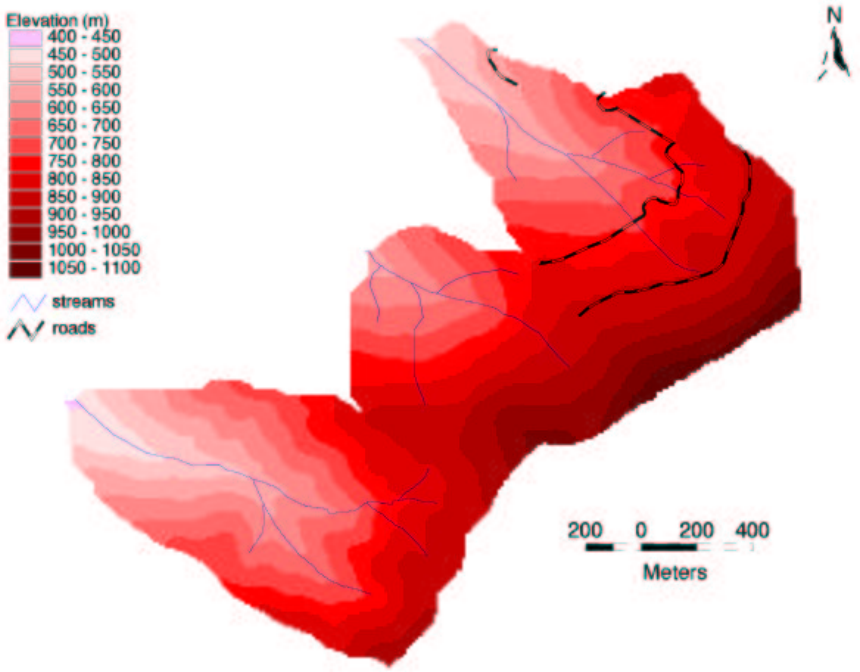

Figure 2.27: Digital elevation model and channel network inputs to DHSVM. Grid resolution=10 m.

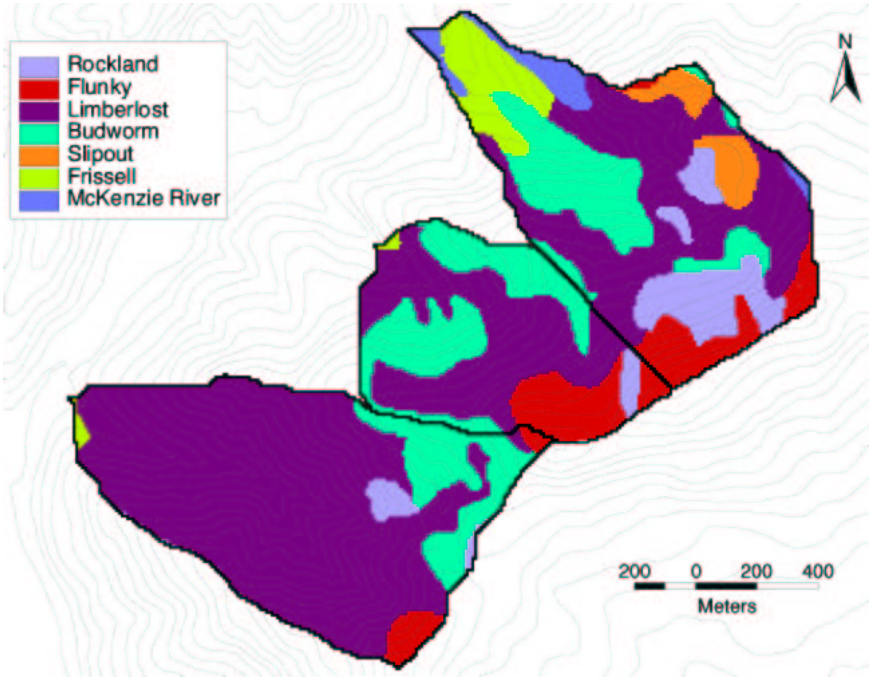

Figure 2.28: Grid map of soil types, based on Dyrness (1969).

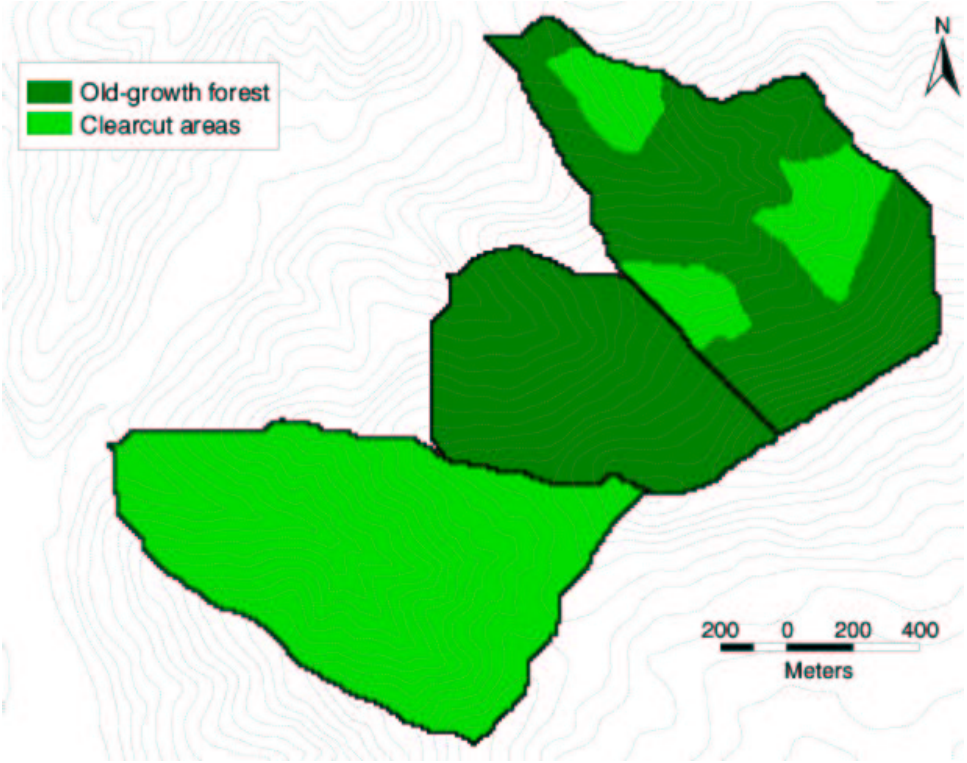

Figure 2.29: Grid map of old-growth and 1960s clearcut areas.

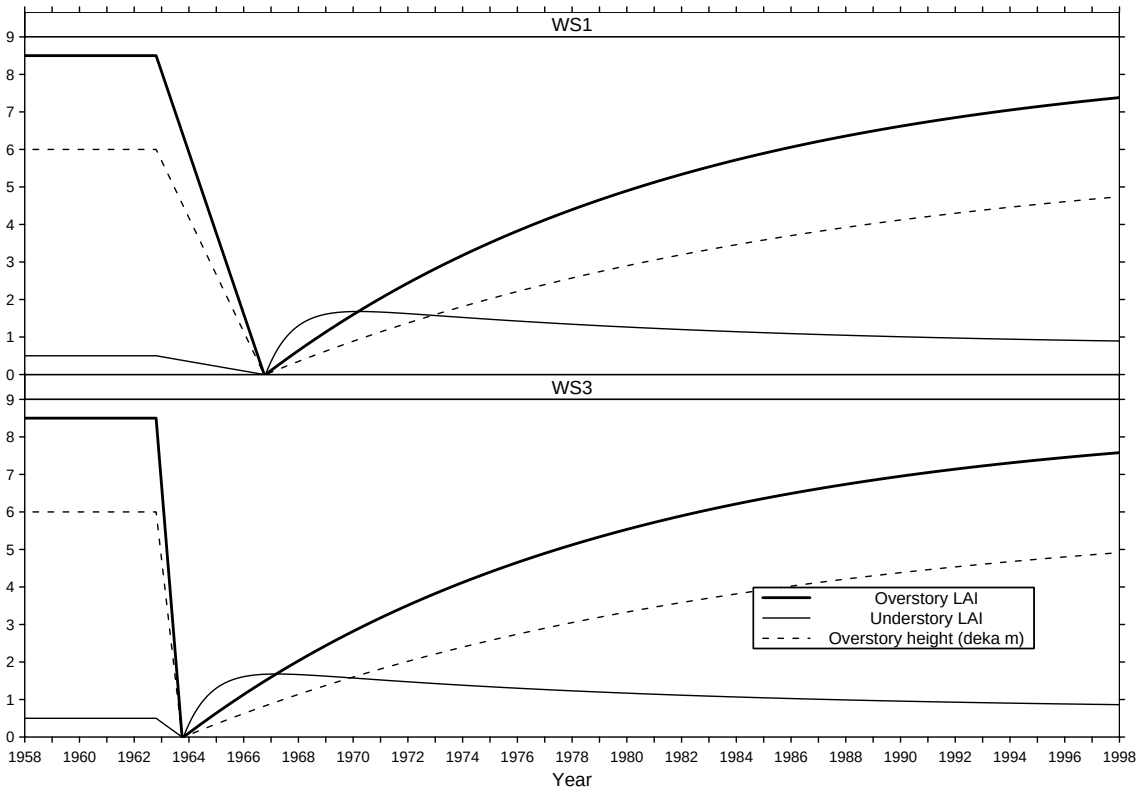

Figure 2.30: Prescribed leaf area index (LAI) and canopy height over time. For describing regrowth in clearcut areas. Overstory canopy height is given in tens of meters.

2.4 Water Balance and Calibration

The first task of any interannual watershed modeling effort is to obtain a reasonable water balance at long timescales. At the HJA, most researchers have assumed that the water balance in the small watersheds can be described as

$$P = Q + ET + \Delta S, \tag{2.8}$$

where P is precipitation, Q is streamflow (runoff), ET is evapotranspiration, and ΔS is change in soil moisture. For the small watersheds at HJA, P and Q are assumed to be adequately measured, and Q is the primary validation variable available for modelers. Most HJA researchers have assumed that the keyed concrete weirs of the WS1,2,3 gaging stations force all groundwater flow to the surface for in-channel measurement, and hence Equation 2.8 lacks a groundwater recharge term. However, it is possible that subsurface flow exits the small watersheds as either shallow groundwater flow near the gages, or as deep groundwater flow with a significant vertical component, as within a larger-scale flow system. On an average annual basis, $\Delta S = 0$, so the feasibility of Equation 2.8 depends on the magnitude of ET required to complete the balance.

ET computed from $P - Q$ on an annual basis can be compared to empirical estimates from similar environments. Using transpiration estimates based on sapflux measurements, and wet canopy evaporation estimates based on eddy-flux measurements, an upper limit for annual ET was estimated as 740 mm (Table 2.11). In almost every year at HJA, implied ET i.e., $P - Q$, was

greater than this independent estimate (Figure 2.31). Either the independent estimate is too low, or groundwater flux/recharge *G* is another loss term in the local water balance. One possibility for underestimating *ET* is neglecting the role of duff, logs, and soil in holding and releasing water. Harmon and Sexton (1995) found that logs alone could store and release about 45 mm/yr at HJA. Nijssen et al. (1997) found evaporation from the moss and litter layer in the BOREAS experiment to be very significant, and modeled it as an upper soil layer with organic-rich physical properties in DHSVM. However, the importance of groundwater flux in catchment water balance has also been demonstrated. Confounding subsurface flow paths in carefully monitored low-order basins have been found in rock types that contain far fewer fractures than the volcanic rock at the HJA (Anderson et al., 1997).

Further insight can be gained from estimates of monthly water balance. Jones (2000) presented a monthly water balance for WS2, assuming Equation 2.8, with estimates of *ET* derived from the Thornthwaite method for potential evapotranspiration. This water balance is compared with the final water balance from this study in Figure 2.32. The cumulative difference between monthly fluxes $P - Q - ET - G$ should be near zero at the end of the average water year. However, in the previously reported water balance there is an error of about 470 mm, or 21% of *P*. The total annual *ET* in that water balance is also about 470 mm, whereas the simulated *ET* in this study is over 600 mm. The amount of loss that cannot be explained by *ET* was assumed to be *G* in this study. This study also presents a different seasonality for *ET*; maximum rates are reached in the spring, when soil moisture is greatest, rather than later in the summer when meteorological conditions are more favorable but soil drought is limiting for transpiration and there is little wet canopy evaporation taking place (Figure 2.32).

The simulated annual water balance for WS1,2,3 is shown in Table 3.1. Both this study and Jones (2000) neglected increases of precipitation with elevation in deriving the water balance. We tried using lapse rates derived from maps of mean monthly precipitation created using the PRISM climate model (Daly et al., 1996). However, those lapse rates led to an 18% increase in annual precipitation over the CS2MET observations, and we were not comfortable trying to incorporate that much additional precipitation into the water balance. Certainly the existence of positive lapse rates for precipitation makes a groundwater recharge term even more plausible. In addition, if precipitation measurements are subject to undercatch, that would further increase the amount of precipitation that must be accounted for.

DHSVM was calibrated by trying to match observed annual, monthly, and hourly *Q* and annual, monthly, and daily *ET* as informed by Table 2.11. Simulated groundwater recharge *G* was used as a remainder term to complete the water balance after matching the target streamflow and *ET* fluxes. Consideration of monthly *P*, *Q*, and *ET* led to the hypothesis that deep groundwater flux was roughly proportional to precipitation; i.e., it mostly occurred during the wet season months. Perhaps the recharge is most active during the wet season through transient and saturation-dependent formation of preferential flow into the bedrock, as found by Sidle et al. (2000) in Japanese hillslopes. We accounted for the apparent seasonality of recharge by scaling unit hydraulic gradient in Darcy's law by the thickness of the saturated soil, so that recharge was proportional to water table height.

The selection of watersheds and time periods on which to base the calibration was based on a disciplined approach that started with the control watershed (WS2) during the pretreatment period (WY58-62), as this would be the situation of a typical forest manager wanting to predict impacts of future harvesting. However, the streamflow response at WS2 during WY58-62 was found to be somewhat anomalous in comparison with other years. The runoff ratio during that time was markedly higher than WS1 and WS3, in comparison with other years (Figure 2.31b). Variable evapotranspiration was unlikely to be the cause of such a large difference, because the forest type was the same across all three basins. However, it seems plausible that regolith permeability and *G* could vary across basins. After the pretreatment period, changing land cover and road

construction played roles in the water balance of the treated watersheds, making interpretation regarding deep groundwater flux more difficult. The runoff ratio of WS1 clearly increased after harvest, and stayed higher than the others for a long time, but all three watersheds converged again around 1994. During the large flood of February 1996, the gage at WS3 was destroyed in a debris flow, and beginning in that year, the runoff ratio for WS3 is distinctly lower than the others.

To evaluate whether the higher runoff at WS2 during the pretreatment period was statistically significant, streamflow was regressed on precipitation for the WY58-62 and WY58-98 periods (Figure 2.33). The WY58-62 regression line was within the 95% confidence band surrounding the WY58-98 regression line. We inferred from this that high streamflow during the pretreatment period was not significantly different from other years. But from a practical standpoint, we had to incorporate other time periods to achieve a reasonable calibration, and we therefore selected two later periods representative of varied climatic conditions and having observed hourly meteorology input: WY80-83 and WY94-98. We also included WS1 during WY58-62 in the calibration process. No calibration was done with data from the regrowth period of WS1, and WS3 was not used at all. As inferred from the paired watershed study, these basins are supposed to have similar climate, soils, and vegetation. After we account for these differences in the model input, the output should be as good for WS1 and WS3 as it is for WS2. However, there is also the possibility that the representation of the regrowing vegetation is inadequate, the effects of which would be difficult to distinguish from an inadequate representation of groundwater recharge.

The set of parameters that were tuned during calibration were lateral (K_l) and vertical (K_v) hydraulic conductivity, leakage conductivity for groundwater recharge (K_g), and rain and snow temperature thresholds. K_l and K_v were scaled uniformly to maintain relative differences across soil types. K_g was constant across soil types. Adjustment was done in a trial-and-error process.

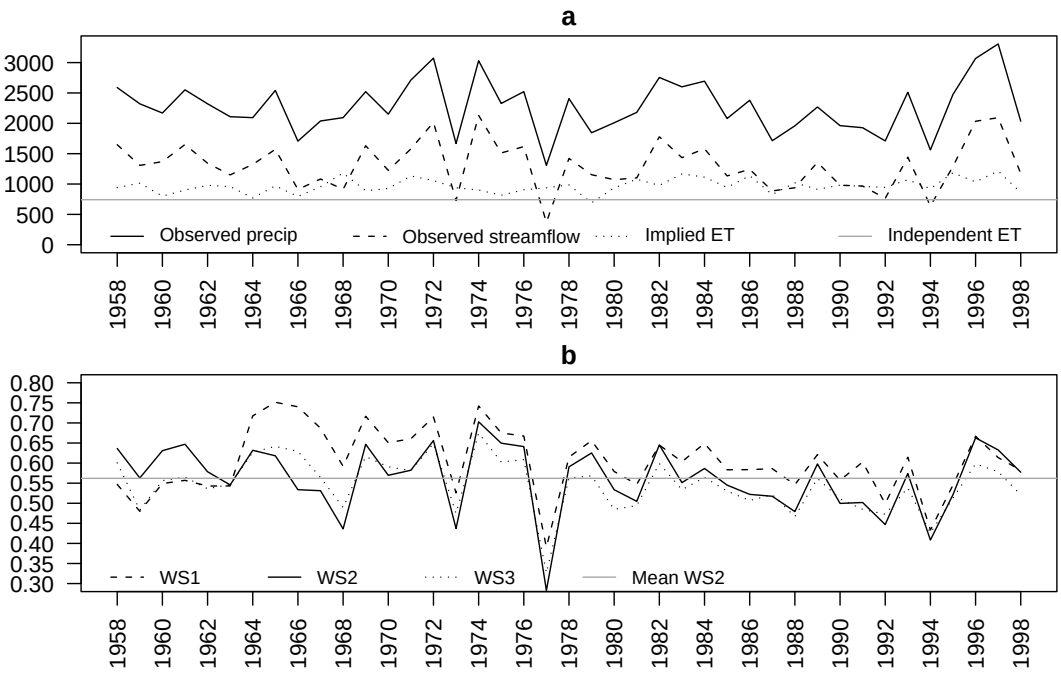

Figure 2.31: Annual fluxes, WS1,2,3. (**a**) Observed precipitation and streamflow and estimated evapotranspiration. Implied *ET* equals difference between precipitation and streamflow and assumes no change in storage or deep groundwater recharge. Independent *ET* equals estimate of *ET* using limited sap flux and eddy flux data from HJA and Wind River, Washington (written communication, Tim Link 2001, Georgianne Moore and Barbara Bond 2001). (**b**) Runoff ratio, streamflow/precipitation.

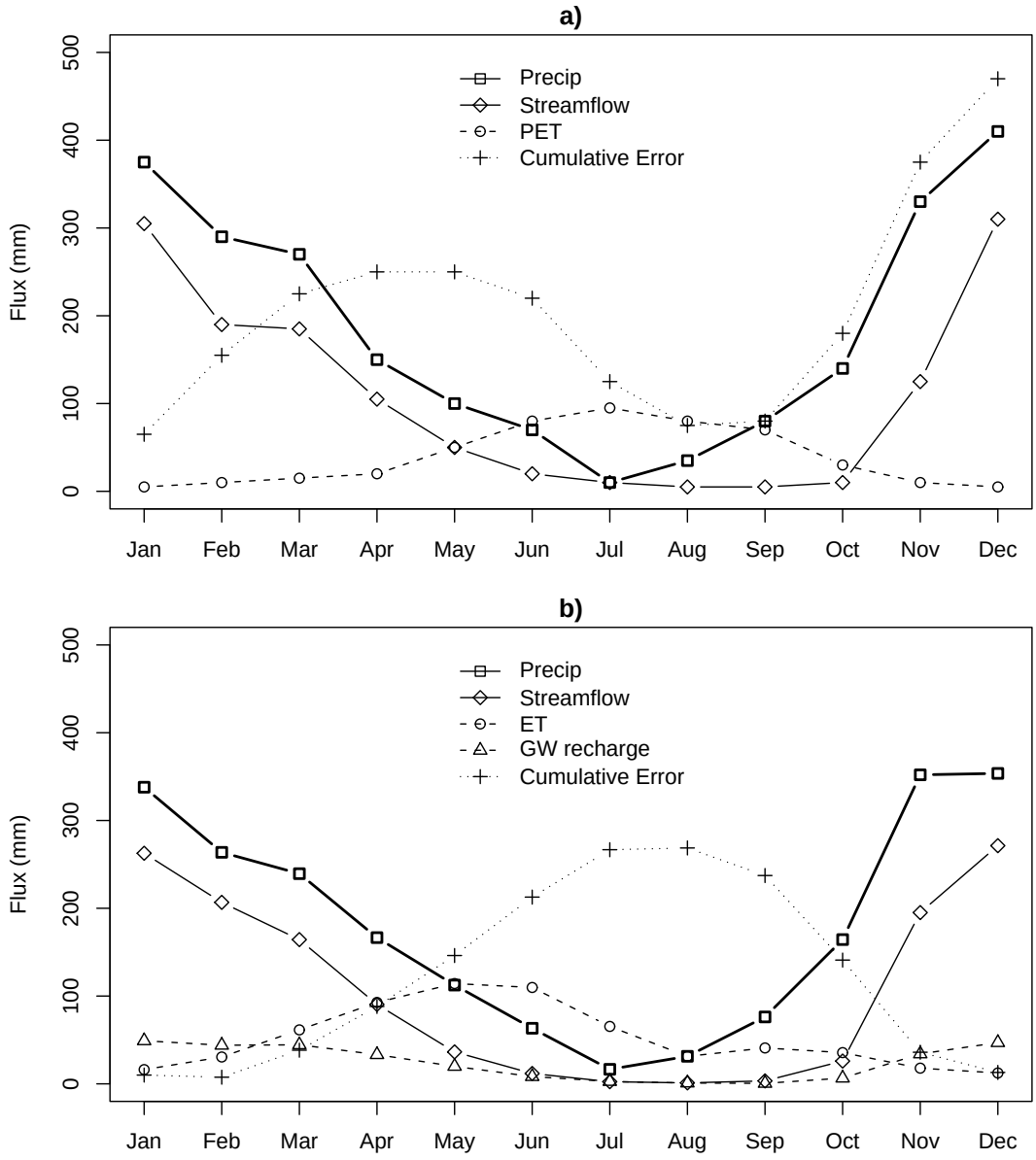

Figure 2.32: Monthly water balance, WS2. (**a**) Water balance as reported in Jones (2000), based on WY52-96. (**b**) Water balance from this study, based on WY58-98. Cumulative error is the cumulative difference of precipitation - streamflow - evapotranspiration - groundwater recharge; error should be 0 at end of year assuming no long-term change in storage. Jones (2000) assumed groundwater recharge=0, but final error is 470 mm.

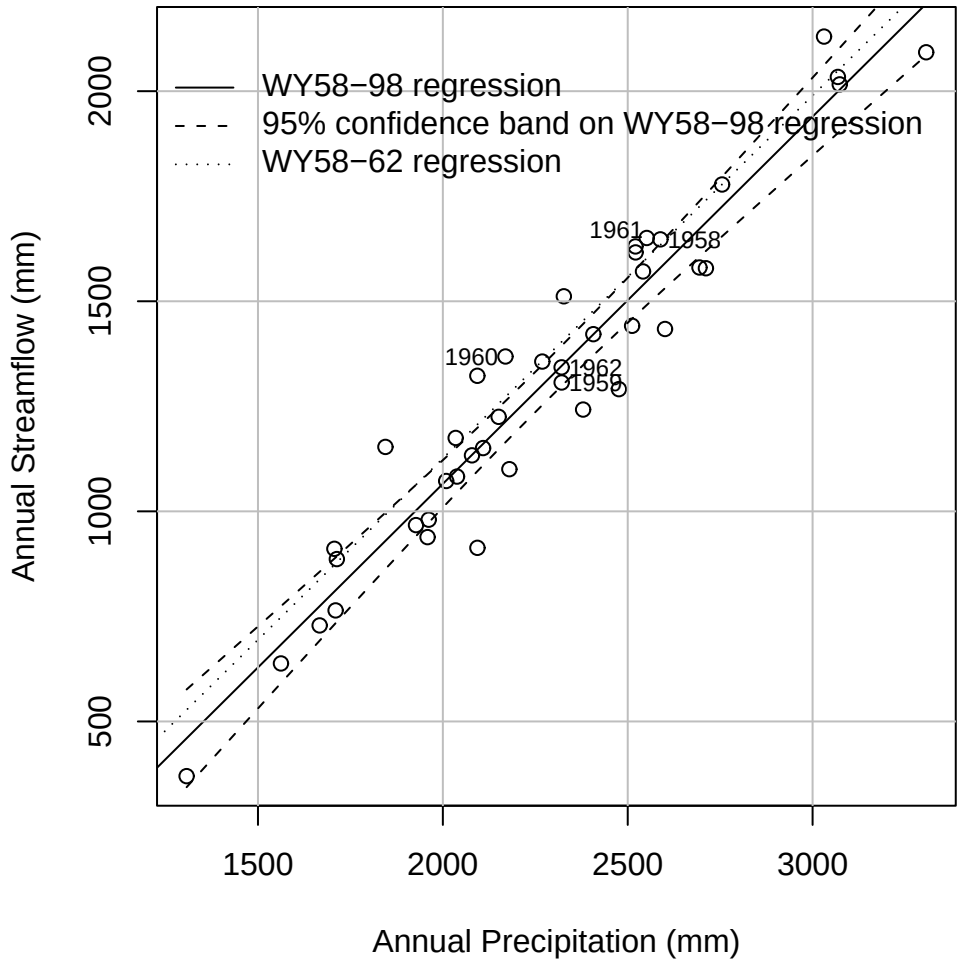

Figure 2.33: Annual observed streamflow regressed on precipitation, WS2. WY58-62 regression is just inside confidence band on WY58-98 regression, suggesting that high streamflow during pretreatment period is not significantly different from other years.

Table 2.11: Independent estimates of daily HJA evapotranspiration. Rates for canopy evaporation (from interception) by month are from eddy flux measurements at the Wind River site (Tim Link, written communication). Rates for transpiration are from sap flux measurements at WS1,2 (Georgianne Moore and Barbara Bond, written communication). Mean daily ET is estimated as a weighted average of canopy evaporation (occuring on wet days), and transpiration (dry days), and is conservatively high, since on many wet days evaporation from interception takes up only part of the day.

			Mean daily flux (mm)		
Month	Average number of wet days	Average number of dry days	Canopy evaporation (on wet days)	Transpiration (on dry days)	Mean daily ET
Oct	12	19	3	1	1.8
Nov	19	11	2	1	1.6
Dec	20	11	1	0.5	0.8
Jan	20	11	1	0.5	0.8
Feb	18	10	2	0.5	1.5
Mar	19	12	3	1	2.2
Apr	18	12	4	1.5	3.0
May	13	18	5	2	3.3
Jun	9	21	6	2.5	3.6
Jul	4	27	5	2	2.4
Aug	5	26	4	1.5	1.9
Sep	8	22	3	1	1.5
Annual total	165	200			742

2.5 Regression Modeling

Statistical methods of Thomas and Megahan (1998) as revised by Thomas (personal communication, 2002) and two new regression methods were applied to simulated peakflows to determine whether model output was of sufficient quality to draw the same conclusions as those based on observations in the previous empirical studies. The first part of the analysis focused on the comparison of historical conditions in WS1 and WS2. The first statistical model was a simple linear regression of WS1 on WS2, as in Eq. 3 of Thomas and Megahan (1998):

$$y_i = A_i + B_i x_i + e_i, \tag{2.9}$$

where y is $\log_e$ of WS1 peakflow ($m^3 s^{-1}$), x is $\log_e$ of WS2 peakflow, A and B are coefficients, e is error, and i is treatment period. Equation 2.9 was applied to the same four recovery periods used by T&M.

Thomas and Megahan (1998) used the following criteria to determine if the relationship between WS1 and WS2 peakflows in a recovery period was different from that of the pretreatment period. If the slope (B), intercept (A), or both were different, they deemed the recovery period to be different from pretreatment. Subsequently, Thomas (personal communication, 2002) identified a

problem with flow units in the original analysis and devised an improved method for testing the similarity of pretreatment and recovery periods. In the new method, slope terms are tested first. If the slope of a recovery period is different from the pretreatment, then the recovery period is judged to be different. Otherwise, analysis continues to test the intercepts. Data from recovery periods where slope is not different from the pretreatment, plus the pretreatment data, are included in fitting a constant-slope regression of the form

$$y = C_1G_1 + C_2G_2 + \cdots + C_kG_k + C_{k+1}x + e, \tag{2.10}$$

where y is $\log_e$ of WS1 peakflow (m^3s^{-1}), x is $\log_e$ of WS2 peakflow, C_i are coefficients estimated by regression, G_i are indicator coefficients identifying each period, with a value of one for treatment period i and a value of zero for others, k is the number of included recovery periods plus one, and e is error. The final step of the revised method is to test the differences between recovery period and pretreatment period intercepts C_i resulting from Equation 2.10, or in other words the vertical separation between constant-slope regression lines.

The second regression model included time as a continuous variable, providing one equation for the whole experiment, as in Eq. 4 of Thomas and Megahan (1998):

$$y = A + Bx + Dt + e, \tag{2.11}$$

where $t =$ time since treatment ended (fractional years), and D is a fitted parameter.

The second part of the statistical analysis compared two scenarios in the same watershed, treated WS1 and untreated WS1. Here Equation 2.9 was used with $y = \log_e$ of peakflows from treated WS1, and x was $\log_e$ of peakflows from untreated WS1. Equation 2.11 was applied similarly. In the WS1 scenarios, all years were recovery years, and these were assigned to four periods with lengths similar to T&M (Table 2.12). Since the watershed was the same in both scenarios, the regression line would have a slope=1 and intercept=0 if there were no treatment effect. Unlike T&M, where the focus was on finding differences between the regressions of the recovery periods and the pretreatment period, here the test of interest was whether the slope was different from one and the intercept different from zero.

To check whether underlying assumptions for regression were met, plots of residuals vs. control, histograms of residuals, and quantile-quantile plots with normal probability were made for all regressions, and inspection of these indicated no problems.

The peakflow datasets for both the historical WS1 vs. WS2 analysis and the hypothetical treated WS1 vs. untreated WS1 analysis are summarized in Table 2.13. Three subsets concerning membership in the original dataset developed by J&G and reused by T&M were created. The first subset comprised all J&G peakflows during the simulation period; i.e., those between 10/1/57 and 7/1/88. In this subset, sample size n of observed peakflows decreased 6%, because the simulation period started later than the J&G analysis. The second subset comprised the J&G events, plus additional observed events that we identified by hydrograph inspection that met the minimum flow standard of 0.03 m^3s^{-1} mentioned in J&G. The third subset was relevant only to the scenario analysis of WS1, and included all peakflows that were identified by the following algorithm.

Peakflow pairs selected by computer algorithm met the following set of conditions for at least one of the parameter sets listed as rows in Table 2.14. A peakflow event had to

1. Have treated peakflow $Q_{pk} > 0.05$ m^3s^{-1};
2. Have an untreated peakflow within 12 hours of the treated peakflow, where the untreated peakflow is defined as a local maximum within a centered 24-hour window;

3. Meet at least one of the following conditions for treated peakflow:

    - Have no more than N occurrences of decreasing flow in the rising limb or N occurrences of increasing flow in the falling limb, as determined from flows separated by lag L hours.
    - Have a rising limb, defined as the N_{limb} number of timesteps before the peak, where the mean flow in the first 2 timesteps was greater than 0.01 m^3s^{-1} and less than $F \cdot Q_{pk}$ m^3s^{-1}; and have a falling limb, defined as the N_{limb} number of timesteps after the peak, where the mean flow in the last 2 timesteps was greater than 0.01 m^3s^{-1} and less than $F \cdot Q_{pk}$ m^3s^{-1}.

Some observed peakflows were not peaks in the model output. In the comparisons involving simulated WS1 flows and simulated or observed WS2 flows, events were included only if peaks were observed in both the observed and simulated flows. This is why, for example, that sample size is less for subset 3 than 1 (Tables 2.13, 3.6). The peakflow had to be observable in the data for the event to be included in all of the WS1 vs. WS2 analysis. The additional, mostly small, peaks that fit J&G criteria but were not included by them increased the sample size such that there were only 3% fewer events in the augmented set compared to the J&G dataset.

For the WS1 vs. WS2 analysis, six different combinations of simulated and observed peakflow sets were created using the three above criteria to provide a comprehensive test (Table 2.13). First, regression datasets involving only observed peakflows were tested to see whether the conclusions of T&M would remain the same with different samples and hourly peaks as opposed to instantaneous peaks (subsets 1,2). Next, a comparison of simulated WS1 peakflows to observed WS2 peakflows was done (subsets 3,4). This test was performed to see whether one could evaluate timber harvest effects using observed streamflow from a control watershed and simulated streamflow from a separate, treated watershed, a task which may be of interest to managers. The final and less difficult test for the model was a comparison of simulated streamflow for both watersheds (subsets 5,6).

The least difficult challenge for the model was the comparison of scenario runs involving simulated streamflow under treated and untreated conditions in the same watershed, here WS1. Our comparison includes subsets involving both climate periods, J&G events, J&G plus additional events, and all events including those picked by algorithm (Table 2.13).

Table 2.12: Recovery periods and met inputs for historical analysis of WS1 vs. WS2, and WS1 scenarios. Dates for WS1 vs. WS2 are same as J&G and T&M. C1 is met input developed from daily CS2MET data; P1 is hourly PRIMET data.

	WS1 vs. WS2	WS1 scenarios	
Met input:	C1, P1	C1	P1
Period	Dates	Water years	
R1	11/66–12/71	58-62	80-84
R2	1/72–12/76	63-67	85-89
R3	1/77–12/81	68-72	90-94
R4	1/82–6/88	73-79	95-98

Table 2.13: Definition of peakflow datasets for regression analysis. Observed and simulated values are hourly flows corresponding to instantaneous peaks used by Jones and Grant (1996) and Thomas and Megahan (1998), except where noted as additional peaks used for this study. The historical comparison of WS1 and WS2 includes events from WY57-88. The scenario comparison of treated and untreated WS1 comprises synthetic events generated with actual meteorology from WY58-98. "All events" refers to J&G events, plus additional events selected manually from the J&G study period, plus peaks selected by algorithm.

Subset	Description
Comparison of historical WS1 and WS2	
1.	Observed WS1 vs. Observed WS2, J&G events
2.	Observed WS1 vs. Observed WS2, J&G + additional events
3.	Simulated WS1 vs. Observed WS2, J&G events
4.	Simulated WS1 vs. Observed WS2, J&G + additional events
5.	Simulated WS1 vs. Simulated WS2, J&G events
6.	Simulated WS1 vs. Simulated WS2, J&G + additional events
Comparison of treated WS1 and untreated WS1 scenarios	
1.	First met period (WY58-79), J&G events
2.	First met period (WY58-79), J&G + additional events
3.	First met period (WY58-79), all events
4.	Second met period (WY80-98), all events
5.	Both met periods (WY58-98), J&G events
6.	Both met periods (WY58-98), J&G + additional events
7.	Both met periods (WY58-98), all events

Table 2.14: Parameter sets for peakflow-selecting algorithm. To be selected, a storm event had to meet the conditions in Section 2.5 with one of the following set of values.

$N(hrs)$	L (hrs)	N_{limb}	F
12	1	3	0.2
24	4	2	0.6
72	24	1	0.8

3 Results

Model simulation results and statistical analysis of them are presented in several sections. First, water balance and goodness-of-fit for streamflow in the historical simulations of WS1,2,3 are described. Then the simulated water balance and predicted streamflow change in the scenario runs is considered. These model runs used the same chronologically correct met input as the historical simulation, but shifted the treatment in time. The last two sections describe the statistical modeling of the historical and scenario simulations.

3.1 Goodness-of-Fit

For the analysis of historical conditions, the mean annual water balance for WS1,2,3 resulted in a streamflow error ranging from -2.6 to +4.2% (Table 3.1). Simulated evapotranspiration was highest in the untreated, old-growth WS2, and lowest in WS1, which experienced the greatest reduction in vegetation. Groundwater recharge was 12-13% of precipitation.

The simulated "hydrologic regime"of WS2, quantified using the methods of Post and Jones (2001), matched reality fairly well (Table 3.2). The main weakness of the model was underpredicting baseflow and overpredicting quickflow, where the simulated and observed hydrographs were separated into components using the algorithm described in Post and Jones (2001).

Streamflow modeling skill was generally highest for WS2 and lowest for WS3 (Table 3.3). Interannual streamflow variation was surprisingly difficult to reproduce, with mean errors for annual streamflow ranging from -8 to +9%, and mean absolute errors ranging from 3 to 9%. Maximum efficiency in simulating hourly streamflow was obtained for WS2 during one of the calibration periods ($E_2 = 0.856$, see appendix for definition of model skill statistics). For E_2, a value less than about 0.6 is typically considered a poor fit, while a value greater than about 0.8 is considered a very good fit. Many hydrologists modeling streamflow are satisfied with a value of around 0.7 at a daily timestep (e.g., Wilcox et al. (1990)).

The drop-off in model skill for other years and other watersheds was not severe except for WS3 during WY80-95, which had $E_2 = 0.664$. Mean annual streamflow errors were less under the WY58-79 meteorology dataset versus the WY80-98 dataset, but among hourly efficiency results there was no pattern.

The highest goodness-of-fit in a single year was obtained for WS2 in WY87, which was not part of the calibration, with $E = 0.920$ (Figures 3.1, 3.2). Peaks and winter baseflow were reproduced well, but spring baseflow was underpredicted. The worst goodness-of-fit occurred with WS3 in WY93, with $E = 0.069$ (Figures 3.3, 3.4). Several WS3 peakflow events were substantially overpredicted, and others were substantially underpredicted. The high runoff and peakflow years of WY96-97 are depicted for WS1 in Figures 3.5–3.8. E was good for this period of great hydrologic interest, at 0.831 and 0.833 for WY96 and WY97, respectively.

The goodness-of-fit obtained at the hourly timescale here compares favorably to the results of the only other published study of modeling the small watersheds over an entire year (Tague and

Band, 2001b). In that study, the model RHESSys was run at a daily timestep and calibrated on WS2 over just one year, WY63, and verified on WS3 over a pretreatment year, 1959. The resulting calibration and verification values for E were 0.77 and 0.7, respectively. Our study involved greater challenge for physically-based modeling: hourly timestep, essentially the entire period of record, and all three watersheds. At a daily timestep over WY58-98, E_2 was 0.825, 0.827, and 0.763 for WS1,2,3, respectively.

Calibration focused on the overall streamflow record, and not surprisingly, model skill was lower for peakflows and individual categories of flow magnitude (Table 3.4). The model tended to overpredict the smallest flows and underpredict the largest flows. In general, model skill was higher for WS2 than for WS1. When considering only peakflows, the smallest events were overpredicted by 39% in WS1 but only by 2% in WS2. The largest peakflows were underpredicted by 36% in WS1 and by 27% in WS2. For all other size classes, predicted peakflows were within 15% of observed values in WS2 and within 30% of observed values in WS1.

Some of the shortcomings of the model application with respect to peakflow simulation are demonstrated in the February 1996 flood (Figure 3.9). During this large rain-on-snow event, described for nearby locations by Marks et al. (1998), most of the observed snowpack at the elevation range of WS1,2,3 was melted off, but the decrease in simulated snow water content was only about 10 mm. In addition to the lack of snowmelt, response times to precipitation inputs seem to be too long. Another factor inhibiting model skill in the pre-WY80 peakflow events is the assumed uniform hourly distribution of precipitation over a given day. Two groups of top ten peakflows were determined for WS1, by magnitude of observed flow and by magnitude of the difference between observed and simulated flow. Four events, including the February 1996 flood, were in both groups. Most were rain-on-snow events prior to WY80. A too-persistent snowpack was inferred as the primary problem in the simulations of most of them. Uniform rainfall over the day and delayed quickflow response also lowered model skill.

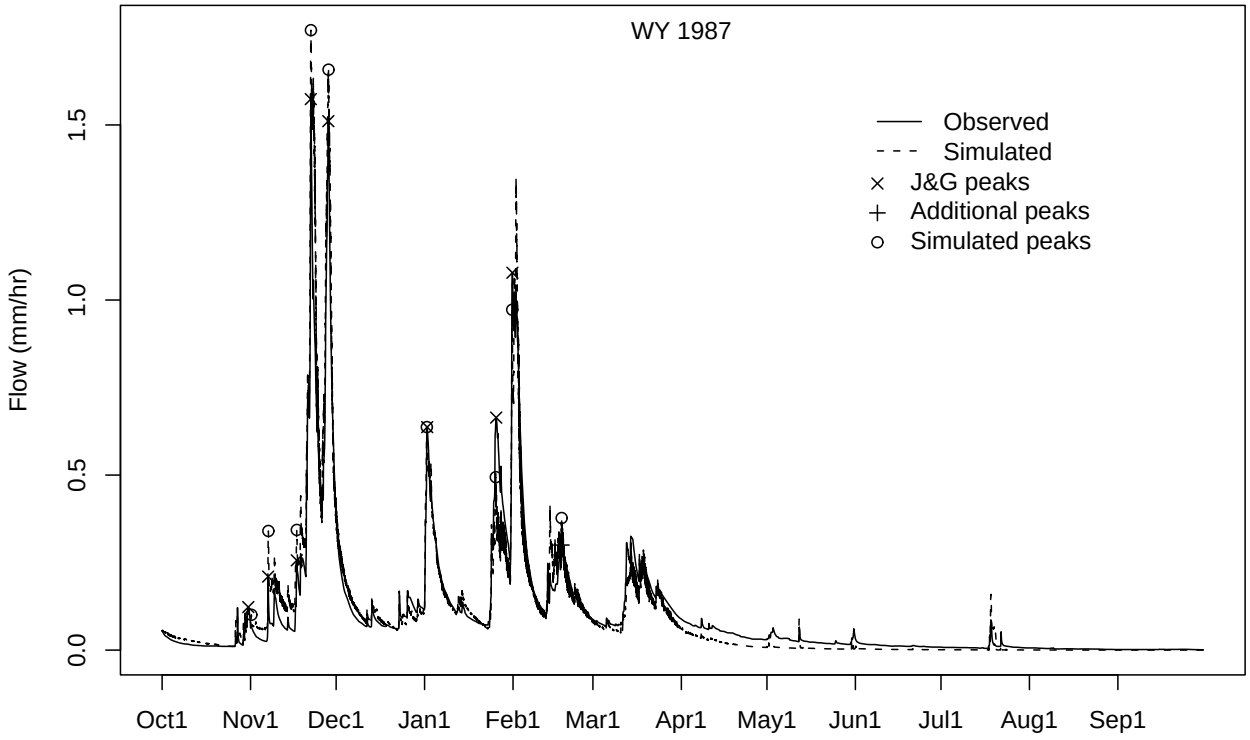

Figure 3.1: Hydrograph, WS2, WY87. Highest goodness-of-fit among all watershed/water year combinations. $E = 0.920, E_1' = 0.753, d_1' = 0.881$.

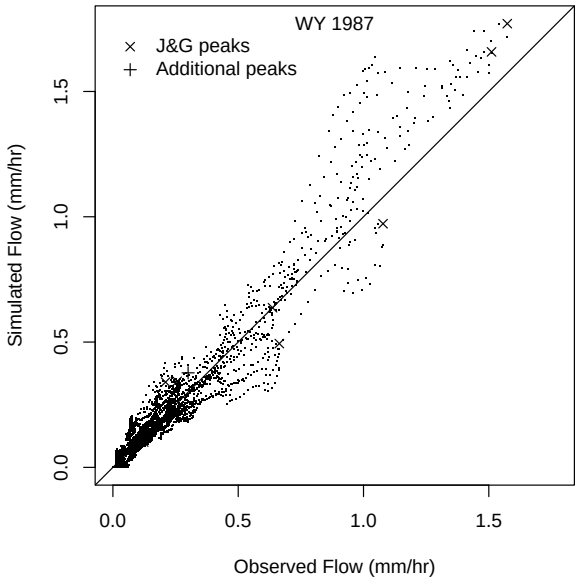

Figure 3.2: 1:1 Plot, WS2, WY87. Highest goodness-of-fit among all watershed/water year combinations. $E = 0.920, E_1' = 0.753, d_1' = 0.881$.

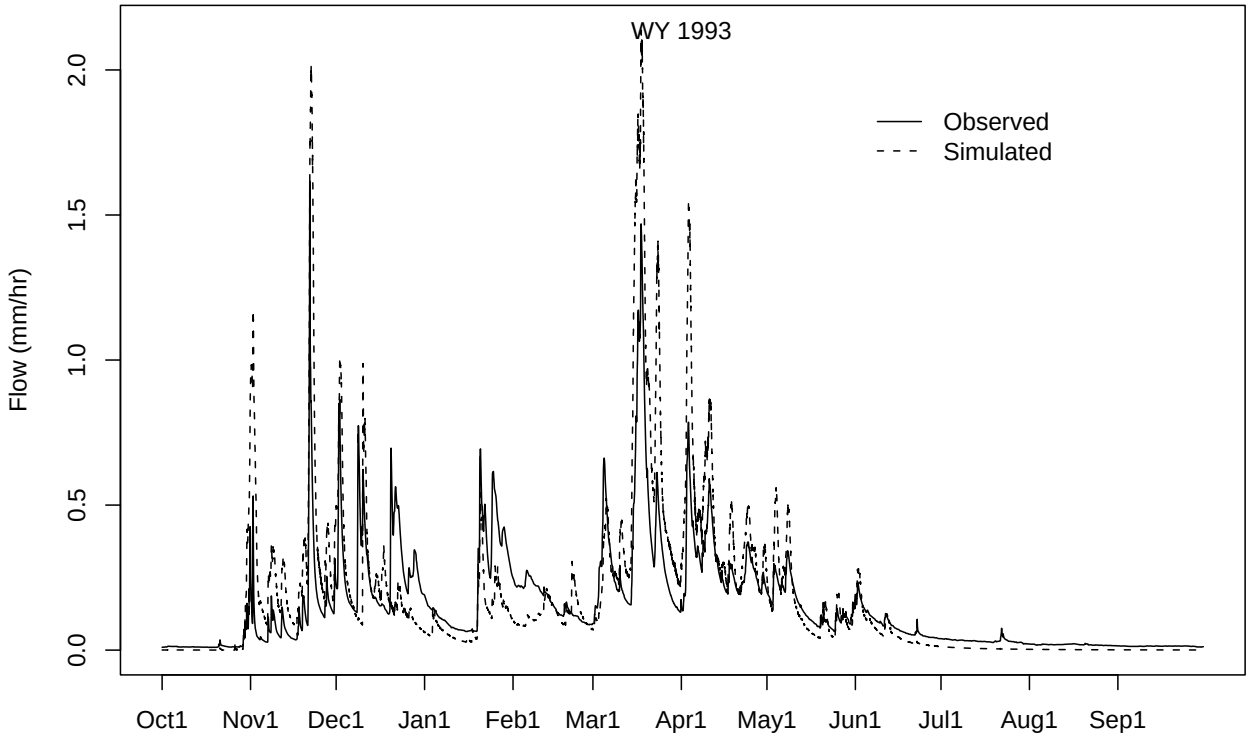

Figure 3.3: Hydrograph, WS3, WY93. Worst goodness-of-fit among all watershed/water year combinations. $E = 0.069, E_1' = -0.031, d_1' = 0.602$.

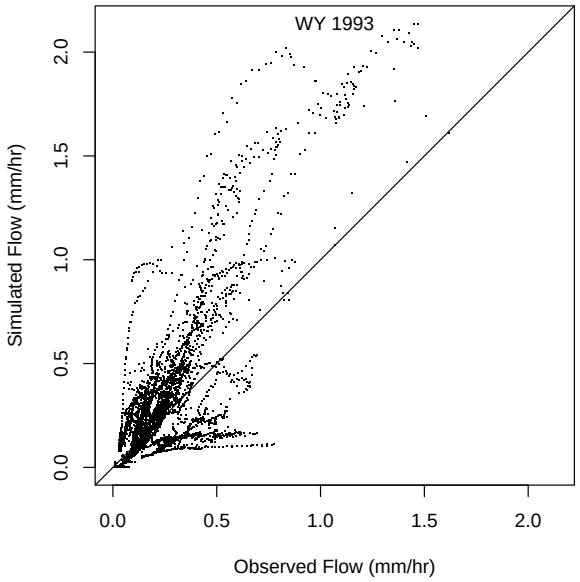

Figure 3.4: 1:1 Plot, WS3, WY93. Worst goodness-of-fit among all watershed/water year combinations. $E = 0.069, E_1' = -0.031, d_1' = 0.602$.

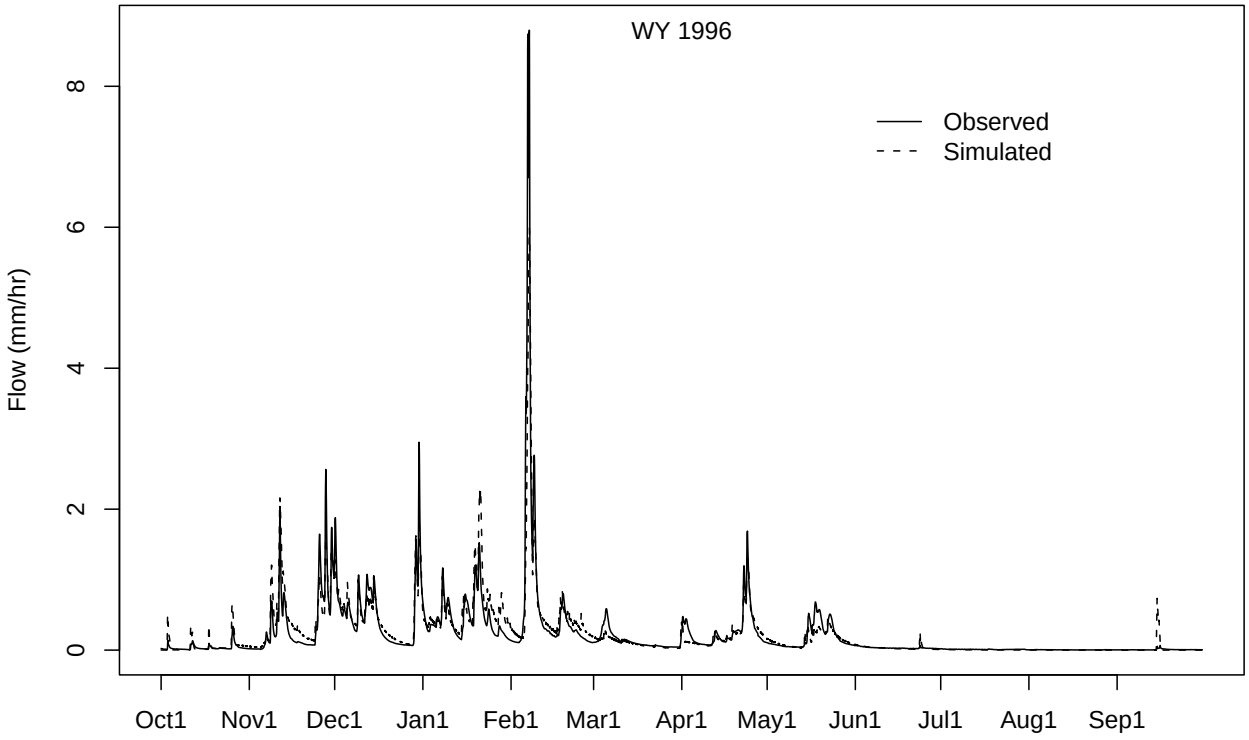

Figure 3.5: Hydrograph, WS1, WY96. $E = 0.831, E_1' = 0.515, d_1' = 0.747$.

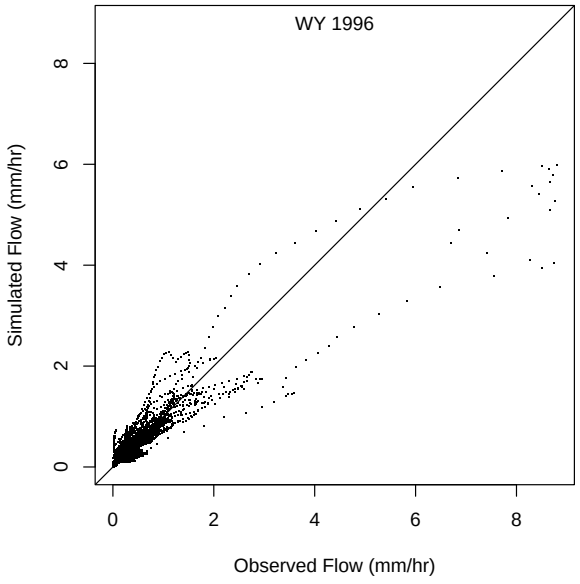

Figure 3.6: 1:1 Plot, WS1, WY96. $E = 0.831, E_1' = 0.515, d_1' = 0.747$.

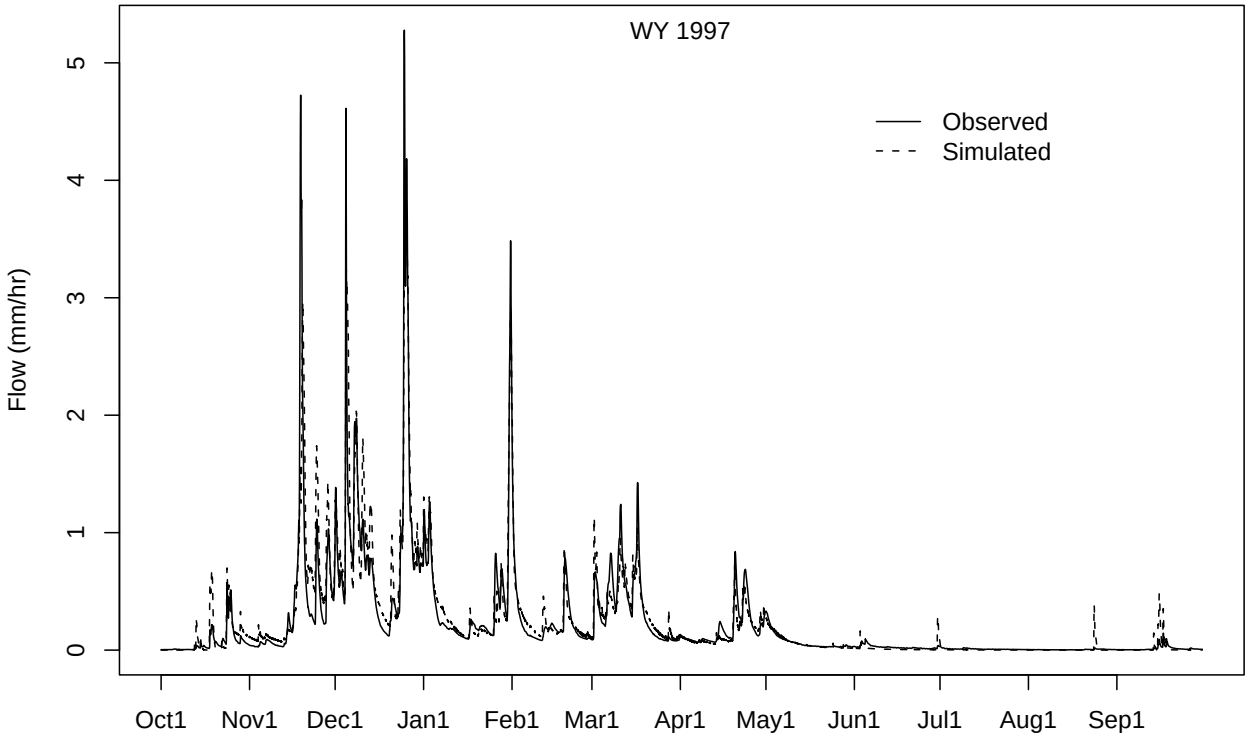

Figure 3.7: Hydrograph, WS1, WY97. $E = 0.833, E_1' = 0.566, d_1' = 0.787$.

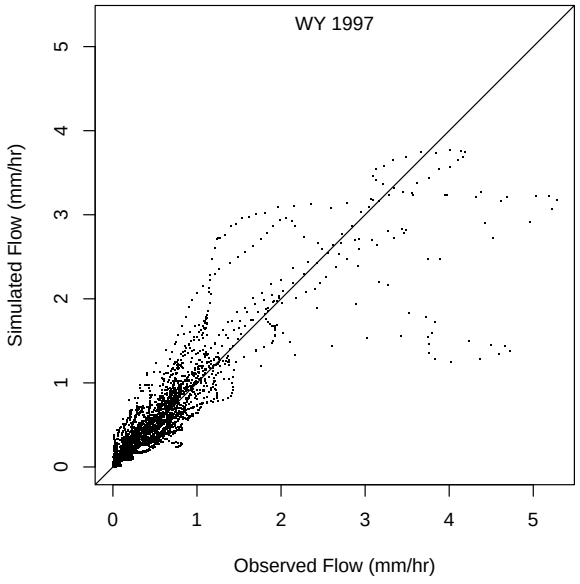

Figure 3.8: 1:1 Plot, WS1, WY97. $E = 0.833, E_1' = 0.566, d_1' = 0.787$.

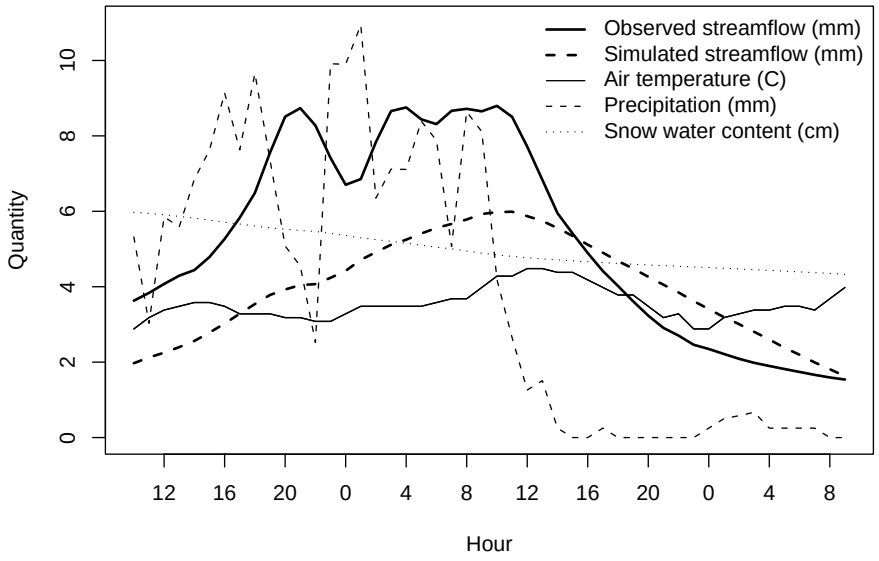

Figure 3.9: Rain-on-snow flood event, 2/6/96–2/8/96, WS1. Observed peakflow=2.49 m^3s^{-1} (8.8 mm/hr).

Table 3.1: Major water balance components, mean annual WY58-98. Precipitation is observed value; other components are simulated. P=precipitation (mm/yr); Q=streamflow (mm/yr); ET=evapotranspiration (mm/yr); GW=groundwater recharge (mm/yr); RO=runoff ratio (Q/P).

Watershed	P	Q	ET	GW	RO	Q error
WS2	2177	1272	628	277	0.58	-2.6%
WS1	2177	1391	536	250	0.64	-0.1%
WS3	2177	1287	599	291	0.59	4.2%

Table 3.2: Hydrologic regime of WS2, using the methods of Post and Jones (2001). Observed and simulated are based on WY58-98. Slope terms are from simple linear regression of annual flow on annual precipitation. CV is coefficient of variation, standard deviation/mean.

Flux	Observed	Simulated
Mean annual streamflow	1306	1272
Mean annual baseflow (%)	40	36
Mean annual quickflow (%)	60	64
Slope, streamflow	0.86	0.87
Slope, baseflow	0.33	0.34
Slope, quickflow	0.56	0.53
CV, daily streamflow	1.78	1.90
CV, annual streamflow	0.31	0.30
CV, daily runoff ratio	4.65	5.02
CV, annual runoff ratio	0.15	0.14

Table 3.3: Streamflow modeling skill for time periods. MEA=mean error of annual streamflow (%); MAEA=mean absolute error of annual streamflow (%); E_2=efficiency; E_1'=first-degree efficiency based on [month,hour] means; d_1'=first-degree modified index of agreement, based on [month,hour,precip] means (see Appendix A).

Watershed	Period	MEA	MAEA	E_2	E_1'	d_1'
		All years				
WS2	WY58-98	-2.3	5.8	0.807	0.506	0.763
WS1	WY58-98	-0.2	5.5	0.789	0.516	0.753
WS3	WY58-98	1.1	5.2	0.738	0.395	0.736
		Calibration				
WS2	WY94-98	-2.1	3.9	0.826	0.594	0.803
WS2	WY80-83	-3	6.8	0.856	0.537	0.777
WS2	WY58-62	-7.9	7.7	0.794	0.476	0.750
WS1	WY58-62	9.2	9.4	0.783	0.461	0.730
		Meteorology Datasets				
WS2	WY80-98	0.8	6.0	0.800	0.517	0.770
WS2	WY58-79	-4.9	5.7	0.811	0.495	0.756
WS1	WY80-98	1.4	5.1	0.804	0.550	0.773
WS1	WY58-79	-1.6	5.9	0.778	0.486	0.734
WS3	WY80-95	5.7	8.0	0.664	0.339	0.720
WS3	WY58-79	-2.3	3.4	0.771	0.423	0.743

Table 3.4: Streamflow modeling skill for flow magnitude categories. Categories (mm/hr): $1 \leq 0.396$; $0.396 < 2 \leq 0.756$; $0.756 < 3 \leq 1.260$; $1.260 < 4 \leq 3.290$; $3.290 < 5$. Categories 1–3 are same as small, medium to small, and medium to large categories, respectively, in J&G; categories 4 and 5 are large events in J&G. Bias=(mean simulated)/(mean observed); d_1=index of agreement based on grand mean ($\overline{O'} = \overline{O}$ in Equation A.6); n=sample size.

	Augmented J&G Events			All Hourly Flows		
Category	Bias	d_1	n	Bias	d_1	n
WS1						
1	1.387	0.200	23	1.130	0.762	3.2e5
2	0.917	0.301	76	0.942	0.355	2.5e4
3	0.837	0.339	91	0.926	0.326	8255
4	0.707	0.457	113	0.856	0.493	4370
5	0.636	0.269	34	0.659	0.320	538
WS2						
1	1.018	0.462	73	0.974	0.769	3.2e5
2	1.021	0.314	102	0.961	0.392	2.2e4
3	0.988	0.451	86	1.042	0.364	8685
4	0.857	0.590	66	0.943	0.510	2858
5	0.735	0.329	10	0.711	0.340	249

3.2 Comparison of Scenario Water Balances

For the scenario analysis involving WS1, the watershed was simulated over WY58-79 and WY80-98 with treated and untreated vegetation states. Under the treated state, the forest was assumed to start regrowing from a clear-cut condition on the first day. Predicted ET was reduced during all months except August and September, with the largest absolute reductions during the period of maximum transpiration, spring and early summer (Figure 3.10). The greatest differences in predicted streamflow are during May, June, and November.

The relative change in streamflow magnitudes between scenarios was also investigated (Table 3.5). As expected, the largest streamflow increases in response to treatment were in the low flow range. Mean hourly flow below the 50th percentile increased by 84% in WS1 and 15% in WS3, but mean hourly flow above the 90th percentile increased only 1.7% in WS1 and not at all in WS3. For the ten largest peakflows, WS1 decreased 1.5% under treatment and WS3 increased 1.1%.

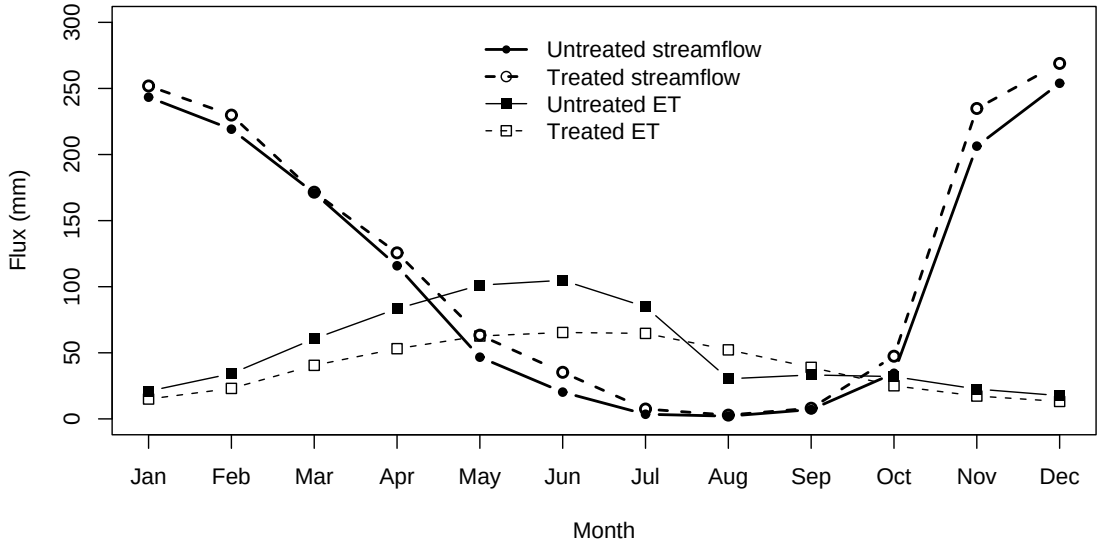

Figure 3.10: Streamflow and evapotranspiration under treatment and no treatment scenarios, WS1, WY80-98. Harvest scenario is regrowth from clearcut, beginning WY80.

Table 3.5: Streamflow change caused by treatment, scenario flow magnitude categories. P_q is percentile of hourly flow. Change is computed from the difference of the means in the first four groups, and from the mean differences of paired peakflows in the Top 10 group.

Category	WS1	WS3
$P_q \leq 0.50$	84%	15%
$0.50 < P_q \leq 0.80$	24%	1.9%
$0.80 < P_q \leq 0.90$	10%	0.8%
$0.90 < P_q$	1.7%	0.0%
Top 10	-1.5%	1.1%

3.3 Statistical Modeling of Peakflows: WS1 vs. WS2

The simple linear regressions of $\log_e$ WS1 on $\log_e$ WS2 peakflows are shown in Figures 3.11–3.16, which are similar to Figure 1 in Thomas and Megahan (1998). The inverse relationship of treatment effect to event size is shown in Figure 3.17, which is similar to Figure 3 in T&M. To simplify the presentation of tabular results, all data subsets are given under one table for each analysis step. The fitted models for each treatment period are given in Table 3.6, which is similar to Table 2 in T&M. Tests of slope differences between recovery and pretreatment periods are given in Table 3.7; constant-slopes models are given in Table 3.8; and tests on the constant-slopes intercepts are given in Table 3.9. These three tables correspond to Tables 3a,b,c in

the 2002 personal communication from Thomas. The estimated time coefficients and their significance are given in Table 3.10.

Statistical results for the two comparisons involving only observed peakflows data (subsets 1,2; Figures 3.11, 3.12, Table 2.13) were practically identical to those obtained by T&M, confirming that shortening or lengthening the list of observed peakflows did not significantly change the outcome. Slope and intercept values were similar, and all recovery period regressions were significantly different from the pretreatment period. When time was used as a continuous variable, (Equation 2.11), all regression terms were significant ($p < 0.005, R^2 = 0.92$) and the time coefficient was negative (Table 3.10).

The comparisons involving simulated streamflow had somewhat different statistical outcomes. Comparing simulated WS1 to observed WS2 (subsets 3,4 in Table 3.6), the pretreatment slopes were about 1.2 compared to 1.0 for the data. Model fit decreased, with R^2 ranging from 0.72 to 0.8. As in T&M, the regression for the second recovery period was found to have the same slope as the pretreatment (Table 3.7), but unlike T&M, the intercept was the also same (Tables 3.8, 3.9). The posttreatment regression lines crossed the pretreatment lines (Figures 3.13, 3.14), indicating that DHSVM and the regression model based on its output predicted treated peakflow to be less than untreated peakflow for some high flow events.

For the comparison of simulated WS1 to simulated WS2 (subsets 5,6), regressions tightened up again, producing higher R^2 values and narrower prediction intervals compared to subsets 3,4 (Figures 3.15, 3.16; (Table 3.6)). Unlike the findings of T&M, all recovery period slopes were found to be the same as pretreatment (Table 3.7), but like the end result of T&M, recovery periods R1,R3,R4 were declared different, because their intercepts were different. Subset 6 was similar to T&M in another respect—the posttreatment regression lines did not cross the pretreatment, implying that even at high flow levels the treated peaks were higher (Figures 3.15, 3.16).

Plots of percent increase in WS1 peakflows vs. WS2 peakflow (Figure 3.17) further illustrate the statistical nature of model output. As with previous analysis, the plots of subsets 1,2 are similar to the results of T&M. For the subsets 3,4, the lines go negative at WS2 peakflows of 0.25-0.35 $m^3 s^{-1}$, indicating again that the model predicts a negative treatment effect on peakflow at high flow magnitudes. As before, subsets 5,6 yielded results closer to the empirical finding of T&M—only the first recovery period goes negative in both cases.

T&M capped off their small watershed analysis with a regression that included time as a continuous variable (Equation 2.11, Table 3.10). Their point estimate of the time coefficient was -0.00628 ($p = 0.004$). Since quality of climate input changed somewhat beginning with WY80, we applied the regression to both WY58-88 and WY58-79. For subsets 1,2, involving just observed peakflows, all time coefficients were negative. For subsets 3–6, involving simulated peakflows for WS1 only or WS1 and WS2, the WY58-88 time coefficients were positive and significant, while the WY58-79 time coefficients were negative and of similar magnitude to T&M, but were not significant.

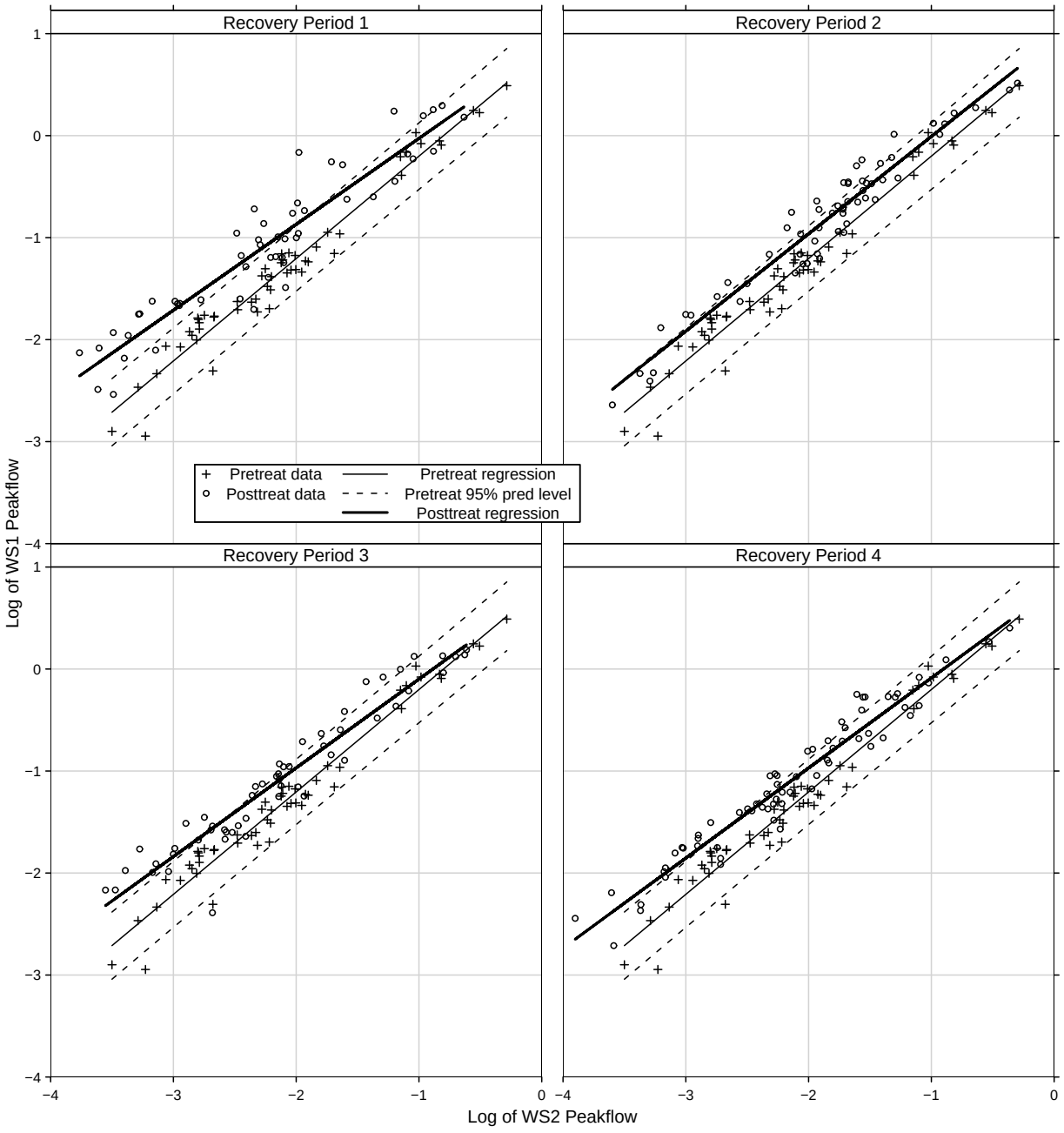

Figure 3.11: Regression line and 95% individual prediction limits for $\log_e$ WS1 on $\log_e$ WS2 during the four recovery periods. **Subset 1: Observed WS1 vs. Observed WS2, J&G peaks after WY57.** Methods after Thomas and Megahan (1998).

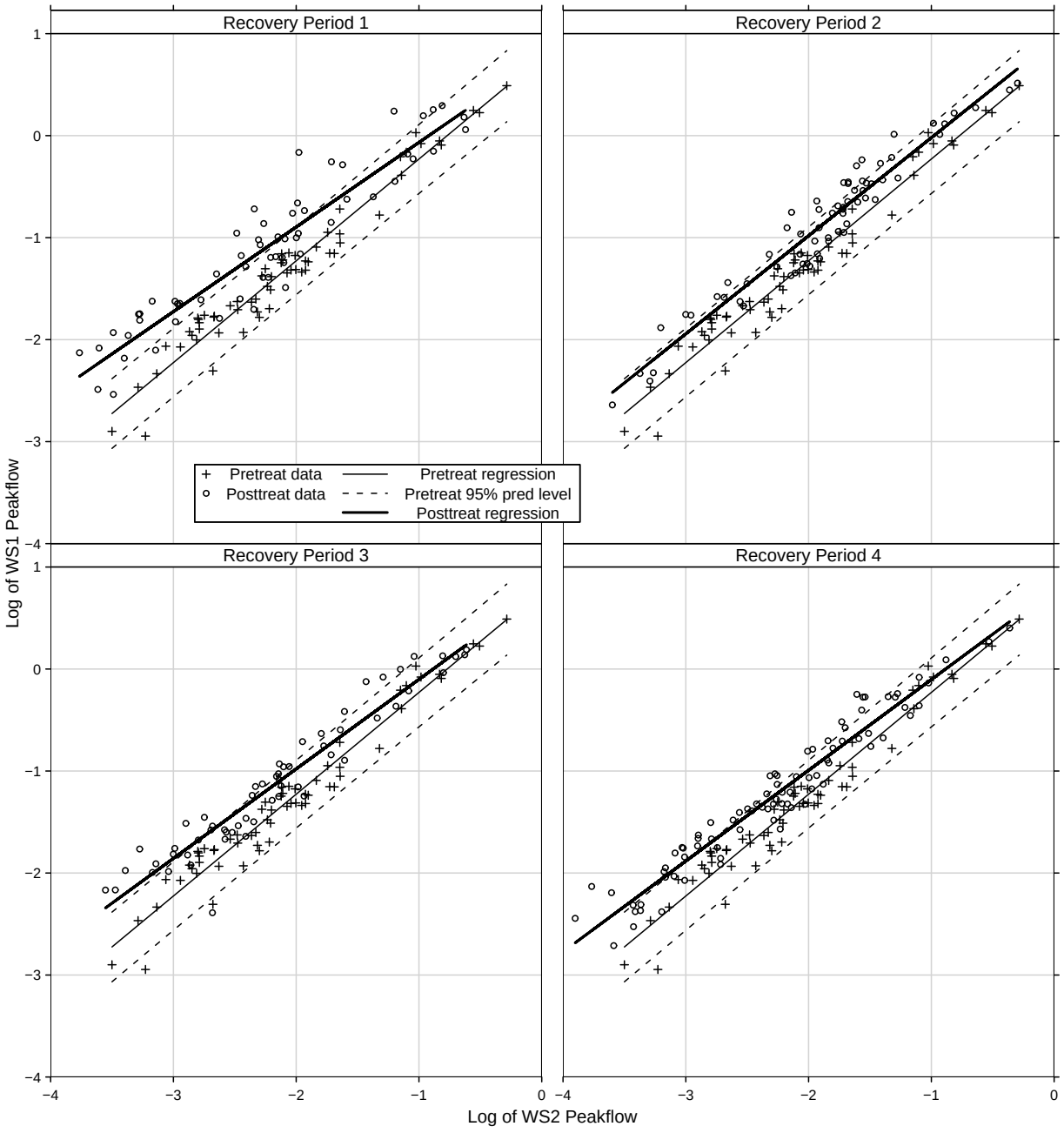

Figure 3.12: Regression line and 95% individual prediction limits for $\log_e$ WS1 on $\log_e$ WS2 during the four recovery periods. **Subset 2: Observed WS1 vs. Observed WS2, augmented J&G peaks after WY57.** Methods after Thomas and Megahan (1998).

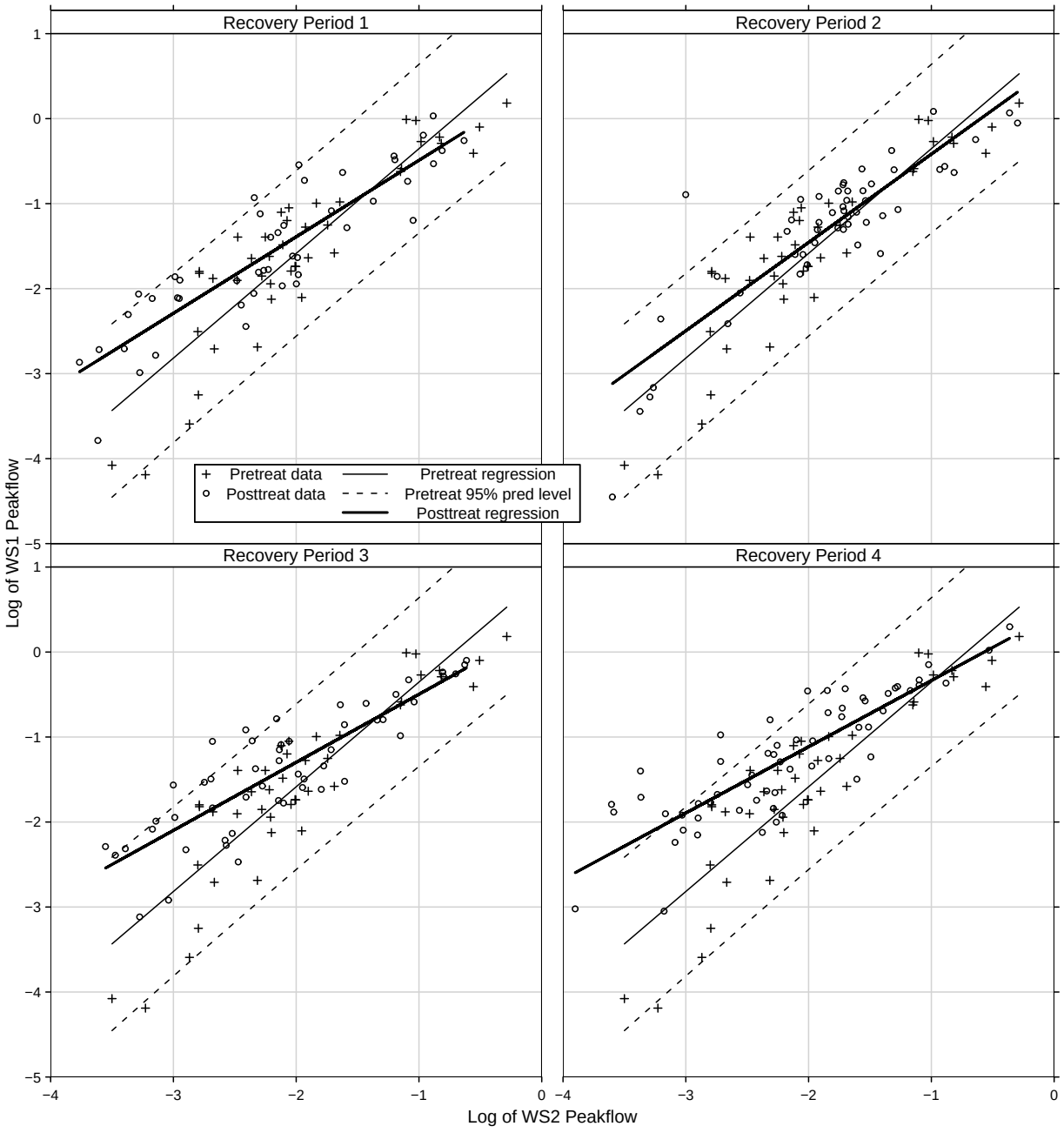

Figure 3.13: Regression line and 95% individual prediction limits for $\log_e$ WS1 on $\log_e$ WS2 during the four recovery periods. **Subset 3: Simulated WS1 vs. Observed WS2, J&G peaks after WY57.** Methods after Thomas and Megahan (1998).

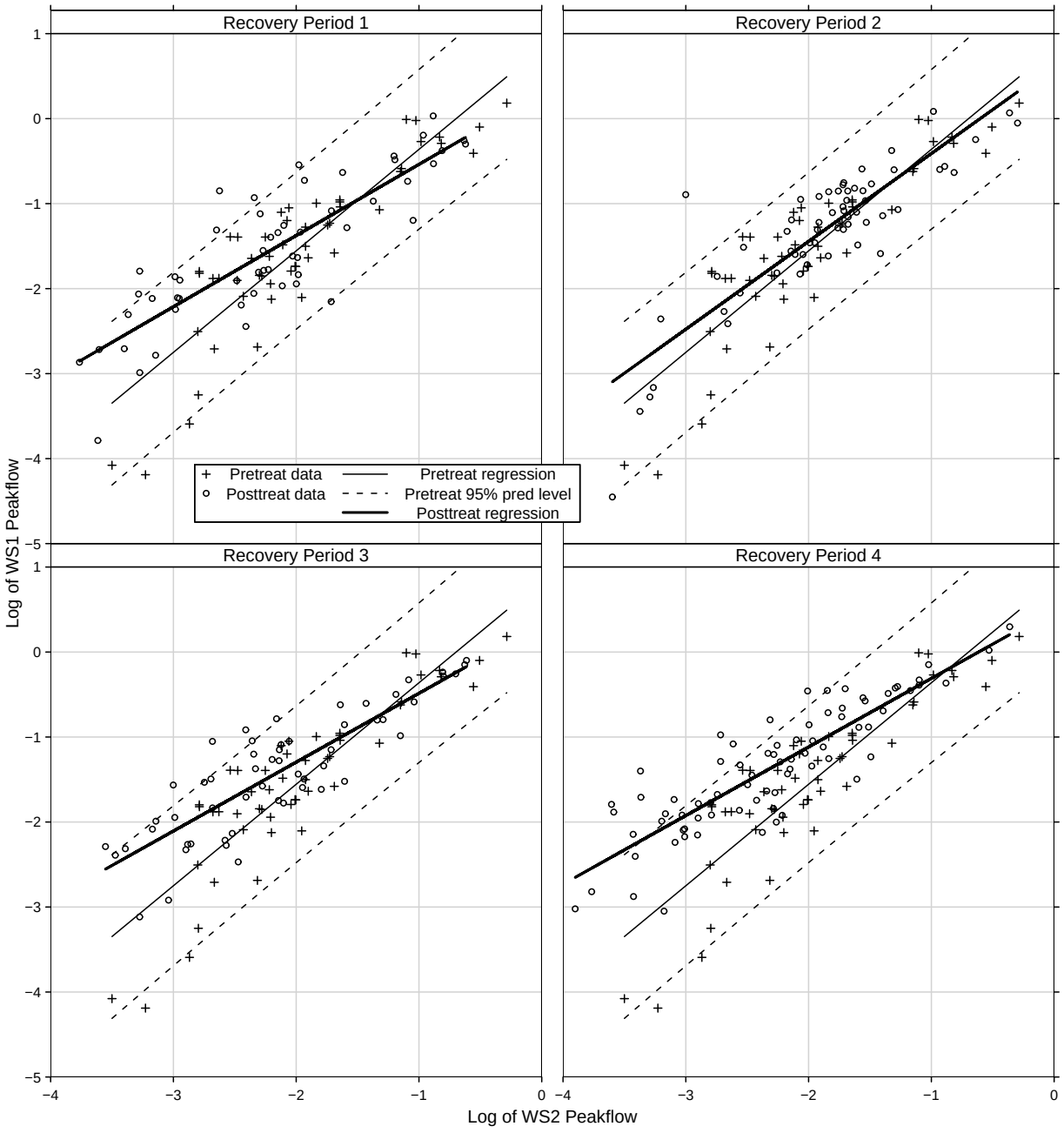

Figure 3.14: Regression line and 95% individual prediction limits for $\log_e$ WS1 on $\log_e$ WS2 during the four recovery periods. **Subset 4: Simulated WS1 vs. Observed WS2, augmented J&G peaks after WY57.** Methods after Thomas and Megahan (1998).

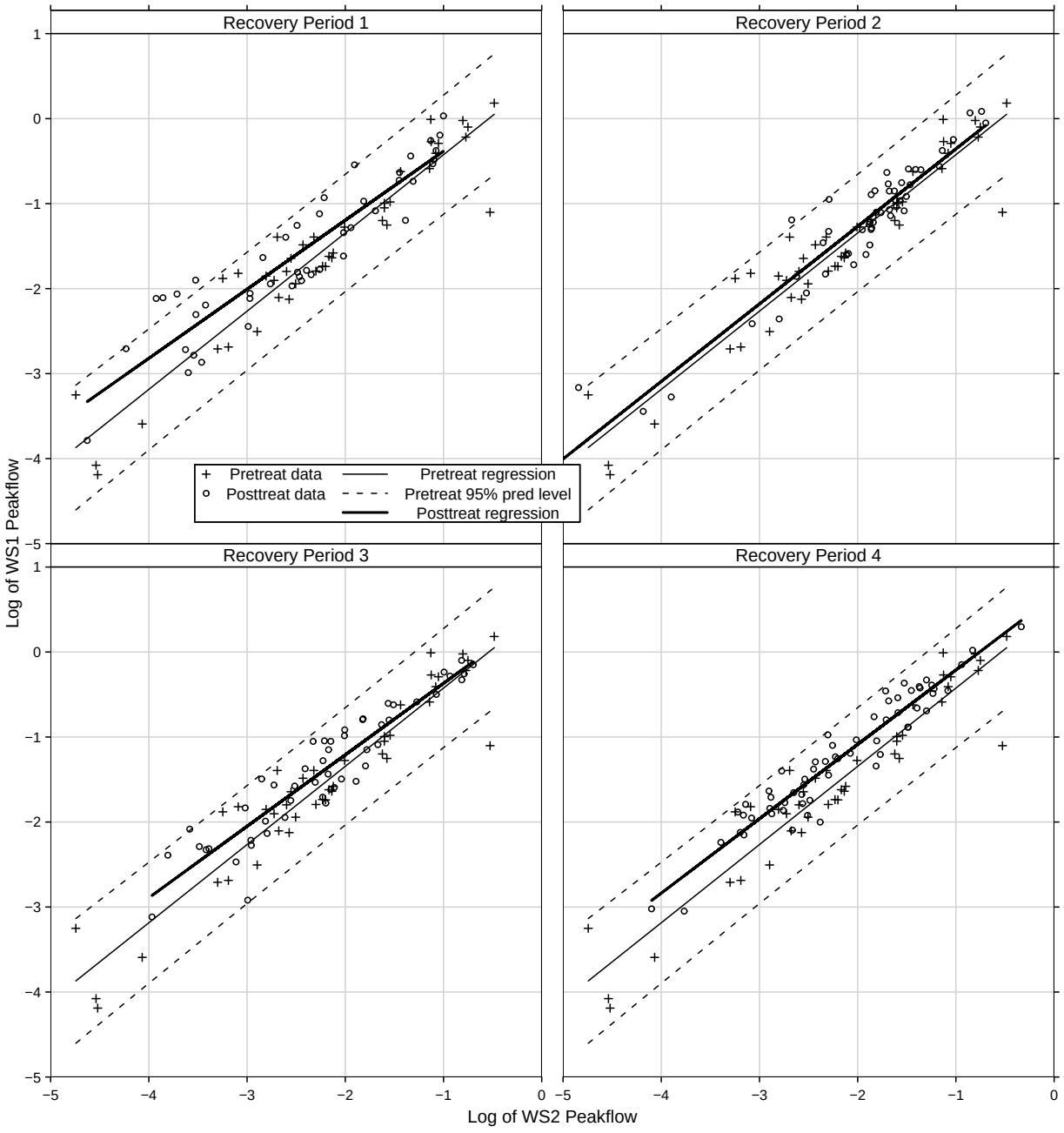

Figure 3.15: Regression line and 95% individual prediction limits for $\log_e$ WS1 on $\log_e$ WS2 during the four recovery periods. **Subset 5: Simulated WS1 vs. Simulated WS2, J&G peaks after WY57.** Methods after Thomas and Megahan (1998).

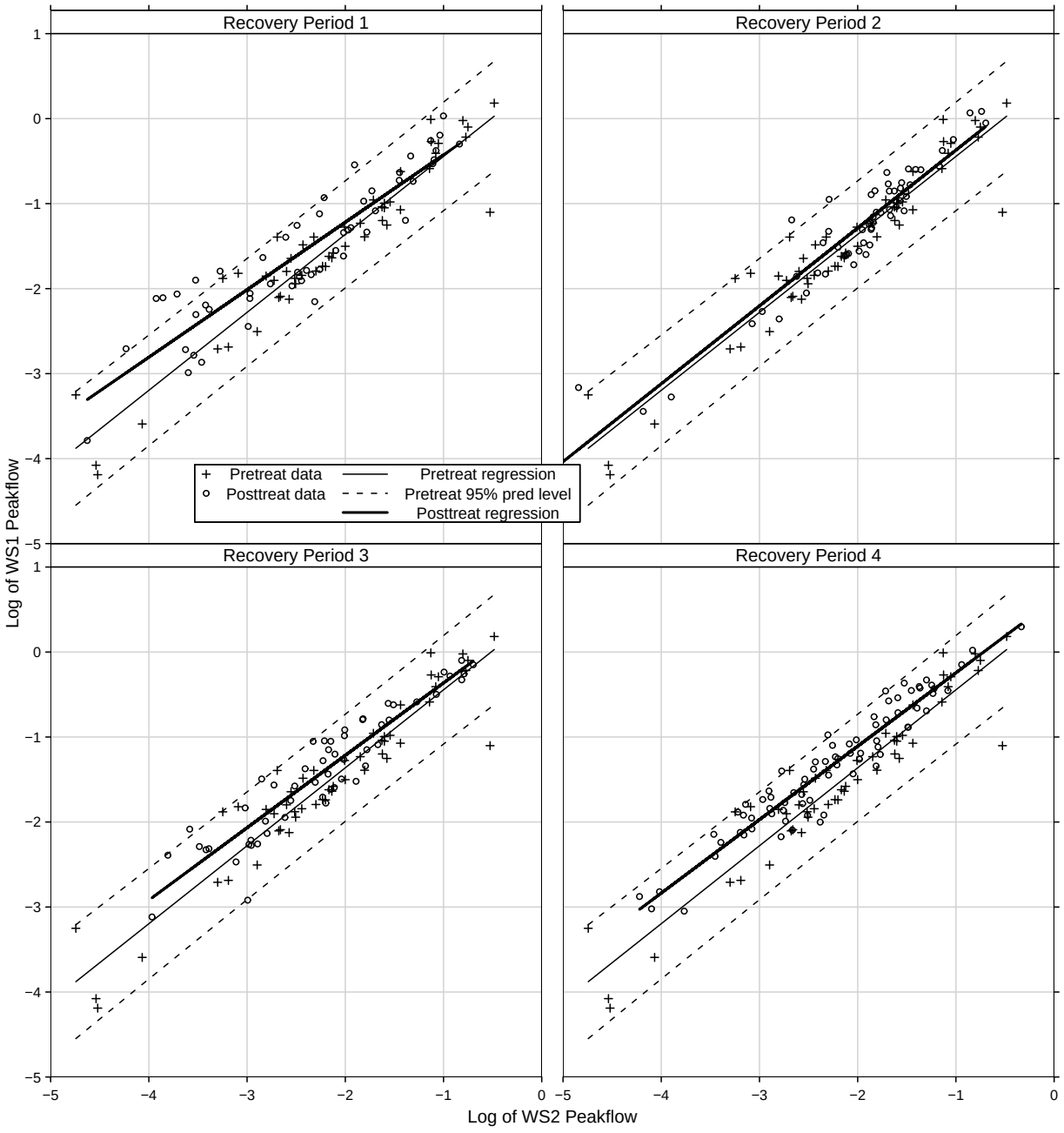

Figure 3.16: Regression line and 95% individual prediction limits for $\log_e$ WS1 on $\log_e$ WS2 during the four recovery periods. **Subset 6: Simulated WS1 vs. Simulated WS2, augmented J&G peaks after WY57.** Methods after Thomas and Megahan (1998).

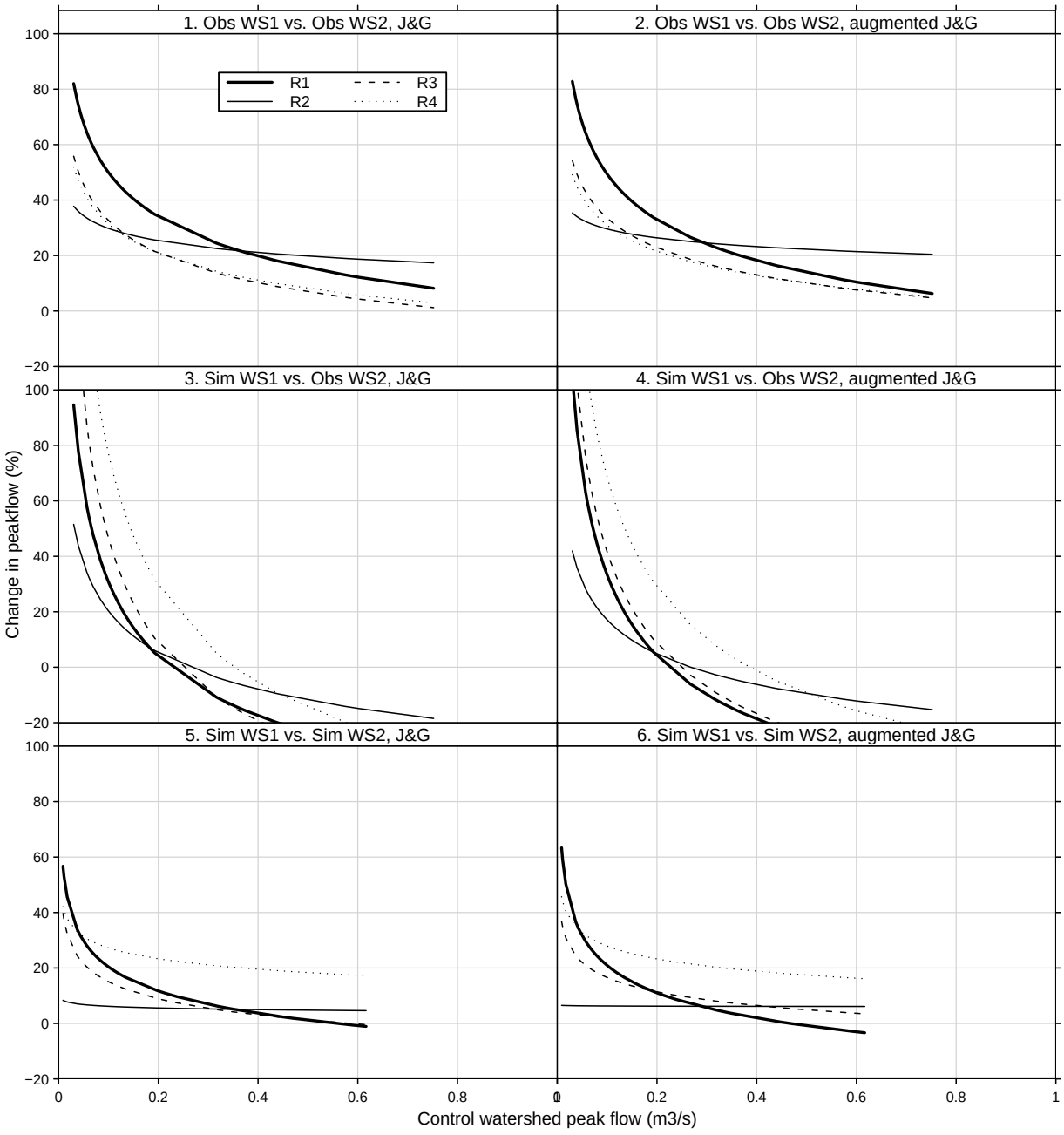

Figure 3.17: Percent increase of WS1 peakflows from control period to recovery periods, vs. WS2 flow rate. Methods after Thomas and Megahan (1998).

Table 3.6: Regressions of $\log_e$(WS1) on $\log_e$(WS2) peakflows. Events after WY57. Original units are in cubic meters per second. s=standard error of the residuals; p=*p*-value for entire model; n=sample size. All models were significant ($p < 0.0001$).

	Estimate		Standard Error					
Period	Slope	Intercept	Slope	Intercept	s	p	R^2	n
Subset 1: Observed WS1 vs. Observed WS2, J&G events								
Pre	1.004	0.803	0.0287	0.0647	0.158	0	0.96	53
R1	0.842	0.815	0.0430	0.1036	0.256	0	0.88	52
R2	0.954	0.946	0.0322	0.0641	0.173	0	0.94	58
R3	0.870	0.771	0.0348	0.0789	0.197	0	0.92	54
R4	0.883	0.796	0.0266	0.0606	0.165	0	0.94	67
Subset 2: Observed WS1 vs. Observed WS2, augmented J&G events								
Pre	0.998	0.769	0.0291	0.0648	0.165	0	0.95	62
R1	0.829	0.763	0.0399	0.0960	0.253	0	0.88	60
R2	0.962	0.942	0.0320	0.0642	0.176	0	0.93	66
R3	0.878	0.776	0.0339	0.0776	0.195	0	0.92	58
R4	0.890	0.787	0.0250	0.0599	0.175	0	0.94	83
Subset 3: Simulated WS1 vs. Observed WS2, J&G events								
Pre	1.232	0.879	0.0982	0.2063	0.476	0	0.8	42
R1	0.900	0.410	0.0708	0.1668	0.399	0	0.79	45
R2	1.039	0.622	0.0835	0.1642	0.432	0	0.76	51
R3	0.801	0.304	0.0676	0.1522	0.379	0	0.74	51
R4	0.779	0.444	0.0624	0.1433	0.375	0	0.73	60
Subset 4: Simulated WS1 vs. Observed WS2, augmented J&G events								
Pre	1.194	0.833	0.0904	0.1894	0.454	0	0.78	51
R1	0.837	0.299	0.0728	0.1721	0.442	0	0.72	53
R2	1.034	0.623	0.0778	0.1549	0.414	0	0.76	59
R3	0.810	0.325	0.0653	0.1486	0.372	0	0.74	55
R4	0.807	0.497	0.0520	0.1261	0.355	0	0.76	76
Subset 5: Simulated WS1 vs. Simulated WS2, J&G events								
Pre	0.920	0.496	0.0490	0.1202	0.337	0	0.90	42
R1	0.812	0.429	0.0522	0.1382	0.339	0	0.85	45
R2	0.912	0.556	0.0390	0.0859	0.253	0	0.92	51
R3	0.841	0.473	0.0465	0.1094	0.269	0	0.87	51
R4	0.875	0.664	0.0354	0.0818	0.212	0	0.91	60
Subset 6: Simulated WS1 vs. Simulated WS2, augmented J&G events								
Pre	0.917	0.473	0.0442	0.1056	0.310	0	0.90	51
R1	0.794	0.369	0.0490	0.1273	0.337	0	0.84	53
R2	0.916	0.546	0.0368	0.0808	0.243	0	0.92	59
R3	0.852	0.488	0.0449	0.1063	0.263	0	0.87	55
R4	0.864	0.620	0.0309	0.0747	0.215	0	0.91	76

Table 3.7: Slope differences between recovery periods and pretreatment period. From regressions of $\log_e$(WS1) on $\log_e$(WS2) peak flows (Table 3.6). Variance is sum of variances estimated for regressions slopes; DF=degrees of freedom. "*" indicates recovery slope is not significantly different from pretreatment slope ($p \geq 0.00625$) and indicates testing of intercepts is needed. Significance level from Bonferroni adjustment for "experimentwise" error (0.00625 = 0.05/8).

Period	Mean Difference	Variance	t-statistic	DF	p-value
Subset 1: Observed WS1 vs. Observed WS2, J&G events					
R1	-0.162	0.00267	-3.128	87	0.0024
R2	-0.05	0.00186	-1.155	106	0.2507*
R3	-0.134	0.00203	-2.975	100	0.0037
R4	-0.121	0.00153	-3.094	112	0.0025
Subset 2: Observed WS1 vs. Observed WS2, augmented J&G events					
R1	-0.169	0.00244	-3.416	107	9e-04
R2	-0.036	0.00187	-0.841	124	0.402*
R3	-0.121	0.00199	-2.7	112	0.008*
R4	-0.108	0.00147	-2.828	129	0.0054
Subset 3: Simulated WS1 vs. Observed WS2, J&G events					
R1	-0.332	0.01466	-2.742	74	0.0076*
R2	-0.193	0.01663	-1.495	83	0.1388*
R3	-0.431	0.01422	-3.615	73	6e-04
R4	-0.453	0.01354	-3.89	71	2e-04
Subset 4: Simulated WS1 vs. Observed WS2, augmented J&G events					
R1	-0.357	0.01348	-3.072	95	0.0028
R2	-0.161	0.01423	-1.346	101	0.1814*
R3	-0.384	0.01244	-3.443	91	9e-04
R4	-0.387	0.01089	-3.71	81	4e-04
Subset 5: Simulated WS1 vs. Simulated WS2, J&G events					
R1	-0.108	0.00513	-1.508	83	0.1353*
R2	-0.008	0.00392	-0.131	80	0.8957*
R3	-0.079	0.00456	-1.176	87	0.2428*
R4	-0.045	0.00365	-0.747	78	0.4575*
Subset 6: Simulated WS1 vs. Simulated WS2, augmented J&G events					
R1	-0.123	0.00436	-1.867	99	0.0649*
R2	-0.001	0.00331	-0.015	99	0.9881*
R3	-0.066	0.00397	-1.04	102	0.3009*
R4	-0.053	0.00291	-0.986	94	0.3268*

Table 3.8: Constant-slope regression models for comparing vertical distance between recovery and pretreatment periods having the same slope (Equation 2.10). Only those recovery periods with slopes not significantly different from pretreatment are included. SD was calculated by squaring residuals around each line and dividing by n−1.

Period	Intercept	SD	n
Subset 1: Observed WS1 vs. Observed WS2, J&G events			
	Slope=0.9797, R^2=0.94		
Pre	0.7511	0.1573	53
R2	0.9931	0.1729	58
Subset 2: Observed WS1 vs. Observed WS2, augmented J&G events			
	Slope=0.9448, R^2=0.94		
Pre	0.6563	0.1677	62
R2	0.9097	0.1751	66
R3	0.9212	0.2	58
Subset 3: Simulated WS1 vs. Observed WS2, J&G events			
	Slope=1.0404, R^2=0.73		
Pre	0.5025	0.4921	42
R1	0.7188	0.4125	45
R2	0.6237	0.428	51
Subset 4: Simulated WS1 vs. Observed WS2, augmented J&G events			
	Slope=1.1093, R^2=0.76		
Pre	0.6652	0.4539	51
R2	0.7641	0.4138	59
Subset 5: Simulated WS1 vs. Simulated WS2, J&G events			
	Slope=0.8748, R^2=0.91		
Pre	0.3952	0.3367	42
R1	0.5832	0.3402	45
R2	0.4812	0.2524	51
R3	0.5473	0.2673	51
R4	0.6632	0.2104	60
Subset 6: Simulated WS1 vs. Simulated WS2, augmented J&G events			
	Slope=0.8693, R^2=0.91		
Pre	0.3681	0.3109	51
R1	0.5511	0.3418	53
R2	0.4506	0.2443	59
R3	0.5271	0.2614	55
R4	0.6317	0.2135	76

Table 3.9: Comparison of intercepts from constant-slope regressions. Variance is $\sum(\frac{SD}{\sqrt{n}})^2$, where *SD* and *n* are from Table 3.8. DF= Satterthwaite's degrees of freedom. "*" indicates recovery intercept is not significantly different from pretreatment intercept ($p \geq 0.00625$), and implies recovery regression is not different from pretreatment.

Period	Mean Difference	Variance	t-statistic	DF	p-value
Subset 1: Observed WS1 vs. Observed WS2, J&G events					
R2	0.2419	0.0009824	7.7187	107	$p < 0.0001$
Subset 2: Observed WS1 vs. Observed WS2, augmented J&G events					
R2	0.2534	0.0009183	8.3621	124	$p < 0.0001$
R3	0.2649	0.0011433	7.8344	110	$p < 0.0001$
Subset 3: Simulated WS1 vs. Observed WS2, J&G events					
R1	0.2163	0.0095467	2.214	78	0.0297*
R2	0.1213	0.0093572	1.2537	80	0.2136*
Subset 4: Simulated WS1 vs. Observed WS2, augmented J&G events					
R2	0.099	0.0069409	1.1878	100	0.2377*
Subset 5: Simulated WS1 vs. Simulated WS2, J&G events					
R1	0.188	0.0052711	2.5892	83	0.0114*
R2	0.086	0.0039492	1.3679	73	0.1755*
R3	0.152	0.0041007	2.3742	76	0.0201*
R4	0.2679	0.0034377	4.5698	62	$p < 0.0001$
Subset 6: Simulated WS1 vs. Simulated WS2, augmented J&G events					
R1	0.183	0.0040999	2.8584	100	0.0052
R2	0.0825	0.0029068	1.531	93	0.1292*
R3	0.159	0.0031376	2.8385	96	0.0055
R4	0.2636	0.002495	5.2773	80	$p < 0.0001$

Table 3.10: Time coefficient in regression model with all treatment periods. Log_e(WS1) was regressed on $\log_e$(WS2) and time in years(Equation 2.11). "*" indicates time coefficient was not significant ($\alpha = 0.05$).

Subset	Period	Estimate	Std. Error	t-value	Pr($>\|t\|$)
1	WY58-88	-0.006119	0.002151	-2.845	0.0048
1	WY58-79	-0.010768	0.005174	-2.081	0.0393
2	WY58-88	-0.006089	0.002015	-3.021	0.0028
2	WY58-79	-0.010570	0.004957	-2.132	0.0346
3	WY58-88	0.019507	0.004632	4.211	< 0.0001
3	WY58-79	-0.006278	0.010524	-0.597	0.5520 *
4	WY58-88	0.017831	0.004236	4.210	< 0.0001
4	WY58-79	-0.009200	0.010180	-0.904	0.3678 *
5	WY58-88	0.006954	0.003109	2.236	0.0264
5	WY58-79	-0.009439	0.007605	-1.241	0.2170 *
6	WY58-88	0.006917	0.002813	2.459	0.0146
6	WY58-79	-0.009278	0.007098	-1.307	0.1930 *

3.4 Statistical Modeling of Peakflows: Treated vs. Untreated WS1 Scenarios

Comparison of simulated WS1 peakflows from scenario model runs eliminated watershed as a factor and provided more clarification of the model's ability to represent treatment effects. In the scenario runs, met inputs (C1 and P1) were chronologically correct, but forest regrowth was shifted to begin at the start of C1 and P1. Regressions of treated WS1 on untreated WS1 are listed in Table 3.11, and plotted in Figures 3.18–3.24. Tests on slopes and intercepts are in Table 3.12 and Table 3.13, respectively. Figure 3.25 is similar to Figure 3 in T&M, except the abscissa is now untreated WS1 instead of WS2.

All regressions were significant ($p < 0.0001, R^2 = 0.91$–0.99), as were all slopes and intercept terms. All slopes were also different from 1, and most intercepts were different from 0, indicating the model output exhibited treatment effects for all recovery periods. In the plots, the 95% confidence band on the regression line crosses the 1:1 line representing no treatment in all subset/recovery period combinations, implying a negative treatment effect at high flow magnitudes. However, this crossing and slope less than 1 are partly due to the influence of small flow magnitude points that are well above the 1:1 line, rather than high flow points below the 1:1 line. The treatment effect clearly declines with time and flow magnitude in all subsets, especially when comparing R1 and R4 (Figure 3.25). In all regressions of treated WS1 on untreated WS1 and time (Equation 2.11), the time term was significant and negative.

Meteorologic input was a confounding factor for the simulation of treatment effects, as seen when comparing model results from the WY58-79 and WY80-98 periods (subsets 3,4, Figure 3.25). Both subsets show a diminishing treatment effect with increasing flow magnitude, but recovery trajectories for the two subsets are different. For simulations with the first met period, percent increases in peakflows for the treated basin decline substantially in recovery period 2 but increase again in recovery period 3. Results for simulations on the second met period concur with expectations, showing a systematic decline in treatment effects over the four recovery periods.

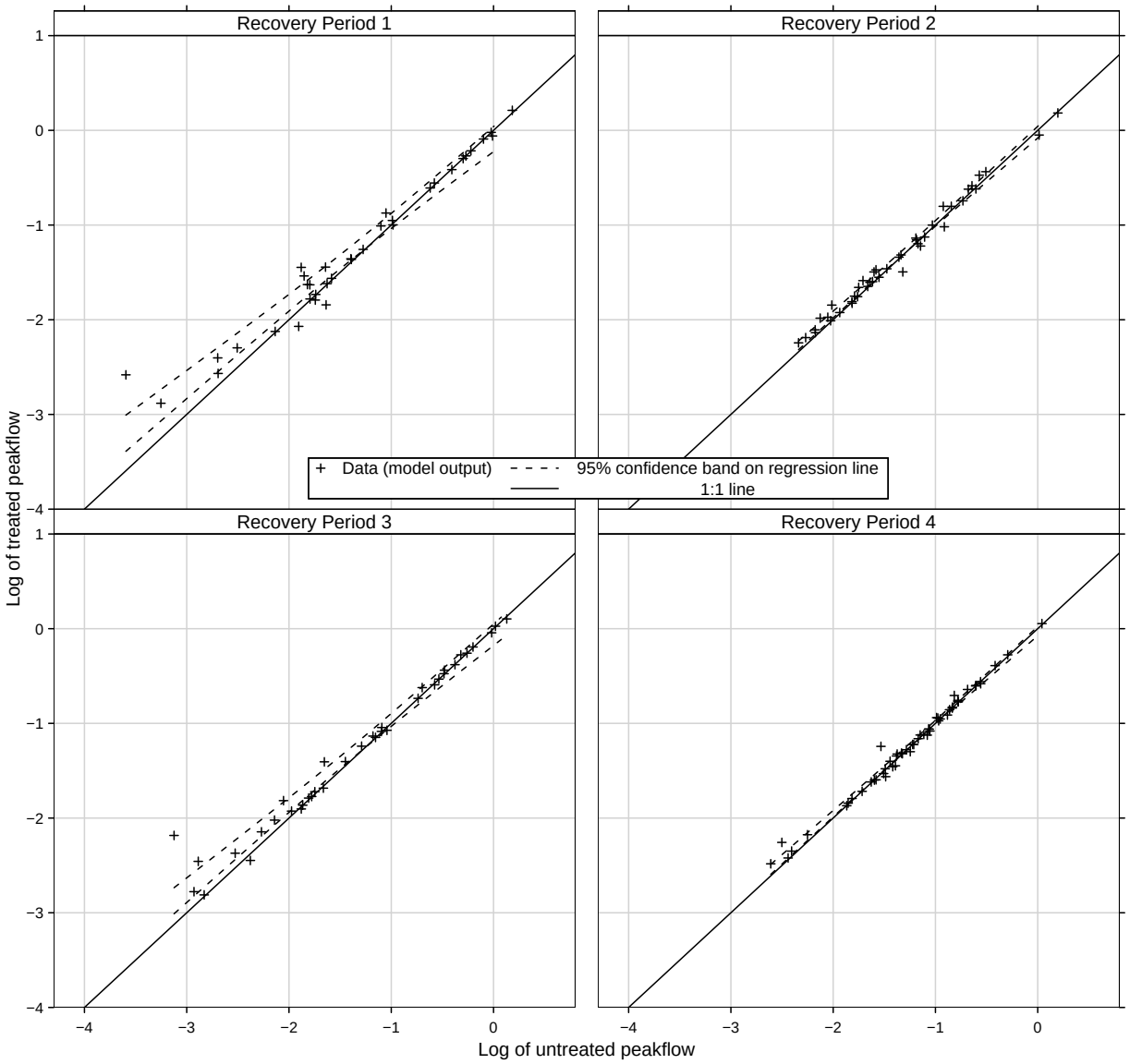

Figure 3.18: Regression of treated on untreated $\log_e$ peakflows from scenarios with WS1. 1:1 line corresponds to no treatment. Confidence band is on the regression *line* (not shown). **Subset 1: First met period, J&G events.**

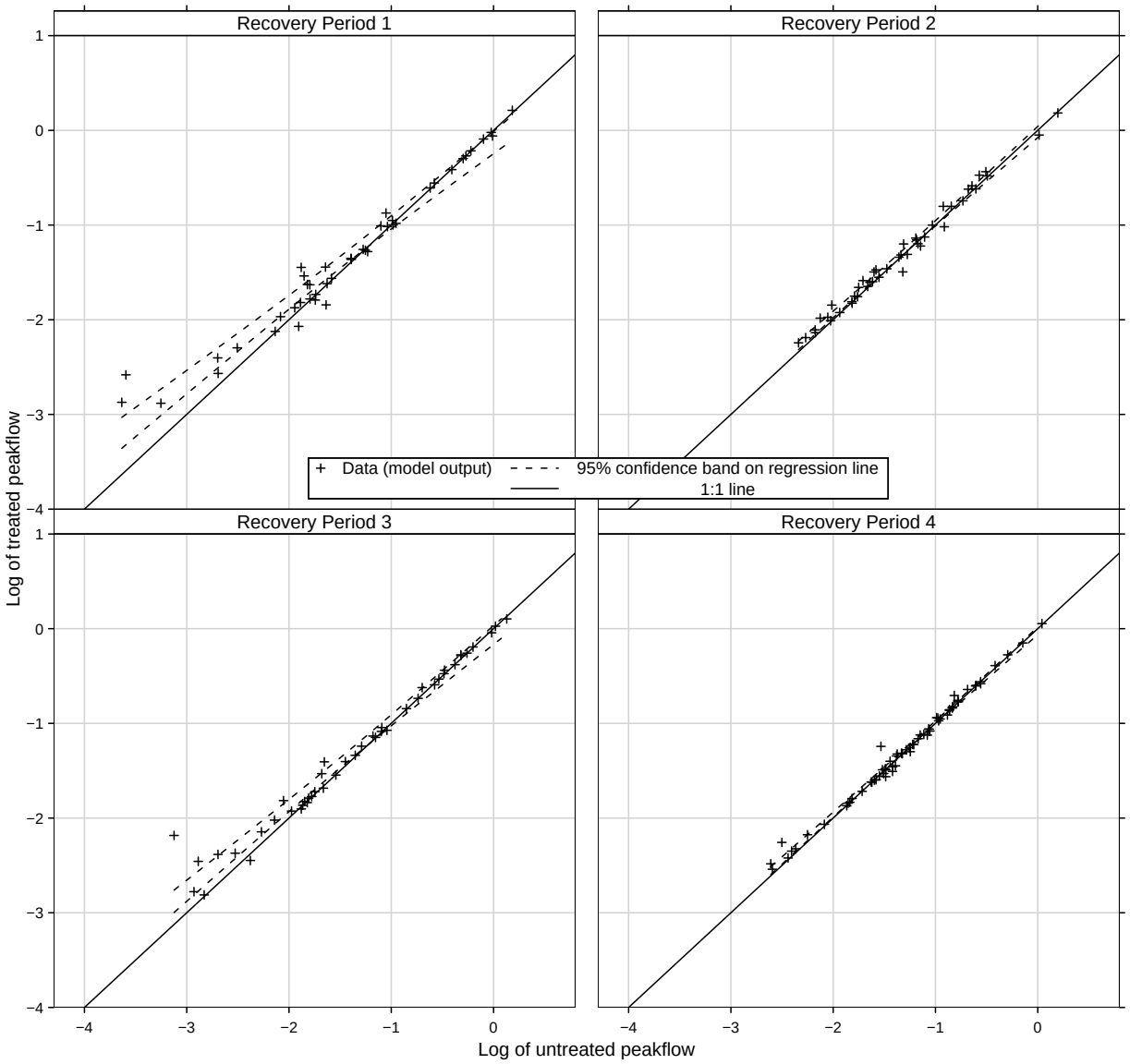

Figure 3.19: Regression of treated on untreated $\log_e$ peakflows from scenarios with WS1. 1:1 line corresponds to no treatment. Confidence band is on the regression *line* (not shown). **Subset 2: First met period, augmented J&G events.**

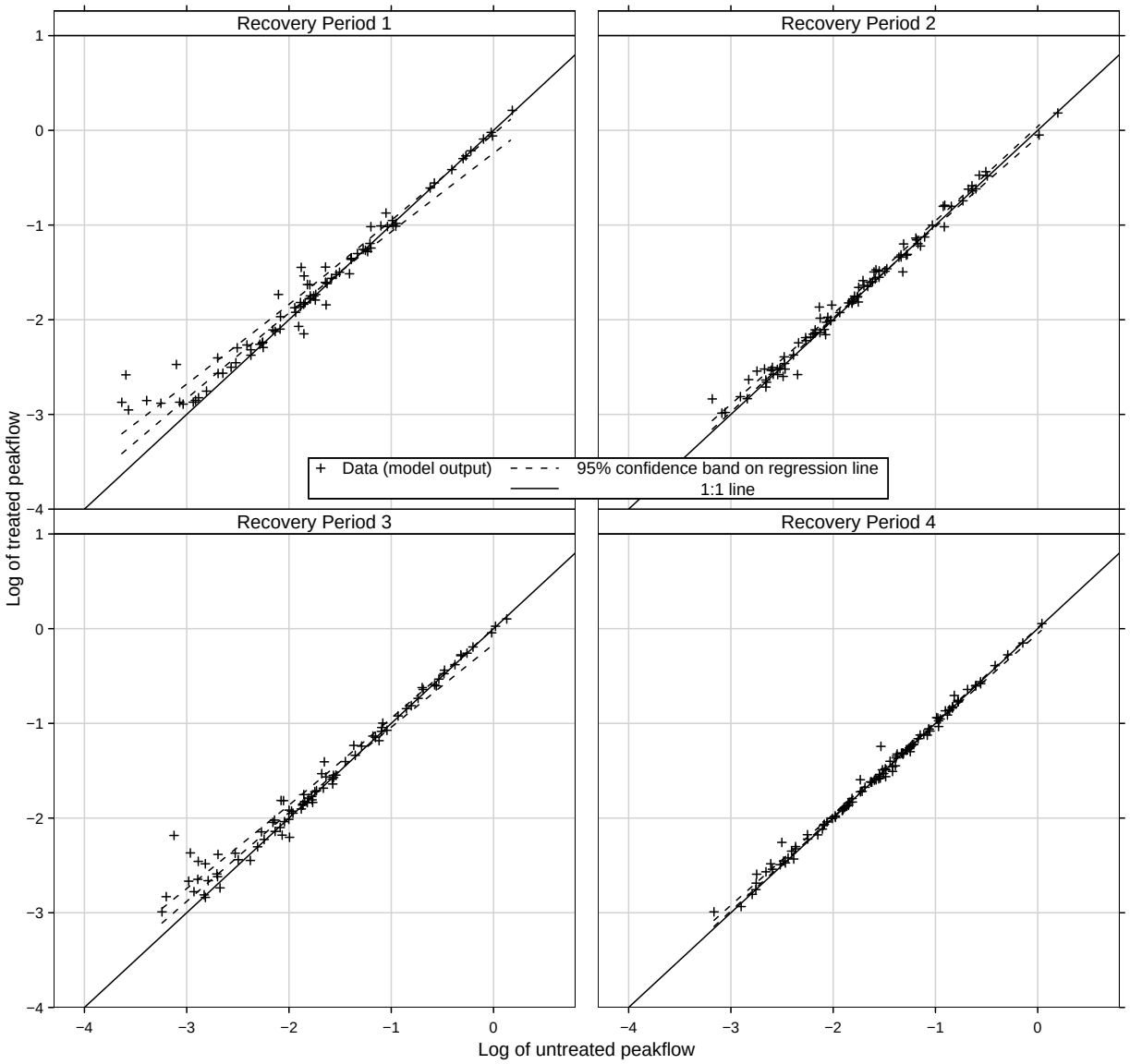

Figure 3.20: Regression of treated on untreated $\log_e$ peakflows from scenarios with WS1. 1:1 line corresponds to no treatment. Confidence band is on the regression *line* (not shown). **Subset 3: First met period, all events.**

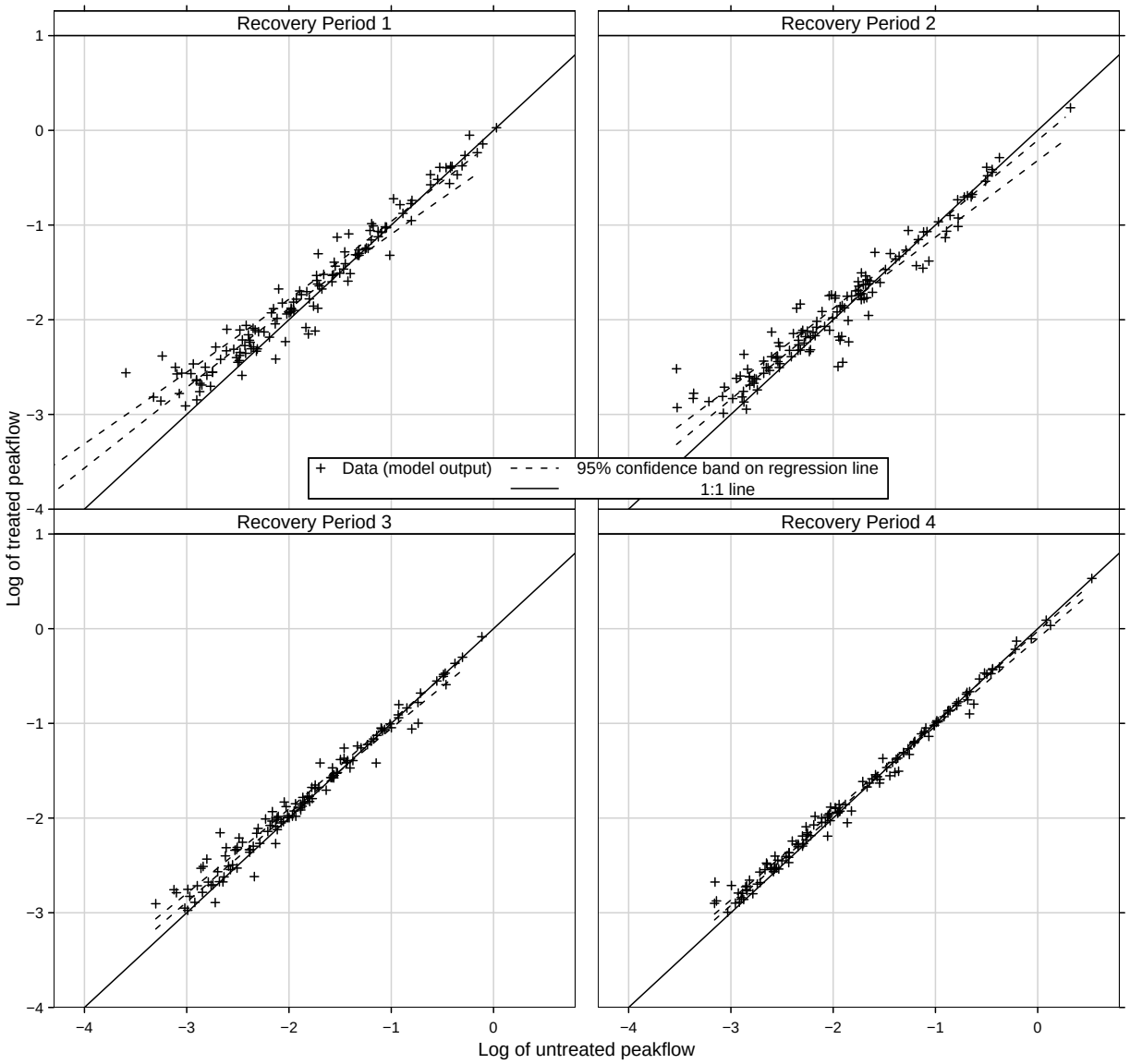

Figure 3.21: Regression of treated on untreated $\log_e$ peakflows from scenarios with WS1. 1:1 line corresponds to no treatment. Confidence band is on the regression *line* (not shown). **Subset 4: Second met period, all events.**

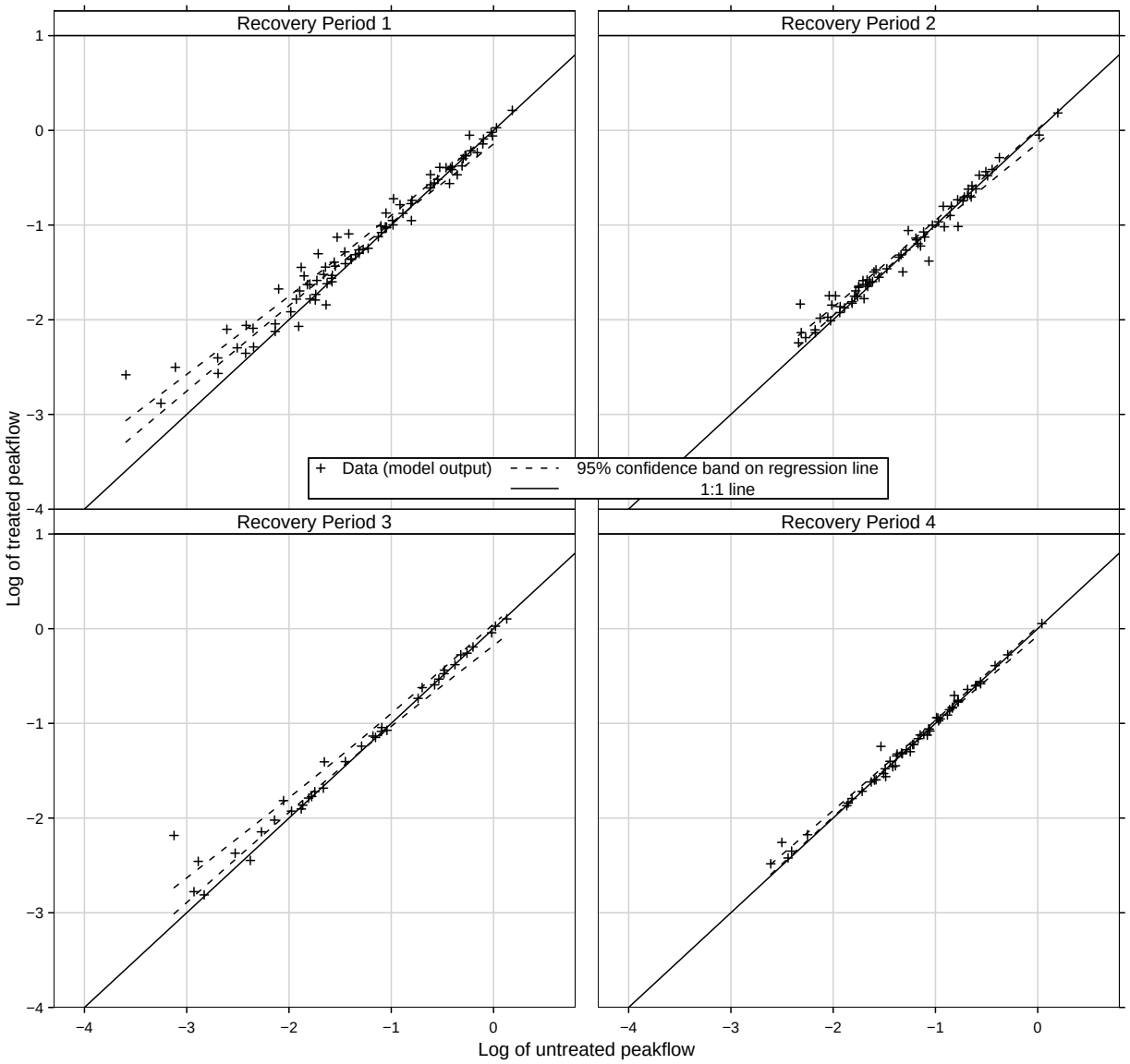

Figure 3.22: Regression of treated on untreated $\log_e$ peakflows from scenarios with WS1. 1:1 line corresponds to no treatment. Confidence band is on the regression *line* (not shown). **Subset 5: Both met periods, J&G events.**

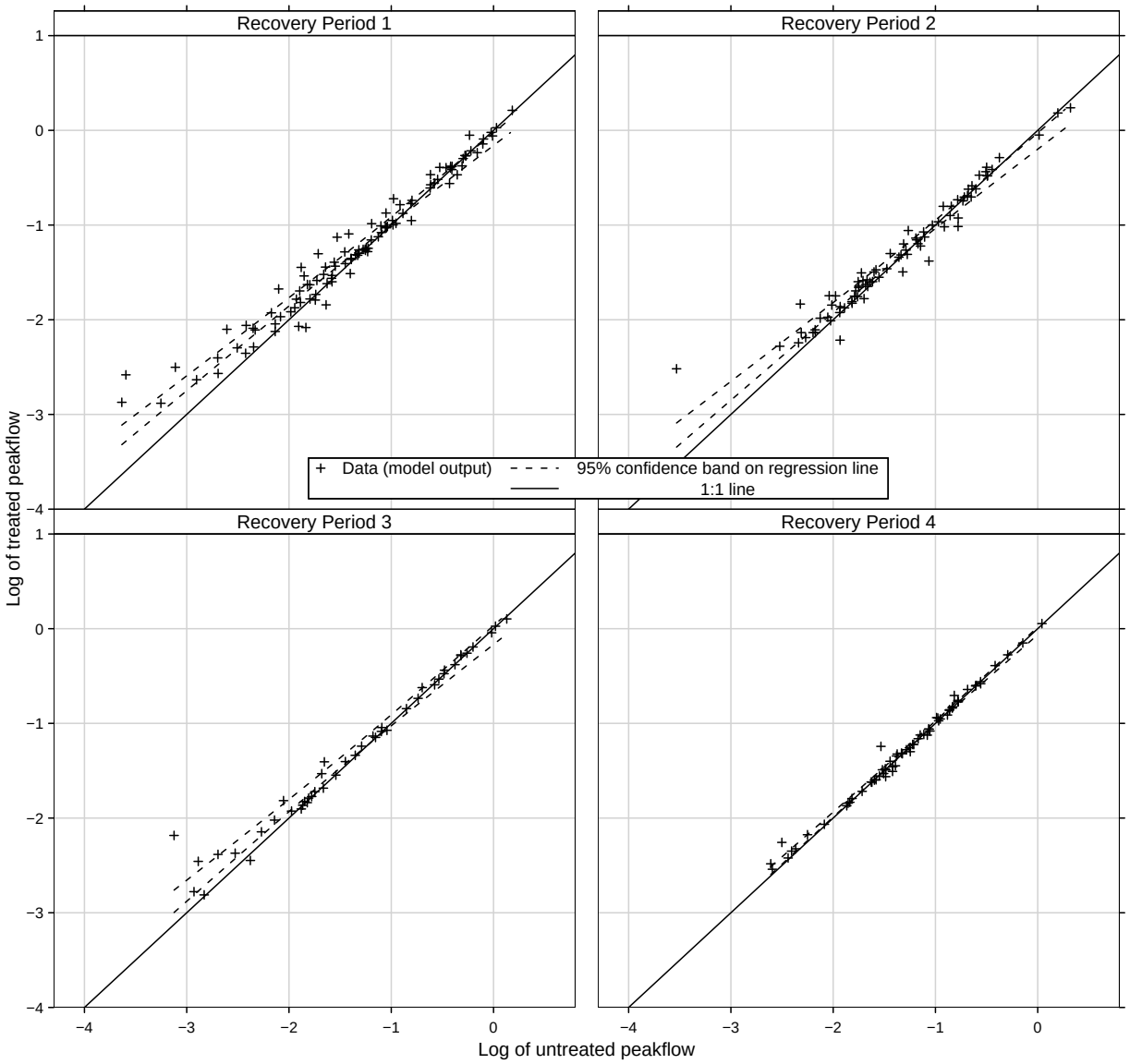

Figure 3.23: Regression of treated on untreated $\log_e$ peakflows from scenarios with WS1. 1:1 line corresponds to no treatment. Confidence band is on the regression *line* (not shown). **Subset 6: Both met periods, augmented J&G events.**

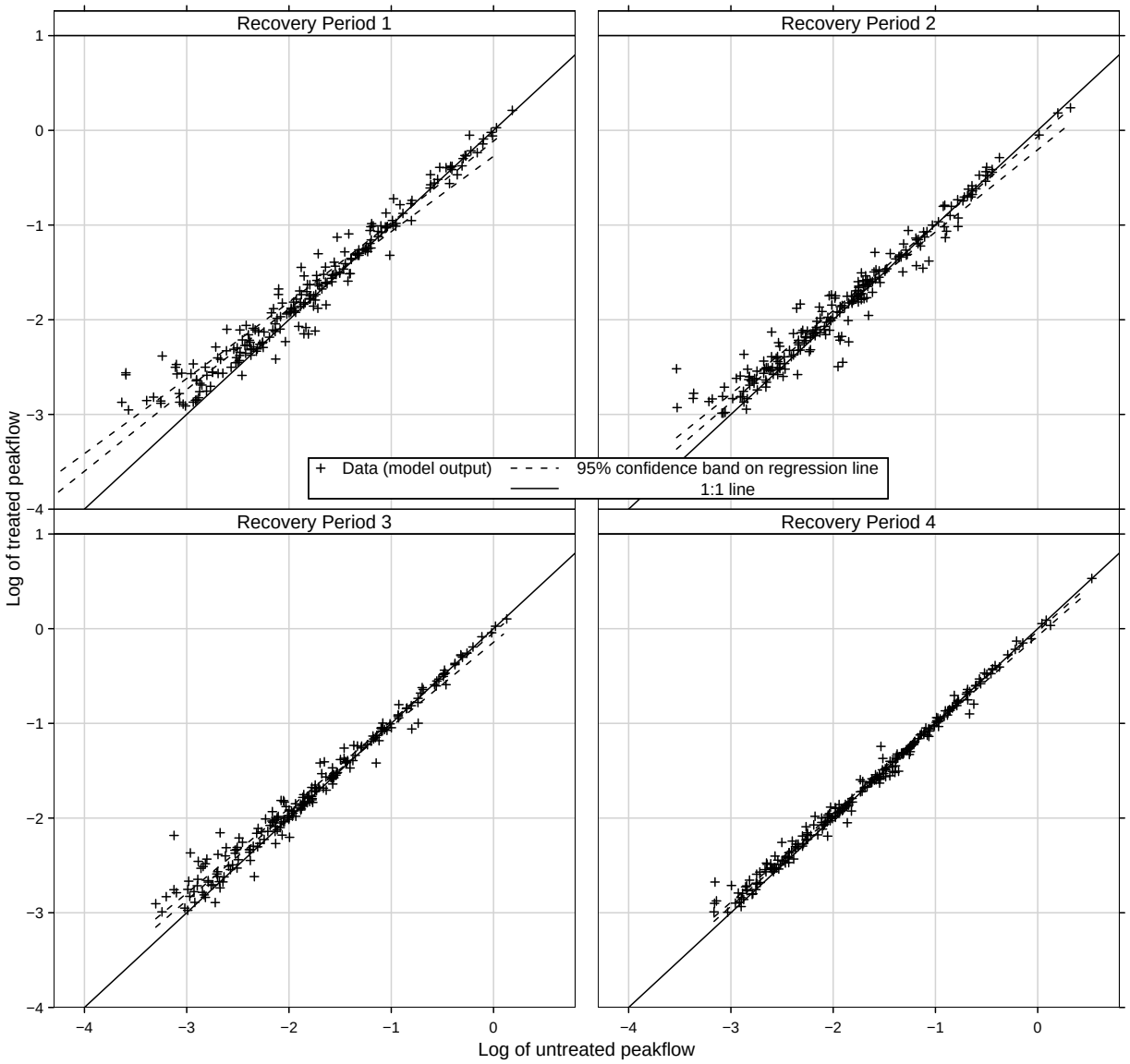

Figure 3.24: Regression of treated on untreated $\log_e$ peakflows from scenarios with WS1. 1:1 line corresponds to no treatment. Confidence band is on the regression *line* (not shown). **Subset 7: Both met periods, all events.**

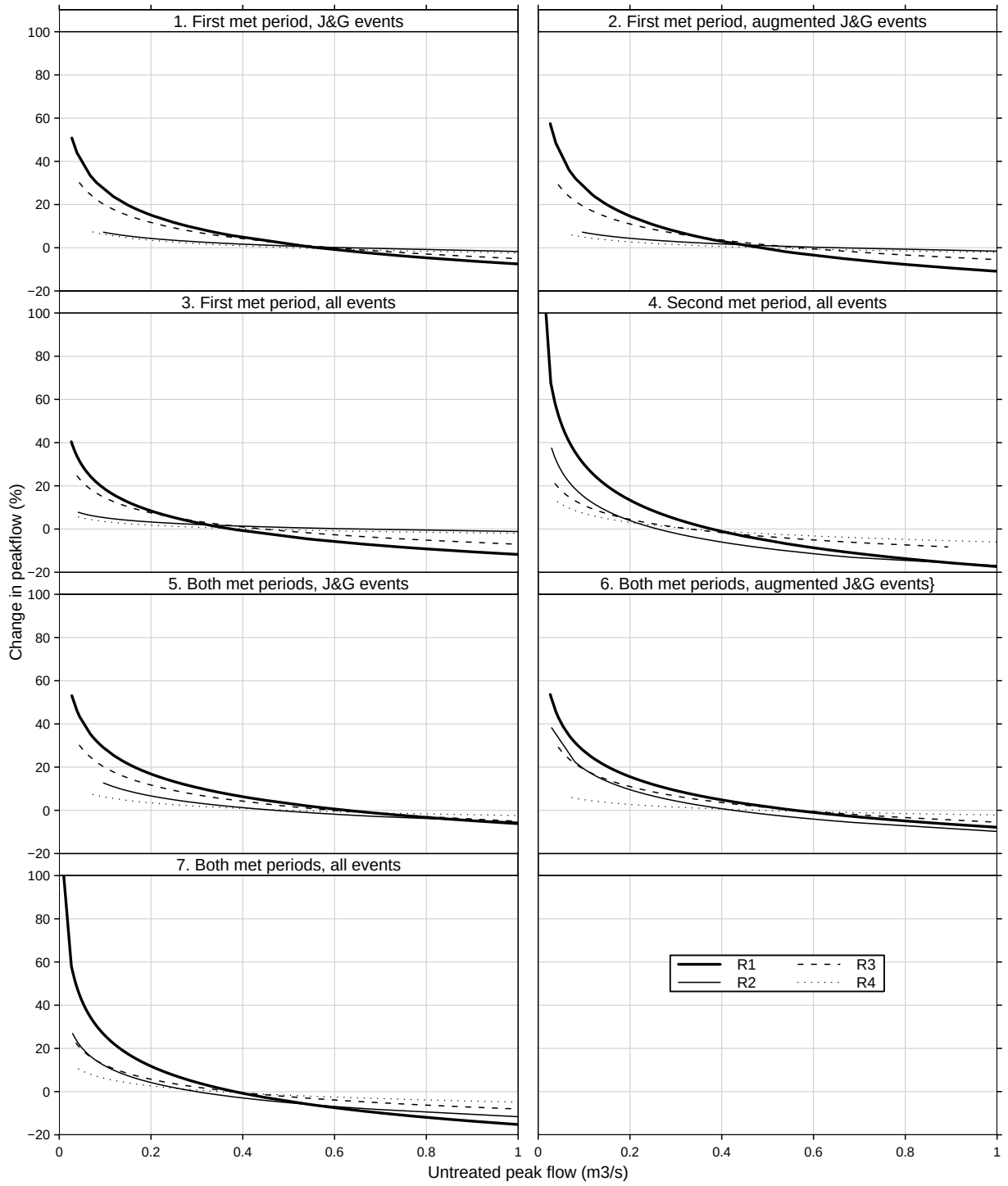

Figure 3.25: Percent increase of WS1 scenario peakflows from untreated to treated cases; vs. untreated flow rate. Methods after Thomas and Megahan (1998).

Table 3.11: Regressions of treated WS1 on untreated WS1 scenarios, using $\log_e$ of the discharges. Original units are in cubic meters per second; s=standard error of the residuals; n=sample size. All models were significant ($p < 0.0001$).

Period	Intercept	Slope	SE(Int.)	SE(Sl.)	s	R^2	n
Subset 1: First met period, J&G events							
R1	-0.092	0.864	0.0518	0.0311	0.17	0.96	35
R2	-0.02	0.963	0.0242	0.0161	0.063	0.99	42
R3	-0.064	0.899	0.0444	0.0271	0.15	0.97	37
R4	-0.027	0.963	0.0193	0.0142	0.058	0.99	54
Subset 2: First met period, augmented J&G events							
R1	-0.129	0.843	0.0466	0.0272	0.163	0.96	44
R2	-0.018	0.963	0.0232	0.0157	0.063	0.99	45
R3	-0.067	0.9	0.0393	0.024	0.14	0.97	45
R4	-0.023	0.97	0.0162	0.0115	0.054	0.99	67
Subset 3: First met period, all events							
R1	-0.139	0.872	0.041	0.0206	0.164	0.96	84
R2	-0.015	0.973	0.0225	0.0116	0.08	0.99	89
R3	-0.083	0.91	0.0329	0.0174	0.137	0.97	86
R4	-0.022	0.976	0.0126	0.0075	0.052	0.99	110
Subset 4: Second met period, all events							
R1	-0.226	0.803	0.0457	0.0223	0.228	0.91	137
R2	-0.211	0.855	0.0432	0.0204	0.179	0.93	133
R3	-0.102	0.913	0.0272	0.0136	0.11	0.97	126
R4	-0.065	0.943	0.0151	0.0077	0.075	0.99	133
Subset 5: Both met periods, J&G events							
R1	-0.074	0.864	0.0285	0.0186	0.142	0.96	87
R2	-0.062	0.925	0.0297	0.0201	0.099	0.97	67
R3	-0.064	0.899	0.0444	0.0271	0.15	0.97	37
R4	-0.027	0.963	0.0193	0.0142	0.058	0.99	54
Subset 6: Both met periods, augmented J&G events							
R1	-0.092	0.859	0.0271	0.0172	0.144	0.96	107
R2	-0.113	0.879	0.0345	0.0226	0.136	0.95	80
R3	-0.067	0.9	0.0393	0.024	0.14	0.97	45
R4	-0.023	0.97	0.0162	0.0115	0.054	0.99	67
Subset 7: Both met periods, all events							
R1	-0.194	0.828	0.0325	0.0161	0.208	0.92	221
R2	-0.136	0.898	0.028	0.0137	0.154	0.95	222
R3	-0.092	0.913	0.021	0.0107	0.122	0.97	212
R4	-0.052	0.953	0.0102	0.0055	0.067	0.99	243

Table 3.12: Slope tests for scenario regressions (Table 3.11) of treated WS1 on untreated WS1 scenarios. All slopes were different from 1.0 ($p < 0.0001$).

Period	Difference	t-statistic	DF
Subset 1: First met period, J&G events			
R1	-0.136	-23.82	33
R2	-0.037	-9.09	40
R3	-0.101	-20.53	35
R4	-0.037	-10.44	52
Subset 2: First met period, augmented J&G events			
R1	-0.157	-34.51	42
R2	-0.037	-9.42	43
R3	-0.1	-24.38	43
R4	-0.03	-12.53	65
Subset 3: First met period, all events			
R1	-0.128	-49.17	82
R2	-0.027	-16.09	87
R3	-0.09	-40.71	84
R4	-0.024	-21.39	108
Subset 4: Second met period, all events			
R1	-0.197	-90.2	135
R2	-0.145	-62.8	131
R3	-0.087	-52.02	124
R4	-0.057	-72.97	131
Subset 5: Both met periods, J&G events			
R1	-0.136	-55.69	85
R2	-0.075	-18.52	65
R3	-0.101	-20.53	35
R4	-0.037	-10.44	52
Subset 6: Both met periods, augmented J&G events			
R1	-0.141	-68.63	105
R2	-0.121	-32.38	78
R3	-0.1	-24.38	43
R4	-0.03	-12.53	65
Subset 7: Both met periods, all events			
R1	-0.172	-138.29	219
R2	-0.102	-84.33	220
R3	-0.087	-92.21	210
R4	-0.047	-103.31	241

Table 3.13: Intercept tests for scenario regressions (Table 3.11) of treated WS1 on untreated WS1 scenarios. "*" means intercept was not significantly different from 0 ($p > 0.0001$)

Period	Difference	t-statistic	DF	p-value
Subset 1: First met period, J&G events				
R1	-0.092	-5.86	33	$p < 0.0001$
R2	-0.02	-2.1	40	0.0419*
R3	-0.064	-4.89	35	$p < 0.0001$
R4	-0.027	-4.15	52	$p < 0.0001$
Subset 2: First met period, augmented J&G events				
R1	-0.129	-9.7	42	$p < 0.0001$
R2	-0.018	-2.1	43	0.0413*
R3	-0.067	-6.11	43	$p < 0.0001$
R4	-0.023	-4.85	65	$p < 0.0001$
Subset 3: First met period, all events				
R1	-0.139	-13.56	82	$p < 0.0001$
R2	-0.015	-2.37	87	0.0202*
R3	-0.083	-10.5	84	$p < 0.0001$
R4	-0.022	-6.98	108	$p < 0.0001$
Subset 4: Second met period, all events				
R1	-0.226	-24.69	135	$p < 0.0001$
R2	-0.211	-20.32	131	$p < 0.0001$
R3	-0.102	-15.14	124	$p < 0.0001$
R4	-0.065	-21.38	131	$p < 0.0001$
Subset 5: Both met periods, J&G events				
R1	-0.074	-12.98	85	$p < 0.0001$
R2	-0.062	-6.92	65	$p < 0.0001$
R3	-0.064	-4.89	35	$p < 0.0001$
R4	-0.027	-4.15	52	$p < 0.0001$
Subset 6: Both met periods, augmented J&G events				
R1	-0.092	-18.08	105	$p < 0.0001$
R2	-0.113	-12.97	78	$p < 0.0001$
R3	-0.067	-6.11	43	$p < 0.0001$
R4	-0.023	-4.85	65	$p < 0.0001$
Subset 7: Both met periods, all events				
R1	-0.194	-38.09	219	$p < 0.0001$
R2	-0.136	-26.67	220	$p < 0.0001$
R3	-0.092	-25.35	210	$p < 0.0001$
R4	-0.052	-33.65	241	$p < 0.0001$

4 Discussion

The simple meteorological modeling techniques resulted in high-quality hourly input for DHSVM. DHSVM was calibrated with met inputs P1 and C1, so it was anticipated that the corresponding model skill would be among the highest. The least model skill resulted with input C2, which had air temperature generated with the basic method and no shift or bias corrections. This highlights the sensitivity of snowfall, and wintertime streamflow, to precipitation phase in this rain-snow transition zone. Streamflow modeling was moderately sensitive to whether precipitation was distributed throughout the day as observed (P1) or uniformly over the day (P4). We anticipated that hourly observations of precipitation would have more impact on model skill in this steep and small watershed.

Applying a physically-based model forces the hydrologist to explicitly consider all of the major terms in the water balance. We identified and addressed a fundamental problem in previously published water balances for the HJA small watersheds. On a mean annual basis, Q and ET cannot explain about 12% of precipitation, using a conservative estimate of P. The monthly water balance suggests that the required additional loss is most active during the winter rainy season. We attribute this additional loss to groundwater flux out of the watersheds. Although we assumed a uniform groundwater recharge conductivity across soil types, the possibility of significant differences is suggested by the varying runoff ratios of the small watersheds during years when landcovers were the same. Rothacher et al. (1967) were the first to point out significant differences in runoff on area-depth basis among WS1,2,3, and suggested variable “deep seepage” might be one cause.

The role of ET has not been adequately explored in these much-studied watersheds. We suggest that more effort be placed on estimating rates of ET and its components at HJA. Ongoing sapflux experiments will be very helpful for constraining transpiration, and new microwave methods may make possible catchment-scale measurements of total ET (Parlange et al., 2001). More analysis of data from similar ecosystems would also help. Vegetation regrowth, one of the key factors for simulating ET, was prescribed simply and independently of local soil, terrain, and microclimate properties. Data on key properties such as LAI are needed for better model input and to guide a dynamic simulation of vegetation. Until we can better constrain such properties, we will be unsure as to how much of current model error is due to inadequate representation of vegetation.

High efficiency (> 0.7) and reasonably low bias in streamflow modeling were achieved at an hourly timestep over almost the entire period of record at HJA, and compared favorably with previous simulation efforts. Model calibration focused on the overall streamflow record, and tradeoffs in producing baseflow and quickflow resulted in a positive bias for low flows and negative bias for high flows. To improve baseflow simulation, we are currently developing a new approach for groundwater movement that will offer a deeper flowpath while still minimizing the number of parameters.

The biggest disappointment of the simulations was the prevailing underprediction of peakflows. The primary areas to improve are the representation of macropore flow and snow dynamics. For this study, we represented macropore flow by limiting infiltration and diverting more water to the surface routing mechanism. That approach did move water down the hillslope faster than subsurface flow, but was limited by the one cell-per-timestep algorithm for moving water from cell to cell. There are two possible solutions to this problem: 1) shorten flow path lengths by increasing the stream channel density, or 2) move water down the hillslope at a rate faster than

one cell per timestep. The second solution would be more in keeping with field observations. A cascade method could be used, wherein cells are processed in descending order of elevation and water moves from one cell to the next all the way down the hillslope within the timestep. A pure cascade, the upper bound on this flow rate, would move all of the surface water on the hillslope to the receiving channel within the timestep. This would be too extreme in most simulations, so either infiltration could be allowed on downslope cells, or a power law method could be used to leave some water behind on each cell so that only some of the water mass reaches the channel during the timestep. Another possible but more complicated scheme could involve representation of macropore flow as a subsurface variably saturated pipe network.

The second cause for underprediction of peakflows was a too-persistent snowpack in rain-on-snow events for both mature and young canopies. Part of the problem was a lack of sensible and latent heat transfer to drive melting. The current scheme for computing vertical wind profile and aerodynamic resistance in DHSVM was not sensitive enough to canopy state and may be overly complex for most applications. Here again we found tradeoffs, in trying to produce enough aerodynamic conductance for turbulent heat transfer to the snowpack, and but not too much conductance for driving evapotranspiration from the canopy. Storck (2000) was apparently successful in resolving these issues for another Pacific Northwest site, and more investigation into the similarities and differences of these sites would be helpful.

Statistical analysis of observed peakflows in previous studies was fairly conclusive but interpretations varied widely. Jones and Grant (1996) argued that forest treatments might increase the entire population of flows. Thomas and Megahan (1998) countered that increases in peakflows could only be detected in the empirical data up to recurrence intervals of approximately 2 years. Our modeling study doesn't improve the empirical insight with respect to peakflows, but does advance the technology closer to the goal of a practical tool for forest management. Although model error was significant and increased with increasing flow, the overall statistical conclusions based on model output were similar to those based on observations. Peakflow increases had an inverse trend with flow rate, similar to the findings of Thomas and Megahan (1998), but in some data subsets and time periods, decreases were predicted at the highest flow rates. Simulated treatment effects were somewhat smaller than previous empirical findings, but were statistically detectable and tended to decline with time. The clearest signals were obtained when comparing two simulations, especially if both were from the same watershed.

Analysis of WS1 scenario peakflows highlighted another problem with simulated runoff generation during rain-on-snow events—some treated peakflows were less than the untreated ones, mostly in medium-to-large events. These simulated events had in common greater snowmelt in the untreated case. The greater simulated snowmelt in the old-growth (untreated) case was caused by 1) greater areal extent of snowcover prior to the storm, and 2) more intercepted snow in the canopy available for rapid melt. Both mechanisms were related to the canopy density; the higher old-growth LAI tended to shelter the snowpack more from solar radiation and also allow more snow to be intercepted by the canopy before the peakflow. Both treatment and no-treatment cases had a ripe snowpack in these events, so throughfall falling on the ground snowpack was passed through to the soil, along with water from melting snow. Because the simulated rate of snowmelt is mostly independent of the snowpack water content, the key difference was the extent rather than thickness of the snowpack—there were many more grid cells holding snow in the old-growth case than in the treatment case. In contrast to this model behavior, Harr and McCorison (1979) found in an HJA field study that a clearcut tended to have more snowpack than a old-growth plot, and that the snowpack retarded water movement in rain-on-snow events, giving the same result of treated peakflow being less than untreated peakflow, but for different reasons. This conflict and others in the literature on rain-on-snow peakflows suggest a need for more understanding of terrain- and canopy-dependent snow accumulation and melt, and further model development.

Finally, the results suggest that our ability to simulate treatment effects is in part a function of the meteorological conditions (met input) driving runoff events. WS1 scenarios had distinctively different recovery trajectories, depending upon the meteorological data used. Simulation with the WY80-98 PRIMET hourly meteorological dataset produced a recovery trajectory with systematically declining treatment effects in time, whereas simulation with the input developed from WY58-79 CS2MET daily data did not.

5 Conclusions

Some common techniques for disaggregating daily meteorological data worked better than others, and in all cases the optimal prediction capability was obtained when some local knowledge was used. The modified sine curve method for air temperature worked significantly better than a [month,hour,precip] baseline mean only when a 2-hour shift was used. A uniform distribution of precipitation over the day was a better predictor than a [month,hour] baseline mean. For atmospheric transmittance, the Bristow-Campbell model calibrated to local conditions performed best, but the [month,precip] baseline mean was better than the Bristow-Campbell model with regional coefficients. For relative humidity, the [month,hour,precip] baseline mean was the best predictor, even compared to methods that used daily H_{min} and H_{max} data. The least effective humidity model used the $T_{min}=T_{dew}$ assumption and diurnal T variation, and should be avoided in modeling this cool, wet climate. Wind speed was the most difficult variable to reproduce, though the [month,hour,precip] baseline mean may have been a reasonably good predictor had measurement height not changed.

Application of the full set of met modeling methods, including timeseries shifts and bias corrections, yielded low-bias, high-efficiency met results for all variables except wind speed. It was possible to extend the hourly record of PRIMET back in time with confidence by making use of daily data from a nearby station CS2MET. Extension of the hourly met record facilitates hydrologic and ecologic modeling over the entire experimental period at HJA.

Alternative met input sets were found to significantly impact the predicted water balance and efficiency of streamflow simulation. For other uses of the model output, such as predicting flood magnitudes with further statistical modeling, the distinction between model runs may be much less than the gap between reality and simulation. The most significant differences in streamflow efficiency were related to differences in precipitation phase and therefore the air temperature method used. Streamflow efficiency was more sensitive to rain vs. snow than even the assumption of uniform precipitation or lack of bias correction when mapping from CS2MET to PRIMET. In the rain-snow transition zone, a hydrologic model calibrated to the temperature regime at a base station may have significant error when applied to a nearby station unless temperature bias is addressed. The most significant differences in water balance were related to increased evapotranspiration when the $T_{min}=T_{dew}$ humidity model was used.

A fundamental problem in previously published water balances at the HJA small watersheds was identified and addressed. Q and ET cannot explain about 12% of precipitation, using a conservative estimate of P, and we attribute this to deep groundwater flux. Explicit resolution of the water balance is a necessary part of physically-based modeling, and in this instance it forced a re-examination of long-held assumptions in a way that purely empirical research had failed to do. As a first step toward improving our understanding of the water balance at HJA, we included groundwater recharge with uniform K_g across soil types. In future modeling work, this term could be allowed vary across soil types along with K_l, and may help capture the variable runoff ratios observed in the WS1,2,3.

Vegetation regrowth was prescribed in a simple way, independent of local soil, terrain, and microclimate properties. LAI is getting less difficult to measure, thanks to LIDAR technology, and measuring LAI at the HJA would be a boon to the modeling community. Until we can better constrain the properties of the regrowing forest that figure directly into models, we will be unsure as to how much of current model error is due to inadequate representation of vegetation. A

prototype version of version of DHSVM with dynamic vegetation provided by the biogeochemical model BIOME-BGC exists (Waichler, 2000) and could be further developed using HJA as a test case. To effectively apply such a model for predicting changes in hydrology caused by changing vegetation cover, we will first need better transient and distibuted data on properties like LAI to verify the vegetation simulation. We will also need to better understand through empirical work why runoff ratio should vary across similar watersheds and through time.

High efficiency (> 0.7) and reasonably low bias in streamflow modeling were achieved at an hourly timestep over almost the entire period of record at HJA. Increases in treatment peakflows with magnitude and statistical significance similar to the previous work of T&M were obtained from the simulations, especially when both peaks were simulated. Peakflow increases had an inverse trend with flow rate, similar in shape to the findings of Thomas and Megahan (1998), but in some data subsets and time periods, decreases were predicted at the highest flow rates. These decreases resulted from simulated rain-on-snow events where rain fell on ripe snowpack, and there was a greater extent of ground snow cover in the old-growth case, providing more snowmelt to augment the rain than in the immature forest case.

The goodness-of-fit of DHSVM in the small HJA watersheds was encouraging. We believe there is room for significant improvement in the representation of macropore flow and snow dynamics. There is also room for improvement in the final calibration, using more sampling of parameter values and techniques like genetic algorithms to partially automate the process. More comprehensive analysis of the optimal spatial representation for these small watersheds would also be productive. It is possible that larger grid cells or even elevation bands would yield streamflow simulations that are just as accurate but with faster runtimes.

We suggest the following areas for further research and development:

- Representation of macropore flow with hillslope cascades or variably saturated subsurface pipe networks
- Critical evaluation of the costs and benefits of a range of DHSVM model structures, spatial resolutions, and temporal resolutions for model performance
- Direct comparison of DHSVM to other watershed models with same dataset
- Simulation of forest treatment effects in other climate and forest types
- Coordination with forest managers to design and implement further model testing and applications involving operational use of model predictions.
- Use of genetic algorithm and distributed computing methods to facilitate testing of large numbers of parameter sets
- Simulation of forest regrowth, biogeochemistry, and hydrology using BIOME-BGC and PHREEQC coupled to DHSVM

References

Anderson, S., Dietrich, W., Montgomery, D., Torres, R., Conrad, M., and Loague, K. (1997). Subsurface flow paths in a steep, unchanneled catchment. *Water Resources Research*, 33(12):2653–2673.

Beschta, R., Pyles, M., Skaugset, A., and Surfleet, C. (2000). Peakflow responses to forest practices in the western Cascades of Oregon, USA. *Journal of Hydrology*, 233:102–120.

Bierlmaier, F. A. and McKee, A. (1989). Climatic summaries and documentation for the primary meteorological station, H.J. Andrews Experimental Forest, 1972 to 1984. Technical report, U.S. Department of Agriculture, Forest Service, Pacific Northwest Research Station, Portland, OR. PNW-242.

Bowling, L. and Lettenmaier, D. (1997). Evaluation of the Effects of Forest Roads on Streamflow in Hard and Ware Creeks, Washington. Technical Report Water Resources Series No. 155, Dept. of Civil Engineering, University of Washington, Seattle, Washington.

Bras, R. (1990). *Hydrology, An Introduction to Hydrologic Science*. Addison-Wesley, Reading, MA.

Bredensteiner, K. C. (1998). An Investigation of Vegetation-Hydrology Interactions in Watershed 1 at the H.J. Andrews Experimental Forest. Master's thesis, Oregon State University. 168 pp.

Bristow, K. and Campbell, G. (1984). On the relationship between incoming solar radiation and daily maximum and minimum temperature. *Agricultural and Forest Meteorology*, 31:159–166.

Clapp, R. and Hornberger, G. (1978). Empirical Equations for Some Soil Hydraulic Properties. *Water Resources Research*, 14(4):601–604.

Cosby, B., Hornberger, G., Clapp, R., and Ginn, T. (1984). A statistical exploration of the relationships of soil moisture characteristics to the physical properties of soils. *Water Resources Research*, 20(6):682–690.

Daly, C., Neilson, R., and Phillips, D. (1996). A statistical-topographic model for mapping climatological precipitation over mountainous terrain. *Journal of Applied Meteorology*, 33:140–158.

Dickinson, R., Henderson-Sellers, A., Rosenzweig, C., and Sellers, P. (1991). Evapotranspiration models with canopy resistance for use in climate models, a review. *Agricultural and Forest Meteorology*, 54:373–388.

Duan, J. (1996). *A Coupled Hydrologic-Geomorphic Model for Evaluating Effects of Vegetation Change of Watersheds*. PhD thesis, Oregon State University. 131 pp.

Dyrness, C. (1969). Hydrologic properties of soils on three small watersheds in the western Cascades of Oregon. Technical report, Forest and Range Experiment Station, USDA, Portland, OR. Pacific Northwest Research Note.

ESRI (1999). *ArcInfo version 8.0.1 and ArcDoc 8.0.1 on-line documentation*. Environmental Systems Research Institute, Redlands, CA.

Feddes, R., Kowalik, P., and Zaradny, H. (1978). *Simulation of field water use and crop yield*. Wiley, New York. 188 pp.

Gates, D. (1980). *Biophysical Ecology*. Springer-Verlag, New York.

Harmon, M. E. and Sexton, J. (1995). Water balance of conifer logs in early stages of decomposition. *Plant and Soil.*, 172:141–152.

Harr, R. D. and McCorison, F. M. (1979). Initial effects of clearcut logging on size and timing of peak flows in a small watershed in western Oregon. *Water Resources Research*, 15(1):90–94.

Henshaw, D. L., Bierlmaier, F. A., and Hammond, H. E. (1998). The H.J. Andrews climatological field measurement program. In Michener, W. K., Porter, J. H., and Stafford, S. G., editors, *Data and information management in the ecological sciences: a resource guide*, pages 117–122. LTER Network Office, University of Mexico. http://www.lternet.edu/ecoinformatics/guide/henshaw1.fv2.htm.

Holtan, H. (1961). A concept of infiltration estimates in watershed engineering. Technical report, USDA, Washington, D.C. Paper 41-51.

Jenson, S. K. and Domingue, J. O. (1998). Extracting topograhic structure from digital elevation data for geographic information system analyses. *Photogrammetric Engineering and Remote Sensing*, 54(11):1593–1600.

Jones, J. (2000). Hydrologic processes and peak discharge response to forest removal, regrowth, and roads in 10 small experimental basins, western Cascades, Oregon. *Water Resources Research*, 36(9):2621–2642.

Jones, J. A. and Grant, G. E. (1996). Peak flow responses to clear-cutting and roads in small and large basins, western Cascades, Oregon. *Water Resources Research*, 32(4):959–974.

LaMarche, J. L. and Lettenmeier, D. P. (2001). Effects of forest roads on flood flows in the Deschutes River, Washington. *Earth Surface Processes and Landforms*, 26:115–134.

Legates, D. and McCabe, G. (1999). Evaluating the use of “goodness-of-fit” measures in hydrologic and hydroclimatic model validation. *Water Resources Research*, 35(1):233–241.

Maidment, D. R., editor (1993). *Handbook of Hydrology*. McGraw-Hill.

Marks, D., Kimball, J., Tingey, D., and Link, T. (1998). The sensitivity of snowmelt processes to climate conditions and forest cover during rain-on-snow: a case study of the 1996 Pacific Northwest flood. *Hydrological Processes*, 12:1569–1587.

Nash, J. and Sutcliffe, J. (1970). River flow forecasting through conceptual models, Part 1—A discussion of principles. *Journal of Hydrology*, 10:282–290.

Nijssen, B., Haddeland, I., and Lettenmaier, D. (1997). Point evaluation of a surface hydrology model for BOREAS. *Journal of Geophysical Research*, 102(29):367–378.

Parlange, M. B., Pahlow, M., Bou-Zeid, E., and Kumar, V. (2001). Land-atmosphere coupling over complex hilly terrain: case studies. In Band, L. and McDonnell, J., editors, *Chapman Conference on State-of-the-Art in Hillslope Hydrology*, Sunriver, Oregon. American Geophysical Union.

Parton, W. and Logan, J. (1981). A model for diurnal variation in soil and air temperature. *Agricultural Meteorology*, 23:205–216.

Post, D. and Jones, J. (2001). Hydrologic regimes of forested, mountainous, headwater basins in New Hampshire, North Carolina, Oregon, and Puerto Rico. *Advances in Water Resources*, 24:1195–1210.

Richards, F. (1959). A flexible growth function for empirical use. *Journal of Experimental Biology*, 10:290–300.

Rosentrater, L. (1997). The Thermal Climate of the H.J. Andrews Experimental Forest, Oregon. Master's thesis, University of Oregon.

Rothacher, J. (1965). Streamflow from small watersheds on the western slope of the Cascade Range of Oregon. *Water Resources Research*, 1(1):125–134.

Rothacher, J. (1970). Increases in water yield following clear-cut logging in the Pacific Northwest. *Water Resources Research*, 6(2):653–658.

Rothacher, J., Dyrness, C., and Fredriksen, R. L. (1967). Hydrologic and related characteristics of three small watersheds in the Oregon Cascades. Technical report, Pacific Northwest Forest and Range Experiment Station, Forest Service, USDA, Corvallis, Oregon.

Running, S., Nemani, R., and Hungerford, R. (1987). Extrapolation of synoptic meteorological data in mountainous terrain and its use for simulating forest evapotranspiration and photosynthesis. *Canadian Journal of Forestry Research*, 17:472–483.

Sidle, R., Tsuboyama, Y., Noguchi, S., Hosoda, I., Fujieda, M., and Shimizu, T. (2000). Stormflow generation in steep forested headwaters: a linked hydrogeomorphic paradigm. *Hydrological Processes*, 14:369–385.

Storck, P. (2000). Trees, snow and flooding: an investigation of forest canopy effects on snow accumulation and melt at the plot and watershed scales in the Pacific Northwest. Technical report, Dept. Civil Engineering, University of Washington. Water Resource Series, No. 161.

Storck, P., Bowling, L., Wetherbee, P., and Lettenmaier, D. (1998). Application of a GIS-based distributed hydrologic model for the prediction of forest harvest effects of peak flow in the Pacific Northwest. *Hydrological Processes*, 12:889–904.

Szilagyi, J. and Parlange, M. B. (1999). A geomorphology-based semi-distributed watershed model. *Advances in Water Resources*, 23:177–187.

Tague, C. and Band, L. (2001a). Evaluating explicit and implicit routing for watershed hydro-ecological models of forest hydrology at the small catchment scale. *Hydrological Processes*, 15(8):1415–1439.

Tague, C. and Band, L. (2001b). Simulating the impact of road construction and forest harvesting on hydrologic response. *Earth Surface Processes and Landforms*, 26(2):135–151.

Thomas, R. (2002). Revised small-basin regression test in Thomas and Megahan (1998) peak-flow paper. January 22, 2002.

Thomas, R. B. and Megahan, W. F. (1998). Peak flow responses to clear-cutting and roads in small and large basins, western Cascades, Oregon: A second opinion. *Water Resources Research*, 34(12):3393–3403.

Thornton, P. and Running, S. (1999). An improved algorithm for estimating incident daily solar radiation from measurements of temperature, humidity, and precipitation. *Agricultural and Forest Meteorology*, 93:211–228.

Thornton, P., Running, S., and White, M. (1997). Generating surfaces of daily meteorological variables over large regions of complex terrain. *Journal of Hydrology*, 190:214–251.

USGS (1982). Guidelines for determining flood flow frequency: Bulletin 17B of the Hydrology Subcommittee. Technical report, Interagency Advisory Committee on Water Data, Office of Water Data Coordination, United States Geological Survey, Reston, Virginia.

Waichler, S. R. (2000). *Simulation of vegetation and hydrology for climate change analysis of a mountain watershed*. PhD thesis, Oregon State University. 108 pp.

Wemple, B. C. (1998). *Investigations of runoff production and sedimentation on forest roads*. PhD thesis, Oregon State University. 168 pp.

Wigmosta, M. S., Nijssen, B., and Storck, P. (2002). *in Mathematical Models of Small Watershed Hydrology and Applications*, chapter 2. The Distributed Hydrology Soil Vegetation Model, pages 7–42. Water Resources Publications LLC.

Wigmosta, M. S. and Perkins, W. P. (1997). A GIS-based modeling system for watershed analysis. Technical report, National Council of the Paper Industry for Air and Stream Improvement (NCASI).

Wigmosta, M. S., Vail, L. W., and Lettenmaier, D. P. (1994). A distributed hydrology-vegetation model for complex terrain. *Water Resources Research*, 30(6):1665–1679.

Wilcox, B., Rawls, W., Brakensiek, D., and Wight, J. (1990). Predicting Runoff From Rangeland Catchments: A Comparison of Two Models. *Water Resources Research*, 26(10):2401–2410.

A Statistics for evaluating model skill

Bias and several goodness-of-fit measures were the primary statistics used to evaluate model skill in reproducing climate variables and streamflow. The overall approach and several definitions are taken from Legates and McCabe (1999), an excellent reference on goodness-of-fit measures.

Bias B is defined as the ratio of predicted (simulated) mean to observed mean

$$B = \frac{\overline{P}}{\overline{O}} \tag{A.1}$$

where

$\overline{P} =$ mean of the predictions
$\overline{O} =$ mean of the observations

The familiar R^2, or square of Pearson's product-moment correlation coefficient, describes the portion of total variance in the observed data that can be explained by the model, and ranges from 0.0 to 1.0:

$$R^2 = \left\{ \frac{\sum_{i=1}^{N} (O_i - \overline{O})(P_i - \overline{P})}{\left[\sum_{i=1}^{N} (O_i - \overline{O})^2\right]^{0.5} \left[\sum_{i=1}^{N} (P_i - \overline{P})^2\right]^{0.5}} \right\}^2 \tag{A.2}$$

where

$N =$ number of timesteps
$O_i =$ observed value at timestep i
$P_i =$ the predicted value at timestep i

There are two disadvantages of R^2 for describing model skill: 1) any linear relationship between the observations and the predictions, not necessarily a 1:1 relationship, results in a high value of R^2; 2) the squaring of terms gives too much weight to large values. In the case of streamflow, a high R^2 value may indicate good fit of peakflows but mask poor model skill during baseflow periods.

The Nash and Sutcliffe (1970) efficiency E is a tougher test than R^2 and casts the mean of the observations as a benchmark for the model:

$$E = 1.0 - \frac{\sum_{i=1}^{N} (O_i - P_i)^2}{\sum_{i=1}^{N} (O_i - \overline{O})^2}. \quad \text{(A.3)}$$

Values of E tend to be slightly less than R^2 in the case of streamflow.

Three first-degree goodness-of-fit measures from Legates and McCabe (1999) use absolute values of differences instead of squares. The first-degree efficiency is defined as

$$E_1 = 1.0 - \frac{\sum_{i=1}^{N} \mid O_i - P_i \mid}{\sum_{i=1}^{N} \mid O_i - \overline{O} \mid}. \quad \text{(A.4)}$$

E_1 is an improvement over E when evaluating model skill at low and moderate streamflow levels, but the grand mean is still the basis of comparison. A further discrimination can be made by using a baseline mean that involves some kind of seasonal or other categorical variation inherent in the data. For example, the baseline mean for streamflow was defined as the mean for each month of the year, where the mean is taken across all years in the simulation. Avoidance of squaring and use of baseline mean instead of the grand mean provides tougher, more revealing tests of model skill.

The baseline-adjusted, first-degree efficiency is

$$E_1' = 1.0 - \frac{\sum_{i=1}^{N} \mid O_i - P_i \mid}{\sum_{i=1}^{N} \mid O_i - \overline{O'} \mid} \quad \text{(A.5)}$$

where $\overline{O'}$ = baseline mean of the observations, variable in time. Adding another level for specifying the baseline mean is denoted by double prime, E_1''.

All of the above measures of efficiency have a possible range of $-\infty$-1.0. When efficiency=0, the model is no better or worse than the observed mean as a predictor. The closer the baseline mean is to the individual observations, the lower the efficiency is likely to be.

The baseline-adjusted modified index of agreement is

$$d_1' = 1.0 - \frac{\sum_{i=1}^{N} \mid O_i - P_i \mid}{\sum_{i=1}^{N} \left(\mid P_i - \overline{O'} \mid + \mid O_i - \overline{O'} \mid \right)}. \quad \text{(A.6)}$$

d_1' has the advantage of having the same range as the familiar R^2, 0 to 1.0.

B Main DHSVM input files

The main input values are listed below, including filenames of spatial and meteorological input, control variables, and soil and vegetation properties. Following the complete file for WS2 are those lines that were different for WS1 and WS3. These inputs were used for simulations of historical conditions (not scenarios) during WY80-98; inputs for other model runs differed slightly.

WS2

/projects/dhsvm/hja/output/ws2/11-9-01/ws2_input.11-09-01.1140.txt:

```
################################################################################
#OPTIONS SECTION
################################################################################
[OPTIONS]
Radiation                   = INLINE
Format                      = BIN
Extent                      = BASIN
Gradient                    = TOPOGRAPHY              # WATERTABLE
Read Flow Directions        = TRUE
Sensible Heat Flux          = FALSE
MM5                         = FALSE
Precipitation Source        = STATION
Wind Source                 = STATION
Flow Routing                = NETWORK
Hydraulic Routing           = TRUE

Interpolation        = INVDIST #VARCRESS           #INVDIST,NEAREST,VARCREST
MM5                  = FALSE          # TRUE if the MM5 interface is to
                      # be used, FALSE otherwise.  This
                      # option overrides all other met
                      # options
QPF                  = FALSE              # can only be set to true if MM5 is true
                      # setting qpf true will override the mm5
                      # precipitation fields with qpf pseudo stations
                      # defined in the meteorology section
                              # files follow standard met format: but only precip needed
Prism                = FALSE  # interpolate precip based on prism data
                          # Maps for each month will be read from
                      # the same directory as the model state
                          # Maps must be named PrismMap.xx.bin
                      # where xx is month (zeros packed)
                      # PrismMaps must match the DEM dims exactly
Snotel               = FALSE              # if true then all station veg data will be set
                      # to no overstory (i.e. bare)
Outside              = FALSE   # allow met stations outside of bounding box (doesn't help with single-station, non-PRISM situati
Rhoverride           = FALSE              # if true, set local Rh=100% if local Precip>0
Precipitation Source = STATION            # STATION or RADAR
Wind Source          = STATION            # STATION or MODEL
Shading              = TRUE

################ VARIABLE CRESTMAN INTERPOLATION ################################
# The following two options only need to be filled out if the VARCREST
# interpolation scheme is specified above

Cressman Radius        =  10           # radius in model pixels
```

```
Cressman Stations      =   4            # maximum number of stations to
                                      #interpolate on at each pixel

################ LAPSE RATES ##################################################

Temperature Lapse Rate       = CONSTANT
Precipitation Lapse Rate     = CONSTANT

################ Infiltration Rate ############################################
Infiltration                 = VARIABLE

###############################################################################
#MODEL AREA SECTION
###############################################################################
[AREA]
Coordinate System            = UTM
Extreme North                = 4895635.0
Extreme West                 = 560365.0
Center Latitude              = 44.21
Center Longitude             = 122.26
Time Zone Meridian           = 120
Number of Rows               = 79
Number of Columns            = 110
Grid Spacing                 = 10
Point North                  =
Point East                   =

###############################################################################
#TIME SECTION
###############################################################################
[TIME]
Time Step                    = 1
Model Start                  = 10/01/1979-00
Model End                    = 09/30/1998-23

###############################################################################
#CONSTANTS SECTION
###############################################################################
[CONSTANTS]
Ground Roughness             = .01
Snow Roughness               =  0.001
Rain Threshold               =  -1
Snow Threshold               =  1.4
Snow Water Capacity          =  0.06
Reference Height             = 65.0
Rain LAI Multiplier          = 0.000386
Snow LAI Multiplier          = 0.004
Min Intercepted Snow         =  0.005
Outside Basin Value          = 0

################ LAPSE RATES ##################################################

Temperature Lapse Rate       = -0.004
Precipitation Lapse Rate     = 0.0002

###############################################################################
#TERRAIN INFORMATION SECTION
###############################################################################
[TERRAIN]
DEM File                     = /projects/dhsvm/hja/input/ws2_dem.bin
Basin Mask File              = /projects/dhsvm/hja/input/ws2_mask.bin
Flow Direction File          = /projects/dhsvm/hja/input/ws2_fld.bin

###############################################################################
#ELEVATION BAND INFORMATION SECTION
###############################################################################
[ELEVBAND]
ElevBand Input File          = /projects/dhsvm/hja/input/Regional.dat
ElevBand Output File         = /projects/dhsvm/hja/input/ElevBand.out
```

```
################################################################################
#ROUTING SECTION
################################################################################
[ROUTING]

################ UNIT HYDROGRAPH ###############################################
Travel Time File             =
Unit Hydrograph File         =

################ STREAM NETWORK ################################################
Stream Network File          = /projects/dhsvm/hja/input/ws2_stnetwork.dat
Stream Map File              = /projects/dhsvm/hja/input/ws2_stmap.dat
Stream Class File            = /projects/dhsvm/hja/input/stream-class.dat

################ ROAD NETWORK ##################################################
Road Network File            = none
Road Map File                = none
Road Class File              = none

################################################################################
#METEOROLOGY SECTION
#Road Map File                =
#Road Class File              =
################################################################################
[METEOROLOGY]
Number of Stations           = 1


################ STATION 1 #####################################################
Station Name 1               = PRIMET (phony location, 500m south and east from upper left coordinates--to make sure within wate
North Coordinate 1           = 4895240.   # actual=4895460.; basin middle=4895240.
East Coordinate 1            = 560915.    # actual=559450.; basin middle=560915.
Elevation 1                  = 430.0
Station File 1               = /projects/dhsvm/hja/met/primet_hourly_WY80-98.dat

# number of lapse rates (1 or 2) if they are variable and break elevation
Number Temp Lapse Rates 2    = 1
Number Precip Lapse Rates 2  = 1
Elevation Break Point 2      = 1402.

################ IPW FILES #####################################################
IPW Table File               =
IPW Map File                 =

################ RADAR #########################################################
Radar Start                  =
Radar File                   =
Radar Extreme North          =
Radar Extreme West           =
Radar Grid Spacing           =
Radar Number of Rows         =
Radar Number of Columns      =

################ 3.0 MODEL #####################################################
Number of Wind Maps          =
Wind File Basename           =
Wind Map Met Station         =

################ MM5 ###########################################################
MM5 Start                    =
MM5 Temperature File         =
MM5 Humidity File            =
MM5 Wind Speed File          =
MM5 Shortwave File           =
MM5 Longwave File            =
MM5 Precipitation File       =
MM5 Pressure File            =
MM5 Soil Temperature File 0  =
```

```
################################################################################
#SOILS INFORMATION SECTION
################################################################################
[SOILS]
Soil Depth File              = /projects/dhsvm/hja/input/ws2_soildepth.bin
Soil Map File                = /projects/dhsvm/hja/input/ws2_soiltype.bin
Soil Depth Multiplier        =  1
Number of Soil Types         = 7

################ SOIL 1 (44) ###################################################
Soil Description 1           = Budworm
Lateral Conductivity 1       =  0.000363
Exponential Decrease 1       =  2
Maximum Infiltration 1       = 1e-5
Surface Albedo 1             = 0.1
Number of Soil Layers 1      = 3
Porosity 1                   = 0.44 0.46 0.46
Pore Size Distribution 1     = 0.28 0.28 0.30
Bubbling Pressure 1          = 0.3389 .4423 .4118
Field Capacity 1             =  0.35  0.38  0.37
Wilting Point 1              =  0.13  0.14  0.13
Bulk Density 1               = 750. 1400. 1500.
Vertical Conductivity 1      =  2.904e-06  3.63e-05  3.63e-05
Thermal Conductivity 1       = 7.11 6.92 8.01
Thermal Capacity 1           = 1.4e6 1.4e6 1.4e6
Infiltration Coefficient 1   =  8.78e-09
Infiltration Exponent 1      =  1.3
Quick Flow Coefficient 1     =  0.555
Quick Flow Exponent 1        =  2
Groundwater Conductivity 1   =  2.4e-08
Maximum Ground Melt 1        = 0.0

################ SOIL 2 (21) ###################################################
Soil Description 2           = Flunky
Lateral Conductivity 2       =  2.59e-05
Exponential Decrease 2       =  2
Maximum Infiltration 2       = 1e-5
Surface Albedo 2             = 0.1
Number of Soil Layers 2      = 3
Porosity 2                   = 0.45 0.42 0.42
Pore Size Distribution 2     = 0.321 0.353 0.353
Bubbling Pressure 2          = 0.3373 0.1755 0.1755
Field Capacity 2             =  0.35  0.28  0.28
Wilting Point 2              =  0.11  0.08  0.08
Bulk Density 2               = 750. 1400. 1500.
Vertical Conductivity 2      =  2.072e-07  2.59e-06  2.59e-06
Thermal Conductivity 2       = 7.11 6.92 8.01
Thermal Capacity 2           = 1.4e6 1.4e6 1.4e6
Infiltration Coefficient 2   =  8.78e-09
Infiltration Exponent 2      =  1.3
Quick Flow Coefficient 2     =  0.555
Quick Flow Exponent 2        =  2
Groundwater Conductivity 2   =  2.4e-08
Maximum Ground Melt 2        = 0.0

################ SOIL 3 (51) ###################################################
Soil Description 3           = Frissell
Lateral Conductivity 3       =  0.000395
Exponential Decrease 3       =  2
Maximum Infiltration 3       = 1e-5
Surface Albedo 3             = 0.1
Number of Soil Layers 3      = 3
Porosity 3                   = 0.42 0.43 0.43
Pore Size Distribution 3     = 0.239 0.223 0.223
Bubbling Pressure 3          = 0.2044 0.2876 0.2876
Field Capacity 3             =  0.31  0.33  0.33
Wilting Point 3              =  0.13  0.14  0.14
Bulk Density 3               = 750. 1400. 1500.
```

```
Vertical Conductivity 3      =  3.16e-06  3.95e-05  3.95e-05
Thermal Conductivity 3       = 7.11 6.92 8.01
Thermal Capacity 3           = 1.4e6 1.4e6 1.4e6
Infiltration Coefficient 3   =  8.78e-09
Infiltration Exponent 3      =  1.3
Quick Flow Coefficient 3     =  0.555
Quick Flow Exponent 3        =  2
Groundwater Conductivity 3   =  2.4e-08
Maximum Ground Melt 3        = 0.0

################## SOIL 4 (41) ############################################################
Soil Description 4           = Limberlost
Lateral Conductivity 4       =  0.0001095
Exponential Decrease 4       =  2
Maximum Infiltration 4       = 1e-5
Surface Albedo 4             = 0.1
Number of Soil Layers 4      = 3
Porosity 4                   = 0.44 0.45 0.45
Pore Size Distribution 4     = 0.293 0.281 0.281
Bubbling Pressure 4          = 0.2900 0.3613 0.3613
Field Capacity 4             =  0.33  0.35  0.35
Wilting Point 4              =  0.12  0.13  0.13
Bulk Density 4               = 750. 1400. 1500.
Vertical Conductivity 4      =  8.76e-07  1.095e-05  1.095e-05
Thermal Conductivity 4       = 7.11 6.92 8.01
Thermal Capacity 4           = 1.4e6 1.4e6 1.4e6
Infiltration Coefficient 4   =  8.78e-09
Infiltration Exponent 4      =  1.3
Quick Flow Coefficient 4     =  0.555
Quick Flow Exponent 4        =  2
Groundwater Conductivity 4   =  2.4e-08
Maximum Ground Melt 4        = 0.0

################ SOIL 5 (54) ############################################################
Soil Description 5           = McKenzie River
Lateral Conductivity 5       =  0.000409
Exponential Decrease 5       =  2
Maximum Infiltration 5       = 1e-5
Surface Albedo 5             = 0.1
Number of Soil Layers 5      = 3
Porosity 5                   = 0.46 0.46 0.47
Pore Size Distribution 5     = 0.227 0.176 0.148
Bubbling Pressure 5          = 0.5856 0.8434 1.099
Field Capacity 5             =  0.39  0.41  0.42
Wilting Point 5              =  0.17  0.2  0.22
Bulk Density 5               = 750. 1400. 1500.
Vertical Conductivity 5      =  3.272e-06  4.09e-05  4.09e-05
Thermal Conductivity 5       = 7.11 6.92 8.01
Thermal Capacity 5           = 1.4e6 1.4e6 1.4e6
Infiltration Coefficient 5   =  8.78e-09
Infiltration Exponent 5      =  1.3
Quick Flow Coefficient 5     =  0.555
Quick Flow Exponent 5        =  2
Groundwater Conductivity 5   =  2.4e-08
Maximum Ground Melt 5        = 0.0

################ SOIL 6 (20) ############################################################
Soil Description 6           = Rockland
Lateral Conductivity 6       =  3.525e-05
Exponential Decrease 6       =  2
Maximum Infiltration 6       = 1e-5
Surface Albedo 6             = 0.1
Number of Soil Layers 6      = 3
Porosity 6                   = 0.40 0.40 0.40
Pore Size Distribution 6     = 0.413 0.413 0.413
Bubbling Pressure 6          = 0.1118 0.1118 0.1118
Field Capacity 6             =  0.22  0.22  0.22
Wilting Point 6              =  0.05  0.05  0.05
Bulk Density 6               = 750. 1400. 1500.
```

```
Vertical Conductivity 6      =  2.82e-07  3.525e-06  3.525e-06
Thermal Conductivity 6       = 7.11 6.92 8.01
Thermal Capacity 6           = 1.4e6 1.4e6 1.4e6
Infiltration Coefficient 6   =  8.78e-09
Infiltration Exponent 6      =  1.3
Quick Flow Coefficient 6     =  0.555
Quick Flow Exponent 6        =  2
Groundwater Conductivity 6   =  2.4e-08
Maximum Ground Melt 6        = 0.0

################ SOIL 7 (45) ############################################################
Soil Description 7           = Slipout
Lateral Conductivity 7       =  4.23e-05
Exponential Decrease 7       =  2
Maximum Infiltration 7       = 1e-5
Surface Albedo 7             = 0.1
Number of Soil Layers 7      = 3
Porosity 7                   = 0.43 0.43 0.44
Pore Size Distribution 7     = 0.291 0.305 0.239
Bubbling Pressure 7          = 0.2244 0.1987 0.3844
Field Capacity 7             =  0.31  0.3  0.36
Wilting Point 7              =  0.11  0.1  0.15
Bulk Density 7               = 750. 1400. 1500.
Vertical Conductivity 7      =  3.384e-07  4.23e-06  4.23e-06
Thermal Conductivity 7       = 7.11 6.92 8.01
Thermal Capacity 7           = 1.4e6 1.4e6 1.4e6
Infiltration Coefficient 7   =  8.78e-09
Infiltration Exponent 7      =  1.3
Quick Flow Coefficient 7     =  0.555
Quick Flow Exponent 7        =  2
Groundwater Conductivity 7   =  2.4e-08
Maximum Ground Melt 7        = 0.0


##############################################################################
#VEGETATION INFORMATION SECTION
##############################################################################
[VEGETATION]
Vegetation Map File          = /projects/dhsvm/hja/input/ws2_vegtype.bin
Number of Vegetation Types   = 2

################ VEGETATION 1 ###########################################################
Vegetation Description 1     = Old growth douglas fir/western hemlock
Overstory Present 1          = TRUE
Understory Present 1         = TRUE
Fractional Coverage 1        = 1.0
Trunk Space 1                = 0.50
Aerodynamic Attenuation 1    =  2
Radiation Attenuation 1      =  0.25
Max Snow Int Capacity   1 =  0.04
Snow Interception Eff   1 =  0.6
Mass Release Drip Ratio 1 =  0.4
Height 1                     =  60  0.5
Summer LAI 1                 =  8.5  0.5
Winter LAI 1                 =  8.5  0.5
Maximum Resistance 1         =  3000  3000
Minimum Resistance 1         =  300  300
Moisture Threshold 1         =  0.15  0.15
Vapor Pressure Deficit 1     = 4000. 4000.
Rpc 1                        = 3.0 3.0
Albedo 1                     =  0.18  0.2

Number of Root Zones 1       = 3
Root Zone Depths 1           = 0.2 0.3 0.4
Overstory Root Fraction 1    = 0.30 0.30 0.40
Understory Root Fraction 1   = 0.40 0.40 0.30

################ VEGETATION 2 ###########################################################
Vegetation Description 2     = Regrown douglas fir/western hemlock
```

```
Overstory Present 2          = TRUE
Understory Present 2         = TRUE
Fractional Coverage 2        = 1.0
Trunk Space 2                = 0.50
Aerodynamic Attenuation 2    =  2
Radiation Attenuation 2      =  0.25
Max Snow Int Capacity   2 =  0.04
Snow Interception Eff   2 =  0.6
Mass Release Drip Ratio 2 =  0.4
Height 2                     =  60  0.5
Summer LAI 2                 =  8.5  0.5
Winter LAI 2                 =  8.5  0.5
Maximum Resistance 2         =  3000  3000
Minimum Resistance 2         =  300  300
Moisture Threshold 2         =  0.15  0.15
Vapor Pressure Deficit 2     = 4000. 4000.
Rpc 2                        = 3.0 3.0
Albedo 2                     =  0.18  0.2

Number of Root Zones 2       = 3
Root Zone Depths 2           = 0.2 0.3 0.4
Overstory Root Fraction 2    = 0.30 0.30 0.40
Understory Root Fraction 2   = 0.40 0.40 0.30


################################################################################
#MODEL OUTPUT SECTION
################################################################################
[OUTPUT]
Output Directory             = /projects/dhsvm/hja/output/ws2/

################ PIXEL DUMPS ###################################################
Number of Output Pixels      = 0

################ MODEL STATE ###################################################
Read Initial State           = TRUE
Initial State Directory      = /projects/dhsvm/hja/state/ws2/
Initial Soil Temperature     = 15.0
Initial Soil Moist Factor    =  0.6
Number of Model States       = 4
State Date 1                 = 10/01/1962-00
State Date 2                 = 10/01/1979-00
State Date 3                 = 10/01/1983-00
State Date 4                 = 10/01/1993-00

################ MODEL MAPS ####################################################
Number of Map Variables      = 1
Map Variable 1               = 404
Map Layer 1                  = 1
Number of Maps 1             = 1
Map Date 1 1                 = 10/3/2000-18

################ MODEL IMAGES ##################################################
Number of Image Variables    = 0

################################################################################
#END OF INPUT FILE
################################################################################
[End]
```

WS1

/projects/dhsvm/hja/output/ws2/11-9-01/ws2_input.11-09-01.1140.txt:

```
Extreme North                = 4895085.0
```

```
Extreme West                = 559335.0
Number of Rows              = 104
Number of Columns           = 172
DEM File                    = /projects/dhsvm/hja/input/ws1_dem.bin
Basin Mask File             = /projects/dhsvm/hja/input/ws1_mask.bin
Flow Direction File         = /projects/dhsvm/hja/input/ws1_fld.bin
Stream Network File         = /projects/dhsvm/hja/input/ws1_stnetwork.dat
Stream Map File             = /projects/dhsvm/hja/input/ws1_stmap.dat
North Coordinate 1          = 4894565.   # actual=4895460.; basin middle=4894565.
East Coordinate 1           = 560195.    # actual=559450.; basin middle=560195.
Soil Depth File             = /projects/dhsvm/hja/input/ws1_soildepth.bin
Soil Map File               = /projects/dhsvm/hja/input/ws1_soiltype.bin
Vegetation Map File         = /projects/dhsvm/hja/input/ws1_vegtype.bin
Output Directory            = /projects/dhsvm/hja/output/ws1/
Initial State Directory     = /projects/dhsvm/hja/state/ws1/
```

WS3

/projects/dhsvm/hja/output/ws2/11-9-01/ws2_input.11-09-01.1140.txt:

```
Infiltration                = CONSTANT
Extreme North               = 4896365.0
Extreme West                = 560535.0
Number of Rows              = 133
Number of Columns           = 145
DEM File                    = /projects/dhsvm/hja/input/ws3_dem.bin
Basin Mask File             = /projects/dhsvm/hja/input/ws3_mask.bin
Flow Direction File         = /projects/dhsvm/hja/input/ws3_fld.bin
Stream Network File         = /projects/dhsvm/hja/input/ws3_stnetwork.dat
Stream Map File             = /projects/dhsvm/hja/input/ws3_stmap.dat
Road Network File           = /projects/dhsvm/hja/input/ws3_rdnetwork.dat
Road Map File               = /projects/dhsvm/hja/input/ws3_rdmap.dat
Road Class File             = /projects/dhsvm/hja/input/rd-class.dat
North Coordinate 1          = 4895700.   # actual=4895460.; basin middle=4895700.
East Coordinate 1           = 561260.    # actual=559450.; basin middle=561260.
Soil Depth File             = /projects/dhsvm/hja/input/ws3_soildepth.bin
Soil Map File               = /projects/dhsvm/hja/input/ws3_soiltype.bin
Vegetation Map File         = /projects/dhsvm/hja/input/ws3_vegtype.bin
Output Directory            = /projects/dhsvm/hja/output/ws3/
Initial State Directory     = /projects/dhsvm/hja/state/ws3/
```